

**Generation and Transmission of Optical
Ultra-wideband Signals for Optical Fiber and
Wireless Communication Links**

**vom Fachbereich Elektrotechnik und
Informationstechnik
der Technischen Universität Darmstadt**

zur Erlangung des Grades
Doktor-Ingenieurs (Dr.-Ing.)

Dissertation

von Mohammadreza Malekizandi, M.Sc.

Erstgutachter: Prof. Dr.-Ing. Franko Küppers
Zweitgutachter: Prof. Dr.-Ing. Manfred Berroth

Darmstadt 2018

Malekizandi, Mohammadreza : Generation and Transmission of Optical Ultra-wideband
Signals for Optical Fiber and Wireless Communication Links
Darmstadt, Technische Universität Darmstadt,
Jahr der Veröffentlichung der Dissertation auf TUPrints: 2018
Tag der mündlichen Prüfung: 21.06.2018

Veröffentlicht unter CC BY-SA 4.0 International
<https://creativecommons.org/licenses/>

Erklärung laut §9 PromO

Ich versichere hiermit, dass ich die vorliegende Dissertation allein und nur unter Verwendung der angegebenen Literatur verfasst habe. Die Arbeit hat bisher noch nicht zu Prüfungszwecken gedient.

Unterschrift: _____

Datum: _____

Acknowledgment

As my academic time comes to an end, I would like to give thanks and acknowledgement for the people who have helped me along the way. Without them, my experience would have been far less than what it was. These people were not only my mentors and educators, but also my support and friends. During this time, the people around me shaped who I am and helped me grow.

My greatest gratitude must go to Professor Küppers, for his support, knowledge, care, and guidance which he so generously gave. Secondly, I would like to thank Dr. Trung for his great supervision over my project and his valuable advice throughout the process. I also could not have succeeded without the help of my colleagues who so kindly shared their knowledge and made it feel as if I was surrounded by friends rather than colleagues.

My next acknowledgement is for the support of my parents who throughout my life have guided and taught me how to live the right way. My brother, as my best friend, has been like a constant that I could always count on. I am also thankful for my wife's support and patience while I was working late nights in the lab and for sharing her knowledge of the English language to improve my writings.

Lastly, there have been many others throughout my life who have made it possible for me to be standing where I am and to them I am also forever grateful.

Zusammenfassung

Der Bedarf an hoher Bandbreite der kabellosen Datenübertragung ist in den vergangenen Jahren durch die immer engere Einbindung smarterer Geräte im Privatleben stark angewachsen. Um den Bedarf hoher Datenraten decken zu können, müssen aktuelle kabellose persönliche Netzwerke (WPAN) zu höheren Übertragungsfrequenzen migrieren. Ultra-Breitband (UWB) Systeme sind aktuell eine der vielversprechenden Technologien für breitbandige kabellose Datenübertragungen auf kurzen Distanzen aufgrund von zahlreichen attraktiven Eigenschaften, wie geringe spektrale Leistungsdichte, große Bandbreite, verbesserte Fähigkeit Hindernisse zu durchdringen, Unempfindlichkeit gegenüber Abschwächung durch Mehrwegausbreitung, der Koexistenz mit weiteren kabellosen Systemen und der Möglichkeit von Gbps-Übertragungsgeschwindigkeiten. Im Jahr 2002 hat die U.S. Federal Communication Commission die unlicenzierte Nutzung des UWB-Spektrums zwischen 3,1 GHz und 10,6 GHz bei einer spektralen Leistungsdichte kleiner als $-41,3$ dBm/MHz genehmigt. Wegen der geringeren spektralen Leistungsdichte ist die kabellose Abdeckung mittels der UWB-Technologie auf wenige Meter beschränkt, während Breitband-Zugangstechnologien eine größere Abdeckung im Bereich von Kilometern fordern. Um diese Anforderung zu erfüllen und um das lokale UWB-Netzwerk mit fest installierten kabelgebundenen Netzwerken zu vereinen, wird die glasfasergebundene UWB-Übertragung (UWBoF) als aussichtsreiche Lösung vorgeschlagen. Das Konzept von UWBoF sieht vor, die UWB Signale über optische Kanäle zu übertragen um die Abdeckung zu erweitern und um von den Vorteilen der Glasfaser zu profitieren, wie beispielsweise die geringen Verluste und die Immunität gegenüber elektromagnetischer Beeinflussung. Darüber hinaus ist es vorteilhaft, das UWB Signal direkt im optischen Bereich zu generieren und zu kodieren, um den Bedarf von breitbandigen elektronischen Komponenten und zusätzlichen elektro-optischen Wandlern zu umgehen. Außerdem hat die optische Erzeugung von UWB-Signalen viele weitere Vorteile, wie das geringe Gewicht und Größe und eine große Abstimmbarkeit.

Diese Arbeit stellt ein neues Konzept für die rein optische Erzeugung von UWB Impulsen vor. Insbesondere ist es das endgültige Ziel eine Technik vorzustellen, die den Anspruch der zukünftigen WPAN-Industrie basierend auf Glasfasern vorzustellen. Diese sind beispielsweise die Einfachheit der Sender und Empfänger, geringe Kosten, die effizienteste Ausnutzung der vorgegebenen FCC-Maske, die Fähigkeit hohe Übertragungsraten (im Bereich von Gbps), eine große Abdeckung (im Bereich von einigen 10 Kilometern) und die Kompatibilität mit Zeit- und Wellenlängenmultiplexverfahren von passiven optischen Netzwerken (TDM-PON und WDM-PON). Dahingehend wird ein einfacher und kosteneffizienter Ansatz basierend auf direkter Modulation eines Halbleiterlasers und auf optischen Filtern untersucht und experimentell

demonstriert. Diese neuartige Technik zur Formung des Impulses wird vorgestellt und die Vereinbarkeit mit der FCC-Maske analysiert, ausgehend von der Bandbreite, der spektralen Leistungsdichte und der kabellosen Reichweite. Es wird der Einfluss der Faserübertragung auf das generierte UWB-Signal basierend auf der vorgeschlagenen Technik untersucht. Experimentell wird eine Reichweite von 60 km erreicht. Die Kompatibilität des Senders mit TDM-PON wird durch die Generation und fehlerfreie Übertragung eines 1,25 Gbps UWB-Signals, sowie eines 10-Gbps-Non-Return-to-Zero-Signals (NRZ) demonstriert. Dabei wird nur eine Lichtquelle in unterschiedlichen Zeitabschnitten der TDM-Architektur eingesetzt. Zusätzlich wird die Leistungsfähigkeit einer bidirektionalen, symmetrischen und WDM-kompatiblen Datenübertragung eines 1,25 Gbps UWB-Signals durch 60 km Glasfaser getestet. Fehlerfreie Datenübertragung wird erzielt. Schließlich wurde die Übertragung eines 2,5 Gbps UWB-Signals durch den Einsatz einer neuen Modulationstechnik im Sender ermöglicht. Die herausragenden Eigenschaften der in dieser Arbeit beschriebenen Technik unterstreichen das enorme Potential von UWBoF für die Zukunft von kosten- und energieeffizienten, sowie breitbandigen WPAN-Anwendungen.

Abstract

The demand for high bandwidth in wireless communication in the past years has been growing rapidly as the personal smart devices are becoming more and more an inseparable part of modern life. Accordingly, the current wireless personal area network (WPAN) has to migrate to a higher radio frequency in order to satisfy the demand for high data rates. Ultra-wideband (UWB) systems are considered to be one of the most promising technologies for short range broadband wireless communication, due to their numerous attractive features such as low power spectral density, wide bandwidth, enhanced ability for penetrating obstacles, immunity to multi-path fading, coexistence with other wireless systems and capability of providing Gbps data transmission. In the year 2002, the U.S. Federal Communications Commission approved the unlicensed use of the UWB spectrum from 3.1 GHz to 10.6 GHz, with a power spectral density lower than -41.3 dBm/MHz. Due to the low power spectral density, the wireless coverage of UWB technology is limited to a few meters, while the broadband access technology demands a larger coverage in range of kilometers. In order to satisfy this demand and also integrate the local UWB environment into the fixed wired network, UWB-over-fiber (UWBoF) is proposed as a promising solution. The concept of UWBoF is to transmit the UWB signals over optical channels in order to extend the coverage area and benefit from the features offered by the optical fiber such as, low loss and immunity to electromagnetic interference. Moreover, generating and encoding the UWB signals directly into the optical domain is highly desirable, in order to avoid the use of wideband electronics and the need for extra optical-electrical conversion. Furthermore, optical generation of UWB signals has many other advantages such as light weight, small size and large tunability.

This dissertation proposes a novel concept on the optical generation of UWB pulses. In particular, the ultimate goal is to introduce a technique which satisfies the demands of the future fiber optic based WPAN industry such as: simplicity in transmitters and receivers, low cost, the most effective utilization of the imposed FCC mask, ability to deliver high data rates (range of Gbps), offering a huge coverage area (range of 10s of kilometers), compatibility with the time-division-multiplexing passive-optical-networks (TDM-PONs) and compatibility with the wavelength-division-multiplexing passive-optical-networks (WDM-PONs). Accordingly, a simple and cost effective approach based on the direct modulation of a semiconductor laser and optical filtering is investigated and experimentally demonstrated. The novel pulse shaping techniques are reported and their compliance to the FCC mask in terms of bandwidth, spectral power efficiency and wireless coverage is studied. The impact of the fiber transmission on the generated UWB signals based on the proposed technique is investigated and a coverage area of up to 60 km is experimentally verified. The compatibility of the transmitter with the TDM-PON

is demonstrated through the generation and error-free transmission of a 1.25-Gbps UWB signal and a 10-Gbps-non-return-to-zero (NRZ) signal with the use of only one single light source and in different time slots of a TDM architecture. Additionally, the performance evaluation of a bidirectional, symmetric and WDM-compatible transmission of 1.25 Gbps UWB over 60 km fiber is performed and error-free transmission is obtained. Finally, transmission of a 2.5 Gbps UWB signal is made possible by employing a new modulation technique in the transmitter. The outstanding achievements of this thesis underline the great potential of UWBoF for the future of smart, cost effective, energy efficient and broadband WPAN applications.

Contents

1	Introduction	1
1.1	Broadband access networks	1
1.1.1	Optical fiber access networks	1
1.1.2	Short-range wireless networks	3
1.2	Wireless technology in progress	4
1.2.1	WMAN	5
1.2.2	WLAN	6
1.2.3	WPAN	7
1.3	Thesis Organization	8
2	UWBoF	11
2.1	UWB	11
2.1.1	Definition and regulation	11
2.1.2	Variants of UWB	13
2.1.3	Advantages of UWB	14
2.1.4	Applications of UWB	15
2.1.5	Challenges of UWB	15
2.2	RoF	16
2.2.1	Advantages of RoF	16
2.2.2	Challenges of RoF	17
2.2.3	Applications of RoF	17
2.3	UWBoF	18
2.4	Summary	18
3	State of the art	20
3.1	IR-UWB photonic generation	20
3.1.1	Phase modulation to intensity modulation conversion	23
3.1.2	Photonic microwave delay-line filter	25
3.1.3	Spectral pulse shaping and frequency-to-time mapping	28
3.2	Contribution of this thesis	29
3.3	Summary	30

CONTENTS

4	UWB system design	32
4.1	Directly modulated semiconductor laser	32
4.2	Principle of operation	34
4.2.1	Numerical calculation	35
4.3	Monocycle generation and wireless propagation	36
4.3.1	Bit-error-rate measurement	39
4.4	Doublet generation and fiber transmission	39
4.4.1	Bit-error-rate measurement	43
4.5	Summary	44
5	Integration to TDM-PON	46
5.1	TDM-PON	46
5.1.1	Chirp analysis of CML	47
5.2	Experimental setup and results	50
5.2.1	Burst mode	50
5.2.2	Downstream PON	54
5.3	Summary	56
6	Integration to WDM-PON	58
6.1	WDM-PON	58
6.2	Proposed UWBoF-WDM-PON architecture	59
6.3	Principle of operation	60
6.4	Experiment	63
6.4.1	Downstream	63
6.4.2	Upstream	65
6.5	Summary	70
7	Spectral efficiency and modulation format	72
7.1	UWB modulation formats	72
7.1.1	Pulse amplitude modulation	73
7.1.2	Bi-phase modulation	73
7.1.3	Pulse shape modulation	74
7.1.4	On-off keying	75
7.1.5	Pulse position modulation	79
7.2	Multipulse pulse position modulation	84
7.2.1	Concept of MPPPM	84
7.2.2	MPPPM signal generation and detection	85
7.3	Summary	88
8	Conclusion and Outlook	91
8.1	Conclusion	91
8.2	Outlook	92

Chapter 1

Introduction

1.1 Broadband access networks

Throughout the past few decades, the demand of business as well as residential bandwidth customers, has expanded worldwide from basic e-mail exchange and limited business file transfer, to rising broadband access in order to support data-intensive applications such as online gaming, high-definition television (HDTV), voice-over-IP (VoIP), video-on-demand (VoD) and highspeed internet. Many of the above applications require data rates faster than hundreds of Mbps. For example, HDTV 1080p calls for 2.97 Gbps. It is therefore predicted that by 2021, annual global IP traffic will reach 3.3 ZB [1]. Global IP traffic from 2005 to 2021 will have increased by almost 127-fold. At the same time, broadband speeds will have also nearly doubled [1]. As a result of these changes, extreme pressure has been placed on the communication network infrastructures to support low cost broadband access of diverse services. The result of this has been a significant evolution of wired and wireless access networks within a very short time span.

1.1.1 Optical fiber access networks

Passive optical networks (PONs) have been known to be the most promising high performance and cost effective solution for broadband access networks [2–6]. The standardization roadmap for PONs is presented in Fig. 1.1. To replace coaxial cable based access systems, fiber-to-the-home (FTTH) is being deployed on a large scale throughout the world. Ethernet PON (EPON) (IEEE 802.3ah, 2004) and gigabit PON (GPON) (ITU-T G.984) are two main FTTH-PON standards which are currently being established. Both solutions cover distances of up to 20 km, use point-to-multipoint topology and time-division multiplexing (TDM) with variable split-ratio, commonly from 32 to 64 users.

Although TDM-PONs offer higher bandwidth than conventional copper based access networks, they are not compatible with different signal formats and data rates. Upgrading the network to support different transmission protocol or higher data rates, requires replacing the electronics in both the optical line termination (OLT) and the optical network unit (ONU).

1 Introduction

Furthermore, next-generation optical access networks are expected to provide much higher bandwidth up to Gbps per user and beyond to satisfy the demand of developing services and applications [2]. Wavelength division multiplexing (WDM) technology offers a new dimension in order to increase the bandwidth for the upgrade of PON to next-generation access networks. In a WDM-PON system, light sources in the ONUs operate at different wavelengths coexisting within the same fiber. There are several advantages of WDM-PON which allow operators to centralize networks and provide high speed access for business, mobile backhaul and FTTH [5–7] as follows:

- Higher bandwidth: each ONU, without sharing, can have its own maximum downstream and upstream bandwidth due to the dedicated wavelength and bandwidth for each one.
- Flexible bandwidth and format: modulation format and data rate can vary among each wavelength channel.
- Higher security: the signal from an ONU is not shared with any other ONUs as WDM-PON has a virtual point-to-point configuration.
- Fast network reconfiguration: due to the flexibility in wavelength distribution.
- Higher upgrade-ability and scalability: due to the specified link and wavelength, the change of one channel does not effect the operation of others.

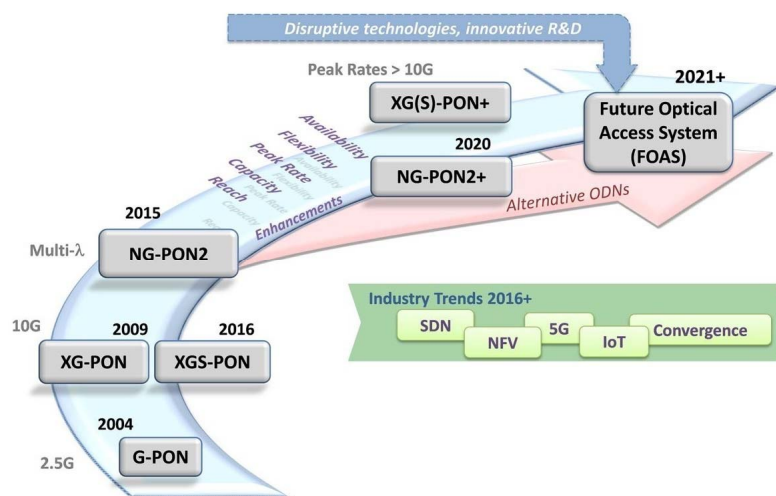


Figure 1.1: PON standardization roadmap [8]. EPON: ethernet passive optical network, GPON: gigabit passive optical network, 10GE-PON: 10 Gbps ethernet passive optical network, XG-PON: 10-gigabit-capable passive optical network, NG-PON1: The first next-generation passive optical network, NG-PON2: The second next-generation passive optical network.

Currently, the major disadvantage of WDM-PONs is the high cost of the equipment related to the remote node and ONUs. Arrayed waveguide gratings (AWGs) are used at the remote node as a wavelength multiplexer/ demultiplexer to combine and separate different wavelengths

of channels. Although they have been largely improved over the past few years, especially to overcome thermal stability issues, their cost is still higher than power splitters used in TDM-PONs. Wavelength dependency causes difficulty in the network upgrades and maintenance as they require manual reconfiguration of the equipment in the end-user side. Several solutions have been introduced to tackle this challenge such as injection-locked Fabry-Perot laser, reflective semiconductor optical amplifier (RSOA), using spectrum sliced broadband light source or tunable laser [7].

1.1.2 Short-range wireless networks

Since the first transatlantic wireless experiment in 1901 [9], end-users have been benefiting from the flexibility, mobility and convenience of numerous wireless communication technologies. Fig. 1.2 shows a few examples of current wireless standards for these networks. Those standards have become popular for different application scenarios, such as long term evolution (LTE) for wireless wide area network (WWAN), global system for mobile communications (GSM), WiFi (IEEE 802.11) for wireless local area network (WLAN), Bluetooth and ZigBee for wireless personal area network (WPAN). In recent years, personal wireless device usage has grown rapidly and resulted in an exponential increase to Gbps in order to support the various multimedia applications, especially video applications [10]. To fulfill these demands, a broadband spectrum is required to support such high data throughput. The challenge however, is that the wireless technologies operate in low frequency bands, which are rather crowded and no longer capable of supporting such high bandwidth requirements due to limited available bandwidth. For instance, for WiFi, there are only 70 MHz in the 2.4 GHz band and 500 MHz in the 5 GHz band. An idea to meet the bandwidth demand is to increase spectral efficiency (SE) over a given bandwidth. SE larger than 1 bit/s/Hz can be obtained by using complex modulation formats, such as quadrature amplitude modulation (QAM) or orthogonal frequency-division multiplexing (OFDM). Utilizing smaller cell sizes (micro- or pico-cells) and reducing the numbers of mobile users (which operate and share the bandwidth) in each cell can also improve the bandwidth for each mobile user. Another alternative to gain high capacity wireless links is to move towards higher RF frequencies, where higher bandwidth is available.

1 Introduction

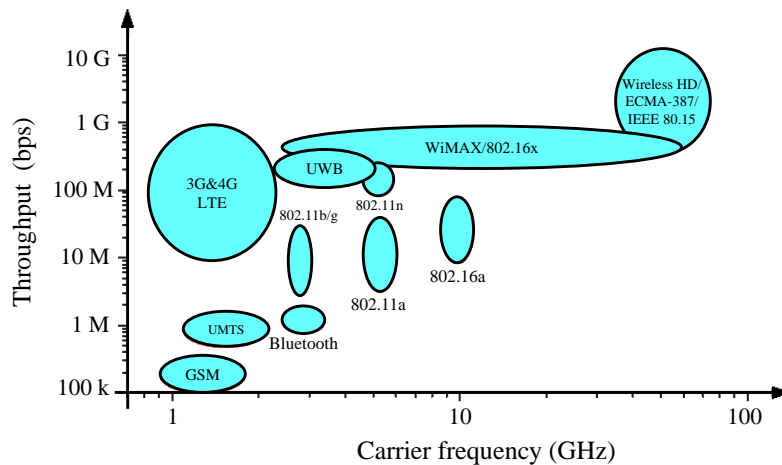


Figure 1.2: Throughput and allocated frequency of some wireless services. UWB: ultra-wide band, GSM: Global System for Mobile Communications, LTE: Long Term Evolution, UMTS: Universal Mobile Telecommunications System, WiMAX: Worldwide Interoperability for Microwave Access.

1.2 Wireless technology in progress

With people becoming increasingly global, the need for communication has increased among both business and family. Nowadays, nothing prevents us from sending audio and video messages anywhere on earth. For instance, students abroad are able to video chat with their parents, while business employees can take part in teleconferences with colleagues on the other side of the world for a rather low cost. Additionally, the form of communication has become richer and more varied. This modern style of communication is all becoming possible due to the swift advancement of information and communication technology (ICT), which is the merger of telecommunication technologies and informatics. It is important to note, that this communication is not only applicable to human interaction. For example, with the invention of so-called smart homes, lighting, heating, ventilation and many other electronic devices can all be controlled automatically [11]. Hence, telecommunication technologies are becoming a significant part of daily life by making it easier to stay connected anywhere in the world, at any time with practically any device.

With the increase in popularity of smart phones and computer tablets there has been a sudden rise in the demand for wireless data capacity and coverage [12, 13]. To fulfill this need, wireless systems are dramatically expanding their capacities as shown in Fig. 1.3. As can be seen, the capacity of WPAN is rising at a much faster rate than the other wireless technologies. One reason for this is the relatively smaller coverage and utilization of high bandwidth wireless technologies, which are capable of multi-Gbps wireless communication, such as UWB (3.1 — 10.6 GHz) and millimeter-wave wireless technologies using the 60 GHz band. Meanwhile, the sharp increase in the capacity of WPAN is an undeniable confirmation of the critical importance of high-speed wireless access required by the end users of communication

networks. Additionally, this illustrates that in-building coverage and capacity have become vitally important because of the fact that hand-held devices are mostly used inside buildings as opposed to from the outside [12]. Consequently, high capacity and energy-efficient in-building networks are becoming necessary. Therefore, this thesis focuses on broadband UWB-over-fiber (UWboF) for high capacity and energy-efficient in-building networks. A general overview of these wireless technologies is discussed in the following sections.

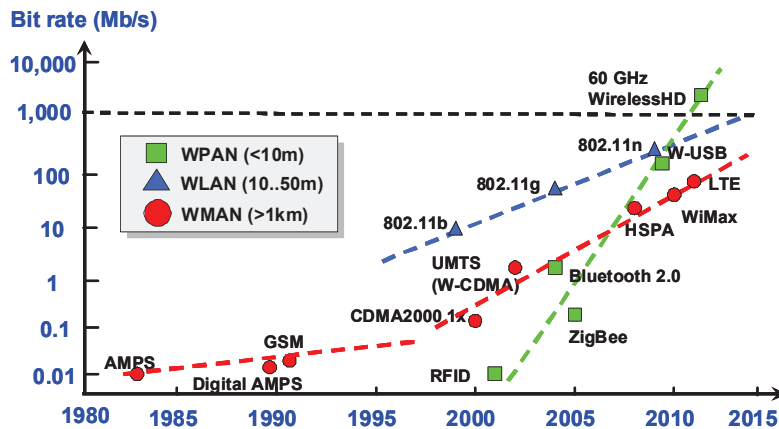


Figure 1.3: Wireless technology trends Ref. [12], Fig. 1.

1.2.1 WMAN

As shown in Fig. 1.3, since the first successful deployment of mobile telephony, mobile communication has been developed into a mass market of high tech products in less than two decades. This unprecedented growth has never been achieved by any other technology, whether radio, television or even internet [14]. From the other side, availability of cellphones has completely changed from once only being used by the wealthy class, to becoming a personal item affordable to everyone. Cellphones in many countries now exceed the number of land-lines, as they can be found even among school aged children. The trend of GSM, universal mobile telecommunication systems (UMTS) and LTE is shown in Fig. 1.3. Typically, the growth in the past was mainly focused on voice and messaging service but nowadays, it is mobile video and internet which encourages the growth.

Data overload is one of the most challenging aspects of the operator's occupation [15]. Cisco Systems predicts a 7-fold increase of data traffic from 2016 to 2021 [13], reaching 49.0 exabytes per month (Fig. 1.4). As a result of this increase, an explosion of mobile data traffic from smart phones and tablets will need to be dealt with by operators [14]. As illustrated in Fig. 1.5, by 2021 laptops will still dominate the amount of data traffic, but newer devices such as tablets and machine to machine (M2M) communication will begin to make up a larger fraction. This shows that communication is not solely limited to human interaction. It is noteworthy to mention that the evolution of the cellular wireless systems is not limited in speed but the main future trend is generalized as [14]: 1) flexible, scalable and energy efficient air interface design,

1 Introduction

2) maximizing of both peak and especially cell-edge data rates and user capacity, 3) guaranteed ubiquitous coverage in high mobility scenarios.

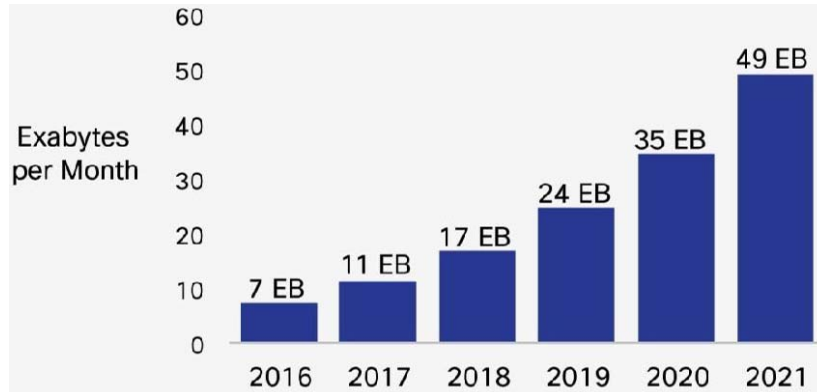


Figure 1.4: Cisco Forecasts 49 Exabytes per month of mobile data by 2021 [13].

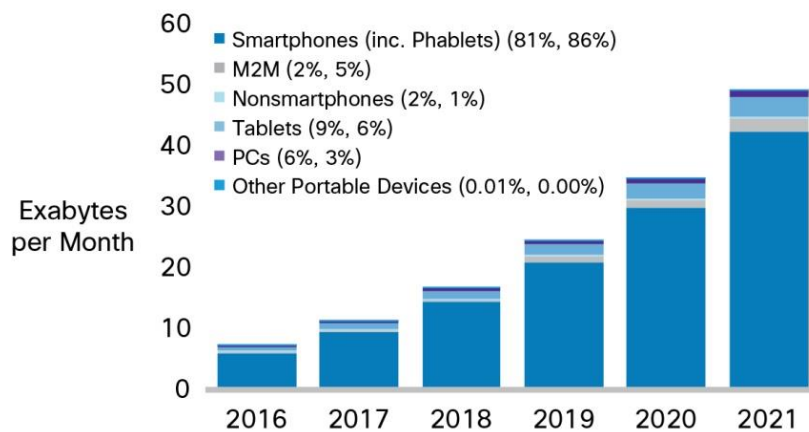


Figure 1.5: Devices responsible for mobile data traffic growth (Laptops and smartphones lead traffic growth) [13].

1.2.2 WLAN

The trend of medium and short range wireless communication is another outcome of the enlargement of radio communication [11]. The WLAN standard IEEE 802.11 (IEEE 1999) was one of the first outstanding products in this segment, which was first introduced in 1997 (Fig. 1.3). Its purpose was to discontinue the use of the LAN wires in homes and offices and was more effective than any of the previous technology up to that point, such as Infrared data association [11]. The release of the upgraded version of IEEE 802.11b led to numerous installations of wireless "hotspots", which were established where several Mbps could be offered to devices such as laptops and personal digital assistance (PDAs) through a wireless

internet connectivity access point, within a range of up to about 100 m. Nowadays, millions of hotspots have been established in key locations throughout the world such as airports, train stations, restaurants and hotels, where people gather in large numbers.

1.2.3 WPAN

In order to cover wearable and hand held devices, another category of technology has been developed, which covers a shorter range of up to 10 m, has low power consumption and provides a wide range of data rates [11]. This branch is called wireless personal area network (WPAN) technologies. Currently, the most common technology of this segment is IEEE 802.15.1 (Bluetooth). WPAN is a rather recent technology and as shown in Fig. 1.3, its data rate is increasing sharply. With the help of this technology, nowadays, laptops, PDAs, mobile phones and other personal devices within a range of 10 m can be easily connected with very low power consumption for battery powered devices. As shown in Fig. 1.3, promising technologies such as UWB and 60 GHz are aiming for very high data rates in this segment. According to [14] short-range wireless communications will be dominating wireless communication in the future, as it is forecast that 7 trillion wireless devices will serve seven billion people by 2020 [14]. Additionally, it is predicted to be a broad spectrum of air interface technologies, network architectures and standards. The air interface technologies might consist of conventional (narrow band) radio, UWB radio, mm-wave communications and optical wireless communications. Furthermore, the offered data rate will be diverse from low (1 bps — 100 kbps), moderate (100 kbps — 10 Mbps) to high (10 Mbps — 10 Gbps). To summarise, WPAN in general and UWB in particular are evolving based on four main issues [16]:

- A growing demand for wireless data capability in portable devices at higher bandwidth but at a lower cost and power consumption than currently available.
- Crowding in the spectrum that is segmented and licensed by regulatory authorities in traditional ways.
- The growth of high-speed wired access to the Internet in businesses, homes and public places.
- Decreasing semiconductor cost and power consumption for signal processing.

In summary, it is abundantly clear that the ultimate goal of all mentioned networks (WMAN, WLAN and WPAN) is to expand capacity. To do so, several techniques have fortunately been introduced such as: additional spectrum (large bandwidth), spectral efficient modulation and coding techniques, advanced multiple antenna techniques (MIMO and beam forming) and the use of smaller and more cells [15]. Among these approaches, reducing the size of deployed radio cells, is the simplest, as it results in a smaller number of wireless users sharing bandwidth within a given radio cell. This is one of the main reasons why WPANs can provide faster wireless data access. Although, to implement small radio cells, utilization of numerous

1 Introduction

antennas is necessary. Furthermore, to improve wireless signal capacity and coverage inside buildings, increasing the antenna density is required, as poor wireless signal propagation causes significant wireless system performance degradation. In order to utilize such a substantial amount of antennas a considerable high-capacity signal distribution network or backbone is required. Optical fiber is one of the most ideal technology to feed the antenna of high-speed wireless systems, due to its large bandwidth, low weight, multi-standard and future proof backbone infrastructure. Hence, this thesis merges the best of both worlds, wireless (unlicensed high bandwidth IR-UWB) and wired (optical fiber) communication systems in order to provide high capacity and energy efficient in-building networks.

1.3 Thesis Organization

The concepts and characteristics of UWB and radio-over-fiber (RoF) systems are discussed in **chapter 2**. The applications, advantages and challenges of each system are fully studied. In order to benefit from the advantages and overcome the challenges, the UWB-over-fiber (UWBoF) is introduced by merging the UWB and RoF systems.

In **chapter 3**, first, a literature review is presented about the traditional approaches of UWB photonic generation. All these known techniques are categorized into three groups based on their concepts. Each category is fully described and explained, and related publications are referenced for further study. Second, the scope and contribution of this thesis is clarified by proposing a novel, simple and cost efficient method for generating the UWB pulses based on the direct modulation of the semiconductor laser and optical filtering. The proposed concept introduces a new category to the traditional ones.

The proposed UWB generation technique is presented in **chapter 4**. First, the theory of the directly modulated semiconductor laser is studied and the principle of operation is explained. Then, the UWB pulses are experimentally generated and the wireless propagation is performed. Next, the impact of the fiber transmission on the generated pulses is numerically and experimentally investigated. It is demonstrated that the proposed transmitter can be adjusted for the different fiber lengths installed in optical access network infrastructure.

The compatibility of the proposed transmitter with the TDM-PON architecture is investigated in **chapter 5**. The chirp behavior of the semiconductor laser is fully studied and measured. Based on the analysis of the laser chirp, the transmitter is developed to be completely compatible with TDM-PON. The bias point of the semiconductor laser is controlled through a burst signal with different amplitudes for different time slots. By a proper selection of the burst amplitudes, non-return-to-zero (NRZ) and UWB signals are generated from a single light source at different time slots in the TDM architecture.

In **chapter 6**, a bidirectional UWBoF system compatible with WDM-PON architecture is presented. In the downstream scenario of the proposed scheme, the desirable UWB pulse shape is obtained by taking advantage of the interference effect of a delay-line interferometer. While the UWB signal is received from one of the DLI outputs and propagated through an UWB antenna, the other output is employed for injection-locking of a colorless Fabry-Perot laser in order to establish an optical carrier for the upstream transmission. A bidirectional data

transmission for the symmetric transmission distance is performed.

The conventional modulation techniques for UWBoF communication are reviewed in **chapter 7**. The advantages and drawbacks of each method are investigated. A new modulation technique based on the position and number of the impulses in a symbol frame duration is proposed, in order to increase the spectrum efficiency. M-ary modulation is enabled by employing the new modulation technique in the transmitter.

Finally, **chapter 8** concludes the study, highlights the outcomes, and provides a prospective for future works in this area.

Chapter 2

UWBofF

In this chapter, the concept, applications and challenges of ultra-wideband (UWB) and radio-over-fiber (RoF) systems are first studied separately. In order to overcome the challenges and benefit from the advantages, the UWB and RoF systems are merged and UWBofF is introduced.

2.1 UWB

As more and more devices are going wireless every day, coexistence among these various wireless technologies is necessary. Since the Federal Communications Commission (FCC) in the USA approved the unlicensed operation of UWB devices in 2002 regarding the emission requirement [17], UWB has become more popular. UWB is able to coexist with other wireless devices, because of its unlicensed operation and low-power transmission. Its inexpensive low-power transceiver, makes it a good candidate for short-to-medium range wireless systems such as WPANs. Subsequently, UWB technology has received great attention and interest from academia, industry and global standardization bodies [18]. The definition of UWB along with its features, challenges, and applications, as well as the FCC regulations, are all discussed in the following.

2.1.1 Definition and regulation

The extensive bandwidth of UWB signals distinguishes them from conventional narrow-band/wide-band ones [19]. According to the FCC, a UWB system is determined to have an absolute bandwidth of at least 500 MHz or a fractional (relative to the center frequency) bandwidth of larger than 20 % [19, 20]. The absolute bandwidth is defined as the difference between the upper frequency f_H and the lower frequency f_L of the -10 dB emission point;

$$B = f_H - f_L \quad (2.1)$$

which is also known as -10 dB bandwidth. From the other side, the fractional bandwidth (B_{frac}) can be calculated as:

$$B_{frac} = \frac{f_H - f_L}{f_c} \quad (2.2)$$

2 UWBoF

where f_c is the center frequency and is given by:

$$f_c = \frac{f_H + f_L}{2} \quad (2.3)$$

From Eq. 2.1 and 2.3, the fractional bandwidth B_{frac} in equations 2.2 can also be expressed as:

$$B_{frac} = 2 \left(\frac{f_H - f_L}{f_H + f_L} \right) \quad (2.4)$$

Due to the large bandwidth of the UWB signal, a set of regulations is enforced on the UWB transmitting systems, in order to benefit from the advantage of UWB without interfering with the other systems [19, 21]. The FCC introduced modern UWB regulations in 2002 [22], for an unlicensed frequency band between 3.1 GHz and 10.6 GHz with a permissible equivalent isotropically radiated power (EIRP) of -41.3 dBm/MHz and a minimum bandwidth of 500 MHz. In order to have a better impression of this level, this is the same level allowed for the radiated noise from an electronic device [23–26]. Consequently, UWB signaling can be assumed as reusing the noise floor for communication applications. The FCC emission mask for indoor applications is shown in Fig. 2.1. It should be noted that the main concern is to not interfere with the extremely power-restricted GPS band (0.96 — 1.61) GHz shown in Fig. 2.1.

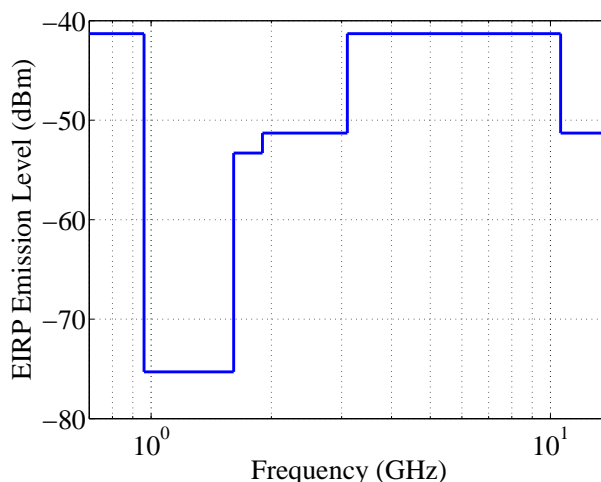


Figure 2.1: FCC emission limit for indoor UWB systems.

It is noteworthy to mention that for different applications the spectral mask is different and the total bandwidth also varies. Moreover, different regions have a different mask; in Europe and in Asian countries the regulations are stricter while in the US and Canada they tend to be more relaxed [21]. UWB regulation for different regions is summarized in Fig. 2.2. Some of these bands require detect-and-avoid (DAA) action in the UWB transmitter. As can be seen in Fig. 2.2, the only common spectrum across these regulations is the band from 7.25 GHz to 8.5 GHz. This is one of the main obstacles for UWB to be successful in the mass market.

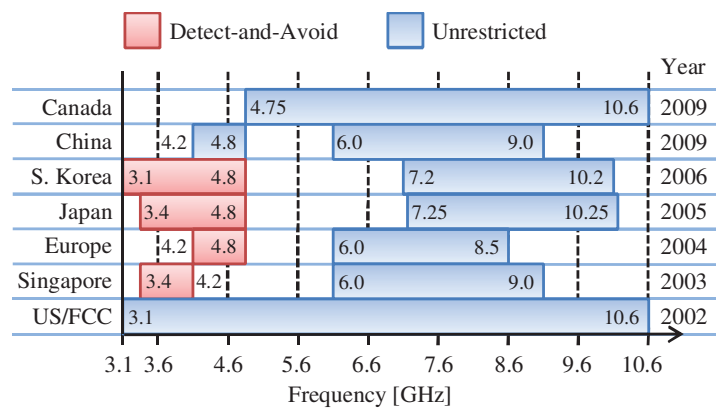


Figure 2.2: UWB intended bands for communications for different regions (Ref. [21], Fig. 1).

2.1.2 Variants of UWB

UWB systems can be classified principally into three different categories: namely carrier-less impulse radio UWB, single carrier UWB and multi-carrier UWB [27].

Carrier-less Impulse Radio (IR-UWB)

IR-UWB is the long-established and traditional approach to UWB communications. It utilizes very short-duty cycle impulses occupying a single band of several GHz. The most important features of IR-UWB are namely the possibility of achieving high throughput, low-power consumption and inexpensive implementation. For modulating the data in the IR-UWB approach, different modulation formats can be used such as pulse polarity modulation (Bi-phase), pulse amplitude modulation (PAM), pulse shape modulation (PSM) and the most common pulse position modulation (PPM) [23, 25, 26]. IR-UWB communication has become more feasible due to the recent developments of both the technical and regulatory sectors of this technology.

Single carrier UWB

In this scenario, a block of pulsed carrier cycles is bandpass filtered and then transmitted to the antenna. The spectrum of the signal can be accurately controlled through this approach. The UWB baseband signal can be easily up-converted to radio frequency with a center frequency of several GHz with the help of a mixer and proper oscillator. The data modulation can be performed the same way as for IR-UWB (i.e PPM, PAM, PSM and ...) and multiple access can be realized by time-hopping or direct sequence spread spectrum [27].

Multi-Carrier UWB (MC-UWB)

In this scheme, multiple carriers are simultaneously used and it is mostly based on orthogonal frequency-division multiplexing (OFDM). To comply with the local regulation (Fig. 2.2), MC-

OFDM based UWB (also known as multi-band-OFDM UWB) is able to turn off some bands dynamically [23, 25–27]. Furthermore, it proposes a good coexistence with narrow band systems.

2.1.3 Advantages of UWB

The advantages of UWB are listed below and briefly described. These advantages are mostly a product of the extremely large bandwidth of UWB signals.

- Large Channel Capacity

The maximum error-free transmitted data rate for an AWGN channel, can be calculated from the Shannons capacity formula:

$$C = B \times \log_2(1 + SNR) \text{ bits/second} \quad (2.5)$$

where C represents the maximum channel capacity, B [Hz] is the channel bandwidth, and SNR is the signal-to-noise ratio of the system. It is obvious from Eq. 2.5 that increasing channel capacity (when $SNR \gg 0$ dB) can be achieved by linearly increasing the bandwidth, while a similar capacity increase would require an exponential increase in power [20, 28]. Consequently, the UWB is one of the best candidates for high-speed data communications.

- Fading Robustness

Due to the UWB signals considerable absolute bandwidth, the UWB receiver can resolve multipath components (MPCs) even in dense multipath environments. The receiver processes the different MPCs separately, and assures that they add up in an optimum way, which leads to a smaller probability of strong fades. This reduces the fading margin and enhances system performance [18]. This enhancement though, comes at the price of complexity in the receiver side.

- High Precision Ranging and Localization

As mentioned above, a UWB receiver is capable of resolving MPCs, considering their large bandwidth. Hence, they can precisely estimate the arrival time of the first signal path. This provides the opportunity of determining the distance between a wireless transmitter and receiver accurately. Accordingly, one of the UWB features is the potential for high-precision localization, which attracts ranging and radar applications [17, 19, 29].

- Superior Penetration Properties

UWB signals are capable of penetrating through obstacles, as their broad spectrum also contains low frequencies. Therefore, UWB systems can operate under both line-of-sight (LoS) and non-LoS (NLoS) conditions. This aspect of UWB makes it feasible for through-the-wall communications and ground-penetrating radars [20].

- Co-Existence with Other Technologies

Due to the low power spectral density of UWB systems, they can coexist with other services such as cellular systems, WLAN, GPS, etc.

2.1.4 Applications of UWB

The described advantages of UWB technology in Sec. 2.1.3 guarantee a huge diversity of applications in military, civilian and commercial districts [24]. Applications of UWB technology are summarized in Table 2.1.

Table 2.1: UWB APPLICATION IN MILITARY AND COMMERCIAL SECTORS [24]

	Military	Commercial
Data communication	Secure LPI/D communications Covert wireless sensor networks (battlefield operation)	Local and personal area networks Wireless streaming video distribution(home networking) Wireless sensor networks (health and habitat monitoring, home automation)
Radar	Through-wall imaging (for law enforcement, fire fighters) Ground-penetrating radar (for rescue operations) Surveillance monitoring	Medical imaging (remote heart monitoring) Ground-penetrating radar (detection of electrical wiring, studs, etc. on construction site) Automotive industry (collision avoidance, roadside assistance) Home security (proximity detectors)
Localization	Personal identification Lost children Prisoner tracking	Inventory tracking Tagging and identification Asset management

2.1.5 Challenges of UWB

Although UWB technology has many advantages, it has, nevertheless, some challenges as well due to the use of nanosecond duration pulses for communications. Many research groups around the world are working on the solutions to deal with those dilemmas, in order to make UWB technology popular and universal. The most challenging issue is regulatory problems. Due to the wide bandwidth of the UWB, strict regulation is necessary to avoid interference between different users of the spectrum. Users of the other technologies need to be convinced that UWB will not harm their existing services.

The other challenge which needs to be addressed is the agreement over the standards for interoperability of UWB devices. There are currently two types of standards for UWB design, and unfortunately, neither side is willing to take steps to overcome this problem. This battle

might become a serious threat to UWB market growth, as consumers will hesitate over which standard to follow [25].

2.2 RoF

Radio over Fiber (RoF) has been introduced to replace the high-power central antenna with the low-power distributed antennas system (DAS) [30]. In RoF technology, the modulated RF signals are distributed to remote antenna units (RAUs) through an optical fiber link. RoF systems usually consist of many base stations (BSs), which are connected to a single central station (CS) (Fig. 2.3). Accordingly, in order to make the BSs cost efficient, the complexity of the system is moved to CS. All switching, routing and operation administration maintenance are done in CS, while BSs have no processing duty and their only task is to convert the optical signal to wireless and vice versa. The RoF-based wireless ‘last mile’ access network architecture was proposed as an alternative for broadband wireless access networks [31].

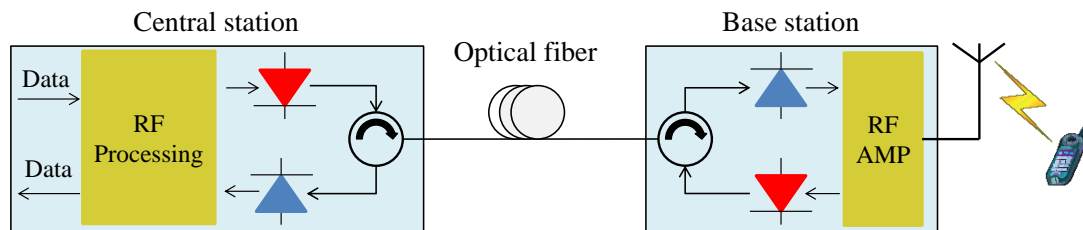


Figure 2.3: RoF architecture.

2.2.1 Advantages of RoF

Some of the advantages of RoF technology are listed below and briefly described.

- **High Bandwidth**
Optical fibers offer three transmission windows with very low attenuation and large bandwidth. The total bandwidth of these three windows exceeds 50 THz for single mode fiber (SMF) [32].
- **Low Attenuation**
As mentioned above, the optical windows have a very low attenuation loss. For instance, the loss in SMF is around 0.2 dB/km and 0.5 dB/km at 1550 nm and 1300 nm, respectively.
- **Immunity to Radio Frequency Interference**
The signal in optical fiber is immune to the electro-magnetic interference, as it is modulated in the optical domain. The optical fiber also offers great privacy and security, due to its immunity to eavesdropping.

- **Low Power Consumption**
As mentioned earlier, all the processing and complex equipment in RoF technology is moved to CS. This reduces the equipment in RAUs, which leads to lower power consumption.
- **Multi-Service Capable**
Utilizing sub-carrier modulation (SCM), the RoF offers flexibility in system operation. In other words, the same RoF network can be shared by multi-operators or provide multi-service traffic.
- **Dynamic Resource Allocation**
Since all the operation and processing in the RoF system is performed at a centralized head-end, the capacity can be allocated dynamically [33]. As an example, during the peak time in a cellular network, more capacity can be allocated to an area with a higher amount of traffic.

2.2.2 Challenges of RoF

The RoF is an analog transmission system, as the modulation and the detection of the light are performed in an analog domain. Consequently, the RoF performance is affected by signal impairments such as noise and distortion. These impairments influence the dynamic range and the noise figure (NF) of the RoF links. In wireless communication systems (such as GSM and WLAN), Dynamic Range is a critical criteria. The received power at the BS from the mobile users (MUs) varies widely (e.g. 80 dB [33]), as an MU can be very close to the BS, while another MU is several kilometers away, but within the same cell.

The noise in the optical fiber links consists of the laser phase noise, laser relative intensity noise (RIN), amplified spontaneous emission (ASE) noise from the amplifiers and the photodiodes shot noise and etc. The chromatic dispersion of the SMF curbs the length of the fiber link and also leads to phase de-correlation causing increased RF carrier phase noise.

2.2.3 Applications of RoF

The main applications of RoF are highlighted in the following:

- **Cellular Networks**
RoF offers very cost efficient routing for mobile traffic (e.g. CDMA, GSM, UMTS) between CSs and BSs. Moreover, the radio coverage in dense urban areas can be extended through RoF [33].
- **Wireless LANs**
With the rise in popularity of mobile devices, the demand for mobile broadband access to LANs is growing quickly. RoF offers a promising solution for the distribution of WLAN signals.

2 UWBoF

- Video Distribution Systems

Both wired (Cable TV) and wireless (IEEE 802.16x) broadband access systems in metropolitan area networks (MAN) can be relayed on RoF.

- Vehicle Communication and Control

Due to RoF's ability to extend the coverage of the road network, it can be used in intelligent transport systems (ITS) and road-to-vehicle communication systems [33], in order to make ITS more manageable and effective.

There is a great desire for a fiber link which is capable of transmitting an entire RF band of several GHz over a long distance. As mentioned above, the losses in fiber link are much smaller than the wireless or wired-coax channel. The ultimate target of this dissertation is to develop a cost effective and power efficient RF-optical link for UWB technology.

2.3 UWBoF

To meet the challenges proposed by the limited reach of UWB wireless communications, the idea of UWB radio over optical fiber is introduced [34, 35]. The main concept is to use optical links with very low loss and broad bandwidth to distribute the UWB signals with a bandwidth of several GHz over long distances. This opens up the door to new aspects and applications of UWB technology. For instance, the coverage area of WPAN can be expanded by up to three fold and give birth to new optical/wireless infrastructures capable of providing 1 Gbps of traffic to and from consumers in the remote node. UWBoF is promising in the area of security as well as it is able to collect data from numerous sensors and cameras through UWB and deliver it over RoF technology [14]. The electrical to optical conversion in UWBoF can be prevented, by generating the UWB signals directly in the optical domain. This is highly desired, as it has many advantages such as light weight, small size, large tunability, and immunity to electromagnetic interference [36]. Many research efforts have been made in order to directly generate UWB pulses in the optical domain. Nonetheless, the proposed techniques are still complex with the use of expensive devices such as optical modulator and mode-locked laser. Among all three variants of UWB categories, IR-UWB over fiber has been selected as the main approach of this thesis. The main objective of this dissertation is to develop a simple IR-UWB transmitter for UWBoF systems based on direct modulation of a semiconductor laser.

2.4 Summary

First, the UWB definition and regulation were studied. The variants of UWB were described, and the advantages were briefly explained. The applications of UWB were categorized and the challenges were reviewed. Next, RoF was studied, the advantages and challenges were discussed and the applications were explained. Finally, UWBoF was introduced by merging the UWB and RoF technologies and taking advantage of their capabilities in order to extend the range of the UWB and benefit from the high bandwidth, low loss, and immunity to electromagnetic interference offered by optical fiber.

Chapter 3

State of the art

3.1 IR-UWB photonic generation

Due to the many profitable features of impulse radio-UWB such as immunity to multipath fading and also simple and inexpensive implementation associated with carrierless (baseband) pulses, IR-UWB is one of the popular choices for UWB communication [37]. Unlike single carrier UWB, the signal is not shifted to the higher frequency using a sinusoidal carrier but instead communicates with a baseband signal composed of subnanosecond pulses [37]. In order to avoid wideband electronics, it is highly desired to generate the UWB pulses directly in the optical domain without requiring an extra electrical-to-optical conversion [35]. Moreover, using optical approaches to generate IR-UWB pulses has many other advantages, such as the light weight of the fiber cable, small size, large tunability and immunity to electromagnetic interference [35].

The main challenge in IR-UWB communication is the design of the waveform. The ultimate goal is to produce a waveform which has a desired wide bandwidth and at the same time can satisfy the FCC regulation as much as possible [37]. IR-UWB pulses are usually based on the Gaussian pulses expressed as:

$$p(t) = \frac{A}{\sqrt{2\pi}\sigma} \left(-\frac{t^2}{2\sigma^2} \right), \quad (3.1)$$

where A and σ stand for the amplitude and spread or shaping factor of the Gaussian pulses, respectively. In order to fulfill the FCC regulation, derivatives of the Gaussian pulse which have smaller DC components are preferred [24, 25]. The higher order derivatives of the Gaussian pulse in the time domain, look like a sinusoidal signal which is modulated by a Gaussian pulse-shaped envelope. The higher the order of the derivative, the more the number of zero crossings in time will be. The higher amount of zero crossings within the same pulse width correspond to a sinusoidal “carrier” with a higher frequency modulated by an equivalent Gaussian envelope. Accordingly, higher order derivative of the Gaussian pulse has been considered as one of the best candidates for UWB transmission [37]. The n_{th} derivative of the Gaussian pulse can be determined from:

$$x^{(n)}(t) = -\frac{n-1}{\sigma^2} x^{(n-2)}(t) - \frac{t}{\sigma^2} x^{(n-1)}(t). \quad (3.2)$$

The Fourier transform of the n_{th} order derivative pulse is:

$$x_n(f) = A(j2\pi f)^n \exp\left(-\frac{(2\pi f\sigma)^2}{2}\right). \quad (3.3)$$

Considering the n_{th} derivative of the Gaussian pulse as the transmitted UWB pulse, the corresponding power spectral density (PSD) can be calculated as:

$$|P_t(f)| = \frac{A_{max}(2\pi f\sigma)^{2n} \exp(-(2\pi f\sigma)^2)}{n^n \exp(-n)}, \quad (3.4)$$

where A_{max} is the maximum peak PSD that the FCC will permit. The first, second and fifth order derivative of Gaussian are depicted in Fig. 3.1. As can be seen, the derivative order and the amount of zero crossings within a pulse width are the same. Figure 3.2 shows the PSD of the first seven order of the Gaussian derivative. As can be seen, the higher the derivative order, the higher the center frequency.

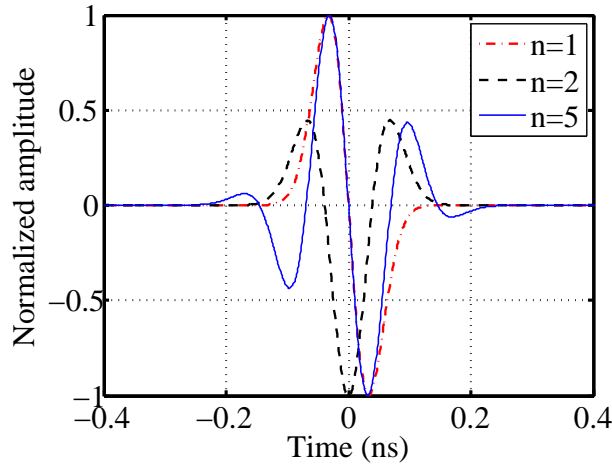


Figure 3.1: Examples of derivatives of Gaussian pulse.

Referring to Fig. 3.2, the low order derivatives ($n \leq 4$) do not comply with the FCC mask around the GPS band (0.96 - 1.61 GHz). This is due to their energy which is mostly stored in the low frequency range. Consequently, the higher order derivatives are preferred as their peak frequency is increased by increasing the derivation order (Fig. 3.2). Accordingly, the fifth order derivative is recommended in [37]. By taking a derivative from the Fourier transform of the n_{th} derivative of the Gaussian pulse (Eq. 3.3) and setting it equal to zero, the frequency peak of the spectrum can easily be calculated from [38]:

$$f_{peak} = \frac{\sqrt{n}}{2\sigma\pi} \quad (3.5)$$

Fig. 3.3 shows the variation of peak frequency based on the pulse shaping factor σ , for the first seven derivatives of the Gaussian pulse. As can be seen, the peak frequency increases

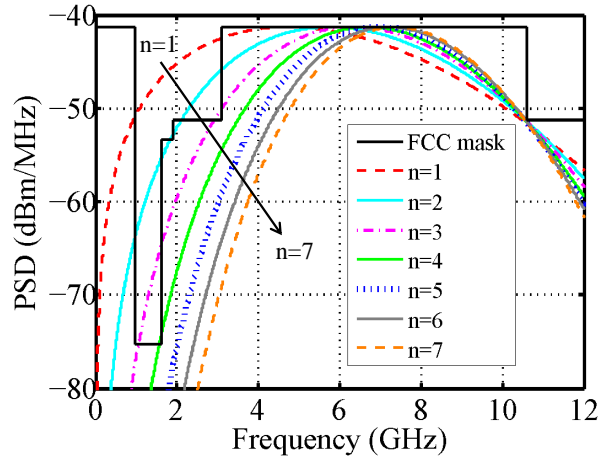


Figure 3.2: PSD of higher order derivatives of Gaussian pulses.

as the pulse shaping factor decreases. From the other side, due to the inverse relationship of the time and bandwidth, as the pulse shaping factor becomes smaller the bandwidth of the signal increases (Fig. 3.4). Hence, as depicted in Fig. 3.3 and 3.4, both peak frequency and the bandwidth of the pulse vary with derivation order and pulse shaping factor. Therefore, in order to comply with the FCC mask and also have the most effective use of it, both the derivation order and the pulse shaping factor should be considered for the pulse shaping [37].

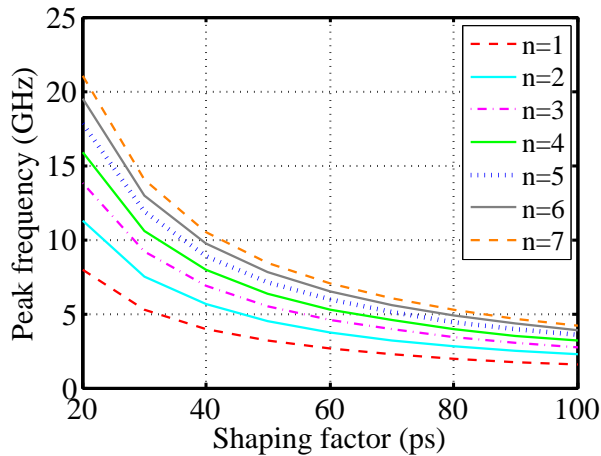


Figure 3.3: Peak frequency versus pulse shaping factor.

The main barrier of UWB communication is the interference with the GPS band. On the other hand, in order to make the IR-UWB preferable for the consumers, some aspects need be considered such as high data rate and low complexity, cost, and power consumption. Consequently, both the FCC-mask and the system requirements must be respected and satisfied. Even though the fifth derivative of the Gaussian pulse is recommended as the best candidate to fulfill the FCC regulation, first order (monocycle) and second order (doublet) Gaussian

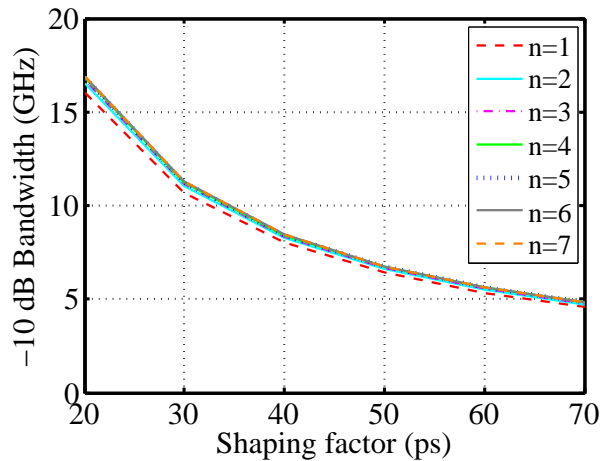


Figure 3.4: Bandwidth versus pulse shaping factor.

derivatives have attracted much attention in microwave photonics research, for the sake of simplicity. Many different methods have been proposed to generate IR-UWB signals optically. However, the most commonly used techniques can be classified into three main categories:

- UWB pulse generation based on phase-modulation to intensity-modulation (PM-IM) conversion.
- UWB pulse generation based on a photonic microwave delay line.
- UWB pulse generation based on optical spectral shaping and frequency-to-time mapping.

The proposed technique in this thesis opens a new scope in IR-UWB photonic generation and adds a new category to the ones named above. The new category is **UWB pulse generation based on frequency-modulation to intensity-modulation (FM-IM) conversion**. In the following sections, the details of the traditional approaches are first reviewed and then the contribution of this thesis to UWBoF is discussed.

3.1.1 Phase modulation to intensity modulation conversion

Monocycle and doublet pulses can be generated by realizing an optical differentiator, which works as a bandpass filter and shapes the input Gaussian pulses. Among all various proposed approaches for implementing an optical differentiator, simple techniques based on PM-IM conversion have been widely studied. PM-IM conversion can be performed by utilizing either a dispersive device (such as SMF fiber) or an optical frequency discriminator [34, 35, 39]. The process of PM-IM conversion is equivalent to bandpass filtering, which shapes the input RF Gaussian pulses to monocycle and doublet pulses. The fundamental principle of the PM-IM conversion technique is fully studied in [34, 35, 39] and the corresponding experimental results of monocycle and doublet pulse generation are demonstrated. For instance, a doublet pulse is obtained in [34, 40, 41], performing PM-IM conversion by employing 25 km SMF fiber as the

3 State of the art

dispersive element with an input of Gaussian pulse with a full-width half maximum (FWHM) of about 63 ps. It is noteworthy to mention that the shape of the generated pulse with this method is highly affected by the length of the SMF, as the transfer function of the system changes by changing the SMF length. Therefore, this approach is not flexible for different applications which need different lengths of fiber. To overcome this problem, using a frequency discriminator as the dispersive element instead of fiber has been proposed. An optical bandpass filter (i.e. fiber Bragg Grating (FBG)) can be used to realize the optical frequency discriminator. As illustrated in Fig. 3.5, UWB pulses with different polarities can be generated by placing the optical carrier at either the left or right slope of the optical bandpass filter [34,39]. Additionally, monocycle and doublet pulses can be generated by employing different portions of the filter transfer function (Fig. 3.5).

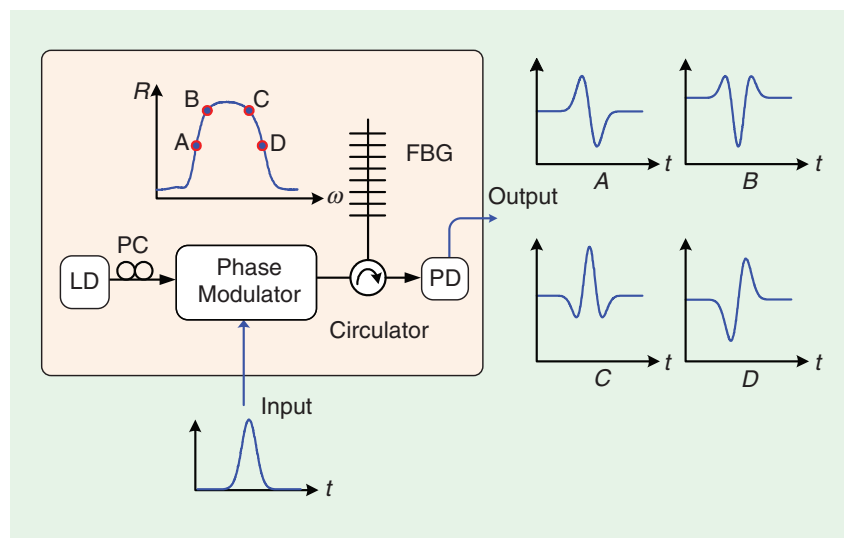


Figure 3.5: UWB pulse generator based on PM-IM conversion (Ref. [35], Fig. 6).

Employing cross-phase modulation (XPM) instead of phase modulation (PM) is another approach for implementing the fundamental principle of the PM-IM method. In this technique, Gaussian pulses are generated all-optically using a femtosecond pulse laser and XPM in a length of nonlinear fiber [40, 42]. In order to achieve the optical XPM, the generated Gaussian pulses are then injected into a length of dispersion-shifted fiber (serving as a non-linear element) together with a continuous-wave probe. FBG can be used as a frequency discriminator to convert the phase-modulated signal carried by the probe to an intensity-modulated signal and generate UWB pulses. More details can be found in [40, 42].

Dong et al. have proposed another alternative technique which is to utilize XPM in a semiconductor optical amplifier (SOA) together with frequency discrimination using an optical bandpass filter [43]. On-chip generation of UWB pulses employing a silicon microring resonator to execute PM-IM conversion is studied in [44]. Although the principle of PM-IM conversion is an attractive approach for carving IR-UWB pulses, it can only generate conventional IR-UWB pulses (monocycle and doublet). As mentioned before, these pulses are not FCC-mask compliant and consequently do not have a high spectral power efficiency. Despite the lack of

flexibility for generating other types of pulses, the complexity and the costs of this approach are relatively less than the techniques described below.

3.1.2 Photonic microwave delay-line filter

IR-UWB pulses can also be generated by using two or three-tap photonic microwave delay-line filters with coefficients of $[1,-1]$ or $[1,-2, 1]$ as shown in Fig. 3.6. As can be seen, this technique requires negative coefficients. In order to avoid optical interference by designing a photonic microwave delay-line filter, the filter needs to work in the incoherent regime using incoherent detection. From the other side, a photonic microwave delay-line filter with incoherent detection usually has only positive coefficients [28]. According to the theory of signal processing, an all-positive-coefficient microwave delay-line filter can only operate as a low-pass filter [28]. To tackle this challenge and achieve bandpass filtering capable of operating in the incoherent regime, huge efforts have been put forth to design and realize photonic microwave delay line filters with negative or complex coefficients [45]. As reported in [46], negative coefficients can be simply implemented by using differential detection.

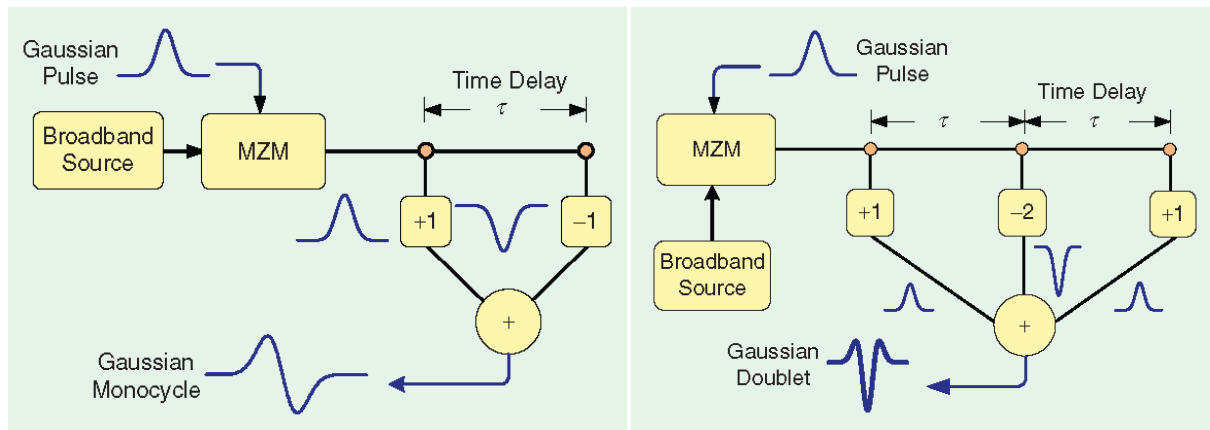


Figure 3.6: Concept of two- or three-tap delay line generation of an IR-UWB pulse (Ref. [35], Fig. 8 and Fig. 11).

The illustrated principle in Fig. 3.6 can be extended for generating n_{th} higher order derivatives by replacing the single wavelength light source with a “ n ”-wavelengths source and employing a $1 \times n$ WDM demultiplexer instead of the 3-dB coupler [45]. It is noteworthy to mention that the negative coefficient in this approach is not generated directly in the optical domain. The fact that “ n ” PDs are necessary for implementing a filter with “ n ” taps, makes the setup complicated and costly. Several techniques have been proposed in order to realize the photonic microwave delay line filter with negative coefficients all-optically. Some of them are briefly explained below:

- Two MZMs that are biased at complementary slopes:
Generating monocycle pulses based on a cascaded Mach-Zehnder modulator (MZM) has been introduced in [47]. By controlling the polarity of the modulators through

3 State of the art

their biasing, and applying proper delay between the modulators, the monocycle pulse with the requested polarity can be generated (Fig. 3.7). Higher order derivatives can be similarly obtained by using a multi laser source, as reported in [48]. In [49], tunable laser sources are replaced by a broadband laser source wavelength which is sliced by utilizing an AWG in order to make the system more cost efficient. Generation of IR-UWB pulses are reported in [50,51] using the same principle, by implementing the intensity modulator based on a Sagnac interferometer containing a traveling-wave phase modulator biased at the nonreciprocal quadrature point.

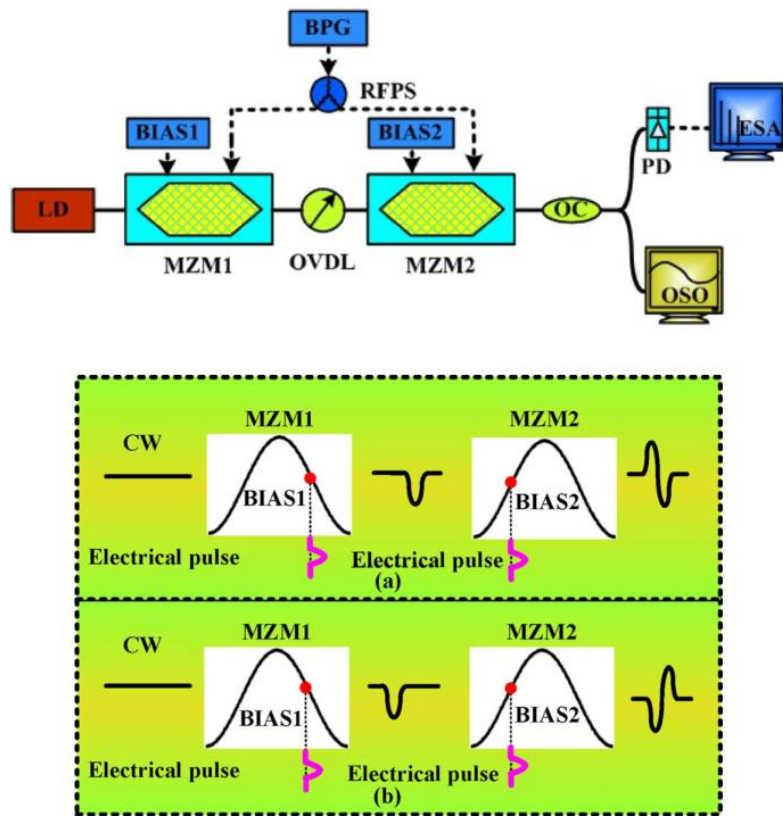


Figure 3.7: Concept of two MZMs biased at complementary slopes (Ref. [47], Fig. 2).

- XGM in nonlinear devices:

Another way to implement the negative coefficient is to take advantage of the cross-gain modulation effect of the SOA. By injecting a high-power pulsed light wave (modulated by a Gaussian pulse) as the pump and lower-power CW light wave as probe into a SOA, a pair of complementary optical pulses can be generated [52]. Due to cross-gain modulation, the power of the probe varies inversely with pump power, which leads to generation of a pair of complementary optical pulses. By applying an appropriate time-delay between the two pulses, a UWB monocycle can be obtained (Fig. 3.8) [34]. Likewise, a doublet pulse can be generated using a three-tap photonic microwave filter

with three coefficients [1, -2, 1] by increasing the number of probe sources to two and applying proper delay [34]. Nevertheless, these techniques are not cost and power efficient, as they require multi-laser sources and high power for cross gain modulation to occur.

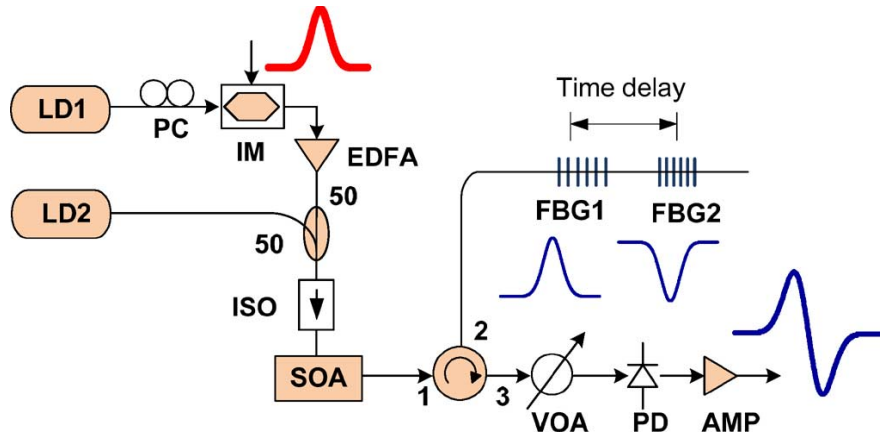


Figure 3.8: UWB monocycle generation based on a two-tap photonic microwave delay-line filter using an SOA (Ref. [34], Fig. 19).

- Cross Polarization modulation (XPolM) in a polarization modulator:
As proposed in [53], monocycle pulses can be obtained using polarization modulation to generate two polarity reversed pulses and utilizing a length of polarization maintaining fiber (PMF) to introduce the appropriate time delay between them (Fig. 3.9). By employing a SOA after the PMF and taking advantage of its gain saturation and recovery principle, doublet pulses can be achieved [54–56]. A switchable optical monocycle and doublet generation has been proposed in [57], using polarization modulation together with balanced detection.

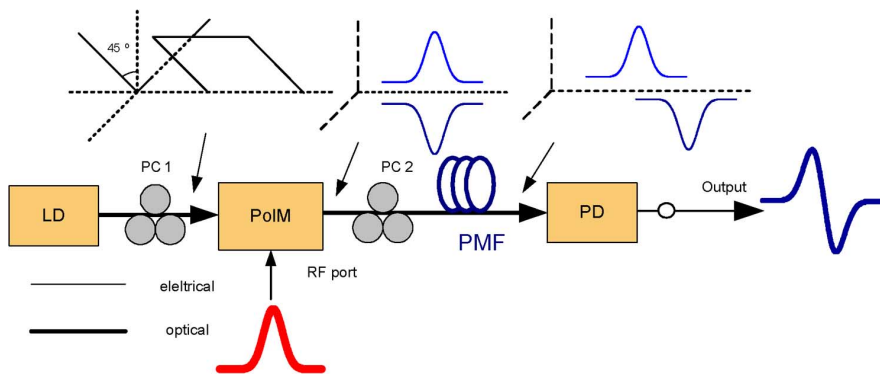


Figure 3.9: UWB monocycle generation using a two-tap microwave delay-line filter based on a PolM. (Ref. [34], Fig. 21).

3.1.3 Spectral pulse shaping and frequency-to-time mapping

Generating the IR-UWB pulses based on optical spectral shaping and frequency-to-time conversion was introduced for the first time by Chou et al. in [58]. They experimentally verified this technique using an optical Fourier transform in free space that made the system bulky and complicated [58]. Afterwards in [59], all-fiber spectral shaping and frequency-to-time conversion to generate the conventional IR-UWB pulses was proposed. The spectrum of a mode-locked fiber laser (MLFL) was carved to a spectral shape corresponding to a monocycle or doublet pulse, using an all-fiber optical spectral shaper. Frequency-to-time conversion was performed by employing a length of SMF as a dispersive medium (Fig. 3.10).

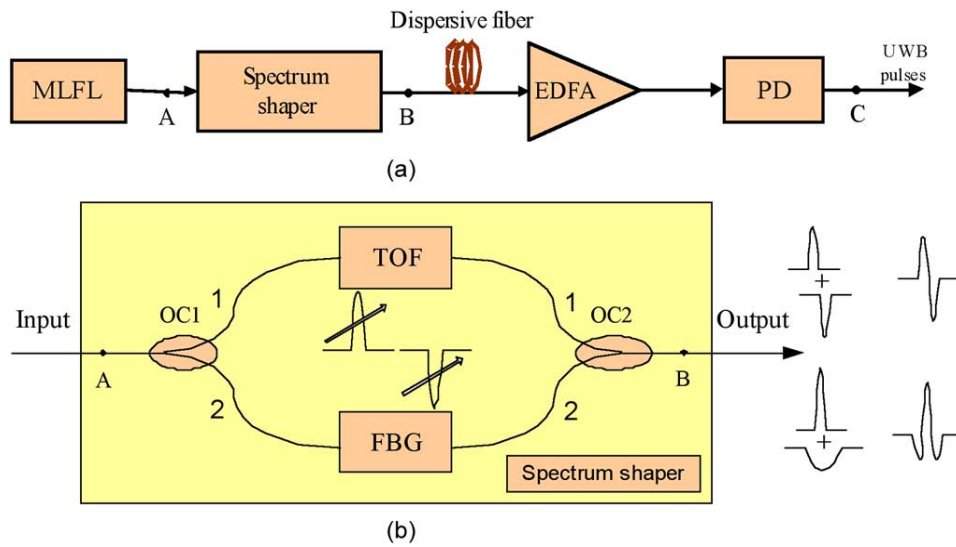


Figure 3.10: (a) Block diagram of the all-fiber UWB signal generation system. (b) All-fiber spectrum shaper configuration. EDFA: erbium-doped fiber amplifier. OC: optical coupler (Ref. [59], Fig. 1).

In [60, 61], a spectral shaper based on FBGs and balanced photodetection is proposed. The transfer function of the FBG in this approach is proportional to the target pulse. Figure 3.11 shows the block diagram of the proposed setup. The required dispersion for the frequency-to-time conversion is provided by a proper length of SMF. Because of the chromatic dispersion (CD) of the optical fiber, generated UWB pulses with these methods suffer from frequency chirp and would be easily distorted. Therefore, dispersion compensation is necessary which makes the system complicated and costly.

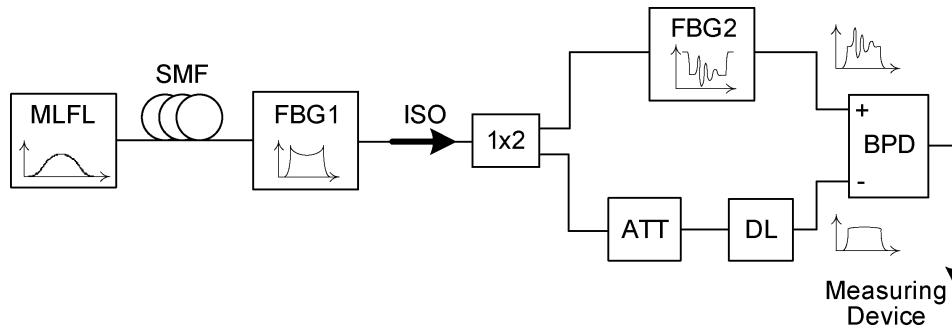


Figure 3.11: Block diagram of the UWB waveform generator (Ref. [61], Fig. 3).

3.2 Contribution of this thesis

As discussed in Sec. 3.1.3, UWB pulses can be generated based on optical spectral shaping and dispersion-induced frequency-to-time mapping. The CD of an optical fiber would strongly affect and distort the corresponding generated UWB pulses, as they suffer from frequency chirp. As a result, the fiber dispersion needs to be compensated and this leads to system complexity and increase in cost. In order to overcome this issue, many different techniques have been proposed to generate UWB signals with zero or small chirp. To do so, external modulators such as the Mach-Zehnder modulator (MZM), polarization modulator (PolM) or optical phase modulator (PM) followed by PM-IM conversion and two- or three-tap photonic microwave delay-line filter with one negative tap coefficient have been utilized as mentioned in Sec. 3.1.1. All aforementioned methods make the system very complicated, bulky and costly.

Meanwhile, other techniques with less complexity have been introduced based on direct modulation of semiconductor lasers [62, 63]. Referring to [62], the monocycle pulses can be achieved by direct modulation of a semiconductor laser and chirp to intensity conversion. As reported in [62], only the transient chirp was used and residual intensity modulation and adiabatic chirp deformed the desired pulse shape, especially when the laser was biased far from threshold. The semiconductor laser was biased near the lasing threshold in [62] and by applying a dark return-to-zero driving pulse, doublet pulses were obtained by employing the overshooting effect.

In this thesis, a very simple and cost efficient method is proposed to generate the UWB pulses based on the direct modulation of a semiconductor laser, optical filtering, and chromatic dispersion in a transmission fiber. The proposed technique opens a new scope in the IR-UWB photonic generation and adds a new category to the traditional ones discussed in Sec. 3.1. The new category is UWB pulse generation based on frequency-modulation to intensity-modulation (FM-IM) conversion. In general, the scope of this thesis is limited to shaping and generation, fiber- and wireless transmission and routing of IR-UWB over fiber.

In this dissertation, the idea of using the direct modulation of a semiconductor laser as a simple and cost efficient UWB transmitter compatible with hybrid PON is developed. First, the generation of the FCC-compliant waveform using direct modulation of the semiconductor lasers is considered. Second, an important issue of the pulse distortion due to the chromatic

dispersion effect in optical fiber is numerically and experimentally investigated. The result is important for adaptability of the transmitter for different accumulative dispersion in different fiber lengths installed in optical access network infrastructure. Third, the proposed transmitter is developed to be completely compatible with TDMA-PON. In this technique, the laser is controlled by a burst signal with different amplitudes for different time slots. Through the proper selection of the burst's amplitudes, NRZ and UWB signals are generated in different time slots by an appropriate chirp of the laser and optical filtering. Via this approach ONUs and RAUs can be supported by a single light source. Fourth, a novel bidirectional UWBoF system, compatible with WDM architecture is presented. In the proposed scheme, a 6th order Gaussian derivative is generated for UWB transmission in a downstream (DS) scenario using a delay-line-interferometer (DLI). While the UWB signal is received from one of the DLI outputs, the other output is utilized to reuse the wavelength by injection locking a colorless Fabry-Perot laser diode (FP-LD). Due to the filtering effect of the FP-LD, a clear optical carrier without intensity modulation is then generated which can be used for upstream (US) baseband (BB) transmission by directly modulating the FP-LD. Fifth, in order to improve the spectral efficiency and optimize the PSD of the signal for the FCC limit, a new modulation scheme is proposed. The concept of this method is based on the position and number of impulses in each symbol time interval. Employing the new modulation technique allows M-ary modulation in the transmitter. Sixth, a replacement for the DFB laser of the transmitter with a tunable MEMS-VCSEL is proposed as a new research opportunity for the future work, which has an extensive wavelength tunability range, smaller footprint, consumes less power, and is cheaper to produce [64]. It makes the whole hybrid PON more reliable and greatly reduces production costs due to the unification of the procurement aspects. The results of this dissertation can be directly applied for commercialization and have the following advantages:

- Generation of NRZ and UWB from only one single light source.
- Simplification and cost reduction of the RAU.
- Compatibility and adaptability of the hybrid PON to the different transmission distances to the ONUs.
- Upgradability and further scalability for future PON systems.

3.3 Summary

As the basis of this dissertation, the IR-UWB was first and fully investigated. A literature review was presented in order to highlight the different techniques and approaches of IR-UWB photonic generation. All introduced methods and techniques were classified into three main categories, namely: PM-IM conversion, photonic microwave delay line and optical spectral shaping. At the end, the scope and contribution of this dissertation to the field of UWBoF was explained by introducing a new scheme based on FM-IM conversion.

Chapter 4

UWB system design

In this chapter, a simple technique is introduced to generate the UWB pulses using direct modulation of a laser and optical filtering. The intensity modulation and the frequency modulation of the directly modulated laser are combined using an optical filter, which performs a photonic electro-optical derivative operation. Gaussian driving pulses are used in order to generate monocycles for ultra-wideband systems.

4.1 Directly modulated semiconductor laser

The optical power and chirping response of the semiconductor laser to the driving current waveform $I(t)$ is determined by means of the large signal rate equations, which describe the interrelationship of the photon density $S(t)$ and carrier density $N(t)$ within the laser cavity:

$$\frac{dN(t)}{dt} = \frac{I(t)}{eV} - \frac{N(t)}{\tau_n} - \frac{g_0(N(t) - N_0)}{1 + \varepsilon S(t)} S(t), \quad (4.1)$$

$$\frac{dS(t)}{dt} = \frac{\Gamma g_0(N(t) - N_0)}{1 + \varepsilon S(t)} S(t) - \frac{S(t)}{\tau_P} + \Gamma \beta \frac{N(t)}{\tau_n}, \quad (4.2)$$

e is the electronic charge, Γ is the mode confinement factor given by the ratio of the active region volume V to the total modal volume, τ_p is the photon lifetime, τ_n is the electron lifetime, g_0 is the gain slope constant, ε is the gain compression factor, N_0 is the carrier density at transparency for which the net gain is zero, and β is the fraction of spontaneous emission coupled into the lasing mode. The output optical power per facet is given by:

$$P = \frac{S(t)V\eta h\nu}{2\Gamma\tau_P}, \quad (4.3)$$

where η is the differential quantum efficiency, h is Planck's constant, and ν is the optical frequency. The small signal analysis of these rate equations can be found in literature works [65–68]. By ignoring the small contribution from the spontaneous emission, the relation between the carrier density change δN and the photon density change δS can be written as follows [68]:

$$(j\omega + \gamma)\delta S = (\tau_P\omega_0^2)\delta N, \quad (4.4)$$

4.1 Directly modulated semiconductor laser

where ω is the modulation frequency, ω_0 and γ are the radial resonance frequency and the damping rate, respectively. The resonance frequency is given by the well-known expression:

$$\omega_0^2 = \sqrt{\frac{g_0 S_0}{\tau_P}}. \quad (4.5)$$

When the laser power is above a few milliwatts, the damping factor is dominated by the nonlinear gain term:

$$\gamma = \frac{\varepsilon S_0}{\tau_P}. \quad (4.6)$$

The chirp (deviation of the optical frequency around the unmodulated frequency) is related to the time derivative of the optical phase by [69]:

$$\delta\nu = \left(\frac{\alpha \Gamma g_0}{4\pi} \right) \delta N, \quad (4.7)$$

α is the linewidth enhancement factor [70]. Combining the Eq. 4.4 and 4.7 gives the following relation between the frequency shift $\delta\nu$ and the photon density change δS :

$$\delta\nu = \left(\frac{\alpha}{4\pi S_0} \right) (j\omega + \gamma) \delta S. \quad (4.8)$$

The first term on the right gives the transient chirp and the second term gives the adiabatic chirp. The transient chirp is proportional to the modulation frequency. The adiabatic chirp is caused by the increase in the carrier density due to nonlinear gain. When the laser bias is far from the threshold, high optical power results in a high damping rate. The frequency shift is dominated by the adiabatic chirp. The FM has the same waveform as the IM, and is advanced in phase compared to the IM. The phase shift between them can be written as:

$$\varphi = \tan^{-1} \left(\frac{\omega}{\gamma} \right). \quad (4.9)$$

As an example, assuming the parameters (Table 4.1) from common high speed DFB lasers [71], the laser output power is about 3.6 mW at a bias current of 60 mA. The damping factor is calculated to be 43.1 s^{-1} . The IM is thus delayed by 22 ps and 15 ps compared to the FM at modulation frequencies of 3 GHz and 10 GHz, respectively.

4 UWB system design

Table 4.1: PARAMETERS FOR 1550 nm DFB LASERS [71]

Active region volume	V	$2e-11 (cm^3)$
Linewidth enhancement factor	α	3.5
Mode confinement factor	Γ	0.2
Gain slope constant	g_0	$1.5e-6 (cm^3 s^{-1})$
Electron lifetime	τ_n	1 ns
Photon lifetime	τ_p	1 ps
Gain compression factor	ε	$1.5e-17 (cm^3)$
Spontaneous emission factor	β	1e-4
Carrier density at transparency	N_0	$1e18 (cm^{-3})$

4.2 Principle of operation

The basic idea of this approach is to use a directly modulated semiconductor laser and optical filtering as a derivative operation, so that the monocycle waveform can be generated with a Gaussian driving pulse. The setup consists of a directly modulated 1550 nm DFB laser and an optical narrow bandpass filter (OBPF), as shown in Fig. 4.1.

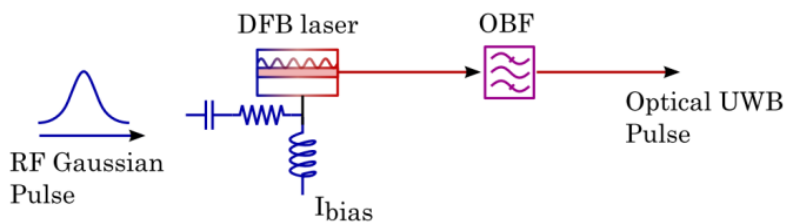


Figure 4.1: Optical UWB signal generation based on direct modulation of semiconductor laser.

When the DFB laser is modulated by an electrical pulse, both intensity and frequency of the laser are modulated (Fig. 4.2.a). The modulated output intensity (related to photon density inside the cavity) is proportional to the driving signal waveform

$$IM(t) = p(t). \quad (4.10)$$

The laser frequency is also modulated due to the carrier density change, including transient chirp and adiabatic chirp. When the laser bias is far from the threshold, the transient chirp can be neglected and the modulated frequency can be written as:

$$FM(t) = \kappa p(t + \tau), \quad (4.11)$$

where κ is the adiabatic chirp coefficient, τ is the delay between intensity modulation (IM) and frequency modulation (FM) of the directly modulated semiconductor laser due to the carrier effect [72]. This delay is inversely proportional to the laser damping factor and was observed

in the literature to be between 15 and 25 ps [73]. The laser output is then sent into an OBPF. The laser spectrum is positioned at the negative slope ($-S$) of the filter which allows negative FM-to-IM conversion (Fig. 4.2.b). At the filter output, the intensity modulation becomes:

$$IM(t) = p(t) - S\kappa p(t + \tau). \quad (4.12)$$

If the filter slope is chosen to be $S = 1/\kappa$ and τ is small enough (about 20 ps) the laser output is thus a negative first derivative of the driving signal waveform:

$$IM(t) = -p'(t). \quad (4.13)$$

The device performs an electro-optical derivative operator which generates monocycle pulses when a Gaussian driving signal is applied (Fig. 4.2.c).

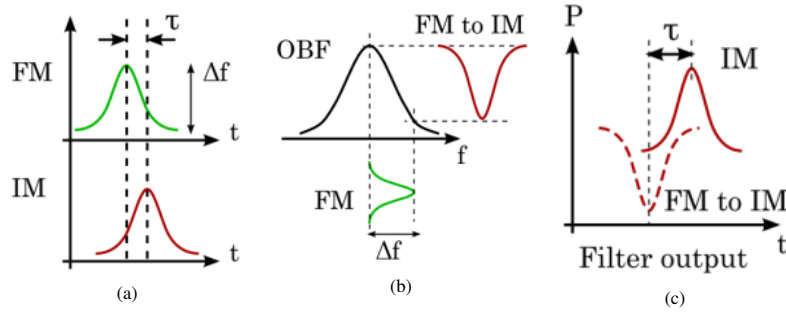


Figure 4.2: (a) Optical FM and IM generated by a directly modulated semiconductor laser, (b) Optical FM-to-IM conversion by the optical band-pass filter, (c) Optical waveform at the filter output. Δf : frequency deviation, $15 \text{ ps} < \tau < 25 \text{ ps}$ (Ref. [74], Fig. 1).

4.2.1 Numerical calculation

Before starting with the experiment and in order to verify the aforementioned theoretical discussion, a simulation is performed. Based on the equations from Sec.4.1 and table 4.1, a 1550 nm DFB laser is modeled in Matlab. The calculated threshold current for the given parameters is 15 mA. An electrical 625 Mbps driving signal is generated at 10 Gbps with a fixed pattern of “1000 0000 0000 0000” (one bit “1” every 16 bits). The bias current and modulation amplitude are set as 45 mA and 35 mA, respectively. A low pass Gaussian filter with a 3 dB bandwidth of 7.5 GHz is modeled to shape the electrical signal into Gaussian pulses with a full width at half maximum of 90 ps. As shown in Fig. 4.1, the DFB laser is then modulated. Fig. 4.3(a) shows the intensity and chirp of the optical signal at the laser output. As can be seen, the FM has the same waveform as the IM and also is advanced in phase, as predicted. The OBPF is modeled as a Gaussian bandpass filter with the order of one and 3-dB bandwidth of 0.06 nm. The OBPF is centered at 1499.997 nm, in order to place the laser spectrum on the negative slope of the filter. Fig. 4.3(b) shows the generated monocycle and the signal chirp.

4 UWB system design

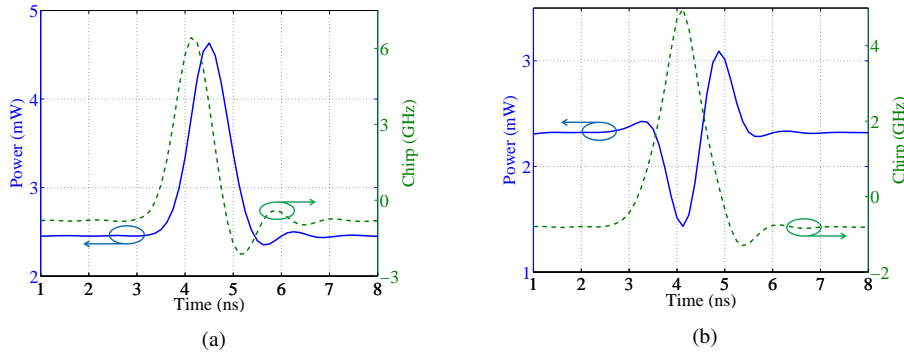


Figure 4.3: (a) Output of the modeled DFB. (b) Output of the modeled OBPF.

4.3 Monocycle generation and wireless propagation

An experiment is performed in order to generate the monocycles based on the concept explained in Sec. 4.2 and study the influences and distortions of wireless propagation through UWB antennas. The experimental setup is depicted in Fig. 4.4. The 625 Mbps driving electrical on-off-keying signal (PRBS $2^7 - 1$) is generated by a pulse pattern generator (PPG) at 10 Gbps with a pattern of “1000 0000 0000 0000” for representing the logical ‘1’ (one ‘1’ bit every 16 bits) and “0000 0000 0000 0000” to represent logical ‘0’. The generated pulses are carved to a Gaussian shape using an electrical lowpass filter with a 3 dB bandwidth of 7.46 GHz.

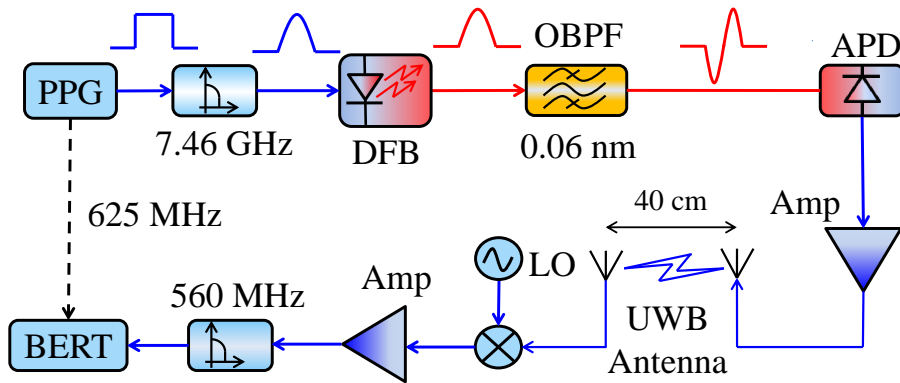


Figure 4.4: Monocycle generation based on FM-IM conversion.

As explained in Sec. 4.2, when the driving signal is applied to the DFB, not only the intensity, but also the optical frequency of the output light is modulated. FM-IM conversion can be achieved by positioning the spectrum of the laser output on the negative slope of an OBPF. The IM and FM are combined and the desired inverse monocycle will be obtained. A commercially available chirped-managed-laser (CML) module consisting of a 10 Gbps direct modulated DFB laser and an integrated optical filter (AZNA DM200-01) is employed in the transmitter for generating the monocycles. The central wavelength, input impedance and

4.3 Monocycle generation and wireless propagation

threshold current of the laser module are 1538 nm, 50 Ω , and 25 mA, respectively and the laser bias current is fixed at 60 mA. The integrated OBPF is a multiple cavity filter with 3 dB bandwidth of 0.06 nm and 10 dB bandwidth of 0.12 nm. The center wavelength of the filter can be tuned by temperature regulation. The generated optical signal is then converted into an electrical signal through an avalanche photodiode (APD) with a 3 dB electrical bandwidth of 9 GHz and amplified using an electrical amplifier with 10 GHz bandwidth. Figure 4.5 shows the generated inverse monocycle and its corresponding power spectral density (PSD) along with FCC mask for indoor transmission. The pulse shape and its electrical spectrum are captured by utilizing an Agilent oscilloscope 86100B and a hp electrical spectrum analyzer 8565E, respectively.

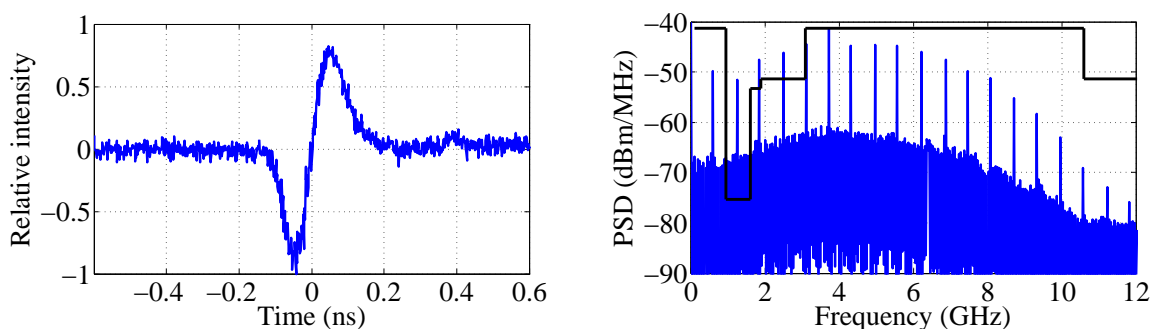


Figure 4.5: Obtained monocycle pulse and corresponding spectrum.

As can be seen in Fig. 4.5, the spectrum of the monocycle does not comply with the FCC mask at the low frequency region. From the other side, indoor wireless systems are designed only for indoor operation and must operate within a fixed indoor infrastructure to avoid any frequency interference. Consequently, it is expected that the UWB antenna removes the unwelcome low frequency components, which leads to reshaping the pulse shape in the time domain. In order to investigate the effect of the UWB antenna on the spectrum and the pulse shape, a pair of spiral antennas are designed and employed for radio transmission. The used antenna and its transfer function (S_{21}) are illustrated in Fig. 4.6. The S_{21} of the antenna is measured by using an Agilent network analyzer E5071C.

Even though the antenna does not completely fit into the FCC mask, it can be seen from Fig. 4.6 that the antenna has highpass filtering behavior and reshapes the spectrum. It is explained in [75] that the antenna transmitting response is related to its receiving response by a temporal derivative. Therefore, the captured waveform in the receiver does not usually resemble the antenna feeding pulse at the transmitter. As reported in [37], because of the derivative aspect of the antenna, output of the transmitter and receiver antennas will be the first and second derivative of input pulse, respectively. As a result, in this experiment, the third order Gaussian like pulse shape is expected after the receiving antenna. The received pulse after wireless transmission and its corresponding PSD along with FCC mask are depicted in Fig. 4.7. The reshaping and the distortion of the received waveform can be explained by considering the spectrum of the monocycle in comparison with the transfer function of the antenna.

4 UWB system design

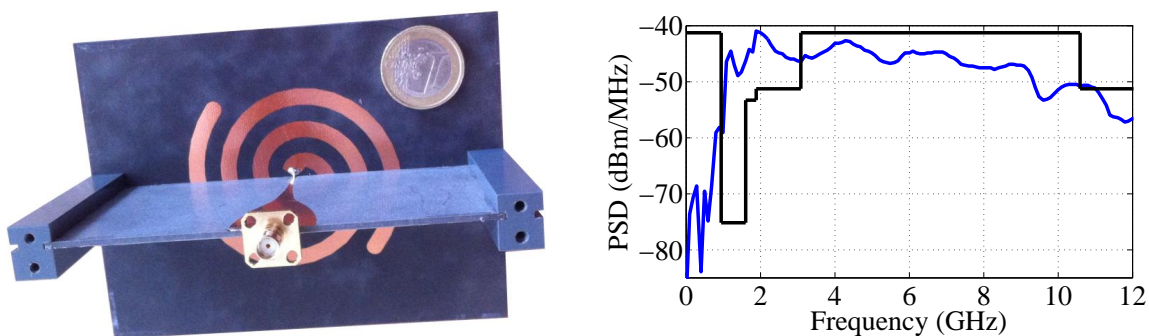


Figure 4.6: UWB spiral antenna and corresponding S_{21} .

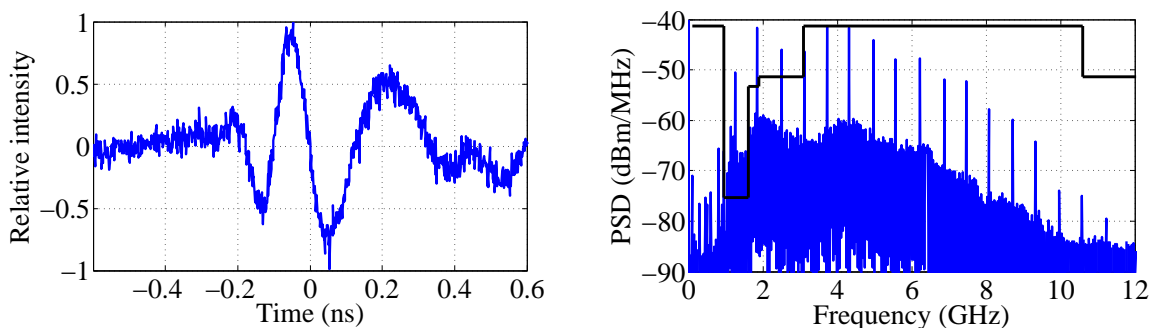


Figure 4.7: Received pulse after wireless transmission and corresponding spectrum.

In order to evaluate the quality of the received waveform in comparison with the transmitted one, Fidelity factor (F) is proposed as [75]. F is the maximum correlation coefficient of two waveforms and indicates the similarity between source pulse $f(t)$ and received pulse $s_R(t)$ and can be calculated from:

$$F = \max_{\tau} \left| \frac{\int_{-\infty}^{+\infty} f(t)s_R(t + \tau)dt}{\sqrt{\int_{-\infty}^{+\infty} f^2(t)dt \int_{-\infty}^{+\infty} s_R^2(t)dt}} \right|. \quad (4.14)$$

F reaches its peak (one), when the two signal waveforms are identical to each other and when they are totally different in shape, the fidelity decreases to the minimum value of zero [75]. Monocycle, doublet and the third order derivative of the Gaussian pulse are generated using matlab and the F between them and the captured waveforms before and after wireless transmission is calculated and presented in Table. 4.2. It can be seen that the captured waveform after radio transmission has the most similarity to the 3_{rd} order derivative of Gaussian pulse, as expected.

4.4 Doublet generation and fiber transmission

Table 4.2: FIDELITY FOR MEASURED AND THEORETICAL WAVEFORMS

	After APD	Monocycle	Doublet	3rd order
After APD	1	0.9643	0.7676	0.8717
After antenna	0.6655	0.6602	0.7098	0.7524

4.3.1 Bit-error-rate measurement

At the receiver, a local oscillator (LO) and an electrical mixer are used to down convert each frequency component of the signal to base band. The base band signal is then amplified using an electrical amplifier with a 3 dB bandwidth of 1 GHz. A lowpass filter with a 3 dB bandwidth of 560 MHz is used to remove the undesired residual high frequency components. Bit-error-rate (BER) is measured at 625 Mbps using a bit-error-rate-tester (BERT) and depicted in Fig. 4.8a. The inset in Fig. 4.8a shows the observed eyediagram of the down converted signal by LO frequency 3.75 GHz when received optical power is -10 dBm. Figure 4.8b shows the received optical power for each spectral component at BER of 10^{-3} . BER and receiver sensitivity show that the spectral components lower than 3.125 GHz and higher than 6.875 GHz are attenuated by the antenna. To avoid distortions and obtain a high fidelity, transfer function of the antenna and the spectrum of source pulse need to match each other and comply with the FCC emission mask to meet the indoor wireless regulation.

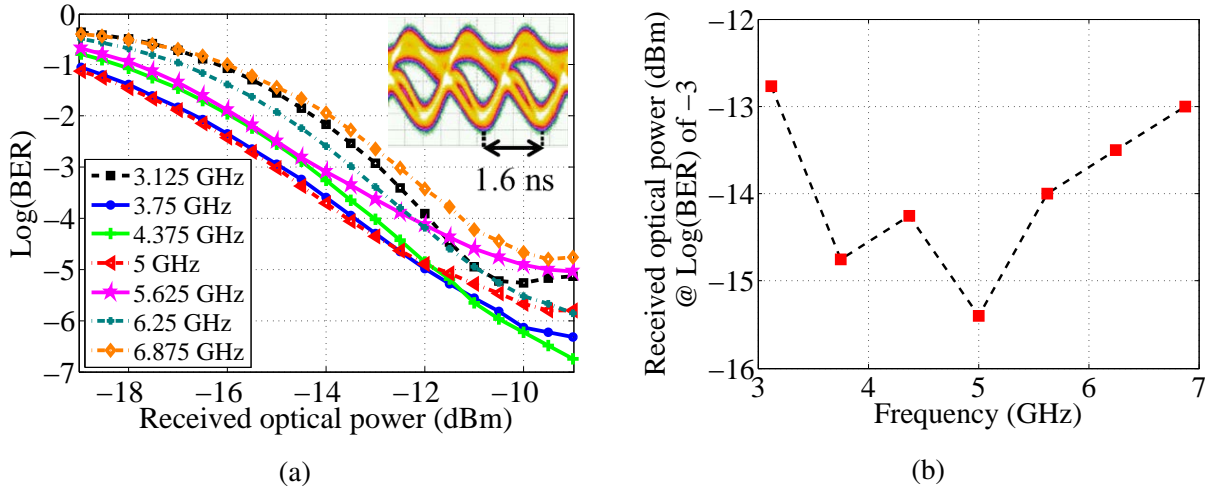


Figure 4.8: (a) Log(BER) vs. received optical power. (b) Receiver sensitivity for different frequency components.

4.4 Doublet generation and fiber transmission

In order to investigate the effect of the chromatic dispersion of SMF on the generated monocycle pulses, the experiment is expanded by adding SMF to the setup in Fig. 4.4. The fiber loss and dispersion are 0.2 dB/km and 17 ps/nm/km at 1538 nm, respectively. The optical

4 UWB system design

power at the fiber input is about 0 dBm and therefore, the influence of the fiber nonlinear effects can be neglected. As the optical pulses are chirped, the intensity waveform is strongly modified by the chromatic dispersion effect in SMF. With a positive frequency shift ('blue chirp'), the group velocity of the pulse is higher compared to the optical carrier. As a consequence, photon energy is transferred from the end to the beginning of the pulse. The experimental setup is schematically depicted in Fig. 4.9. The driving peak-to-peak voltage (V_{pp}) is 1.2 V. As experimentally demonstrated in Sec 4.3, when the driving signal is applied to the DFB, not only the intensity, but also the optical frequency of the light is modulated. FM-to-IM conversion can be performed, by placing the spectrum of laser output on the negative slope of the OBPf, so that IM and FM are combined and the desired inverse monocycle is obtained. As will be explained below, with the use of chromatic dispersion in SMF associated with the laser chirp, doublet pulse can be achieved.

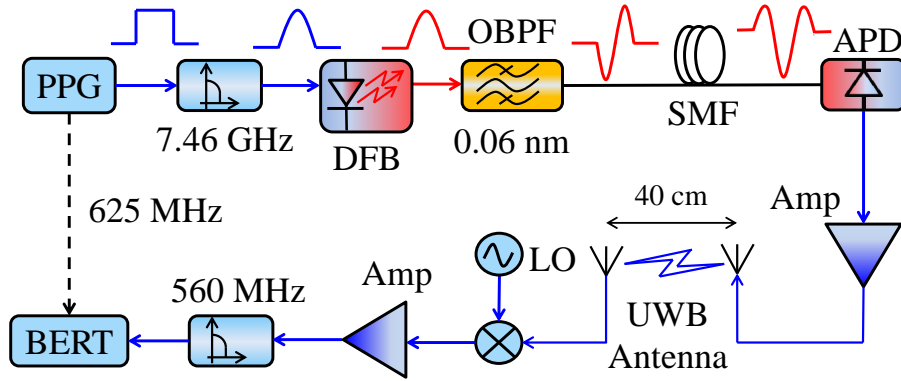


Figure 4.9: Doublet generation using chromatic dispersion in SMF associated with the laser chirp.

In this scenario, the effect of chromatic dispersion on chirped pulses are used to achieve UWB doublets. Therefore, investigating the concepts of a signal complex envelope and the fiber impulse response is necessary in order to study the impact of chromatic dispersion on a chirped signal. The complex envelope of CML output can be mathematically expressed as:

$$E_{CML}(t) = \sqrt{I_{CML}(t)} \exp[j\phi_{CML}(t)], \quad (4.15)$$

where $I_{CML}(t)$ and $\phi_{CML}(t)$ are the intensity and phase, respectively. The phase and chirp of the signal are related as:

$$\phi_{CML}(t) = 2\pi \int_0^t \Delta\nu(t) dt, \quad (4.16)$$

where $\Delta\nu(t)$ is the laser frequency deviation (chirp). The intensity $I_{CML}(t)$ and chirp $\Delta\nu(t)$ can be measured using a time-resolved chirp-measurement technique [76]. $E_{CML}(t)$ can then be achieved through Eq. 4.15 and 4.16. To consider the effect of chromatic dispersion, the fiber impulse response is modeled in form [77]:

$$h_{fiber}(t) = F^{-1} \left(\exp \left[\frac{-j\pi DL\lambda^2 f^2}{c} \right] \right), \quad (4.17)$$

4.4 Doublet generation and fiber transmission

where $D = 17$ ps/nm/km is the fiber dispersion, L is the transmission distance, $\lambda = 1538$ nm is the wavelength, $F^{-1}(\cdot)$ is the inverse Fourier transform operator and c is the speed of light. Fiber attenuation is neglected in Eq. 4.17, as it does not influence the pulse shape. From convolution of the input envelope with fiber impulse response, the output signal complex envelope can be obtained and the output intensity can be calculated as:

$$I_O(t) = |E_{CML}(t) * h_{fiber}(t)|^2. \quad (4.18)$$

The calculated and the experimentally measured pulses after different fiber lengths (0 to 60 km) are compared in Fig. 4.10. The results indicate a good agreement between the measurement and calculation. As the optical pulse is chirped, the chromatic dispersion of SMF modifies the intensity waveform. With a positive frequency chirp, the group velocity of the pulse is higher than the one of the optical carrier and photon energy is transferred from the end to the beginning of the pulse.

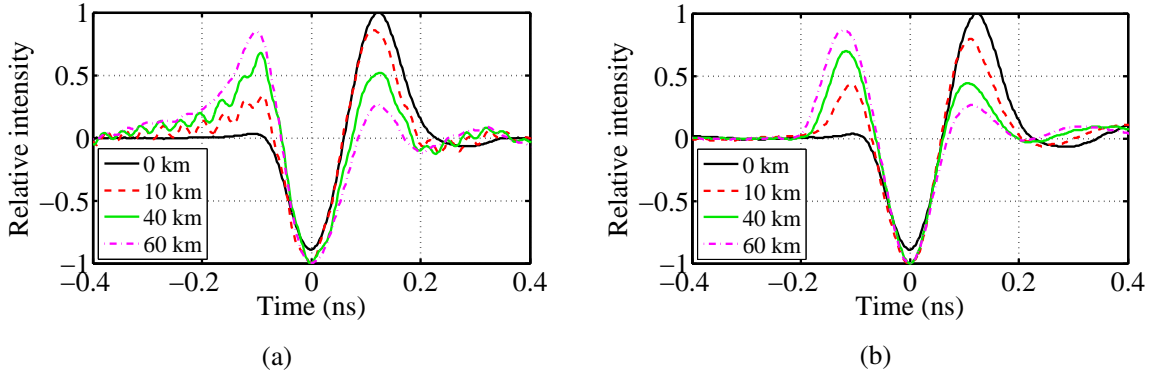


Figure 4.10: Obtained pulse shapes at different fiber lengths. (a) Calculation. (b) Experiment.

Based on this configuration, the doublet pulse is generated after 25 km Fig. 4.11. However, in optical access network infrastructure, different fiber lengths are installed. From the other side, in order to generate the doublet pulses, a specific amount of dispersion is required. As a result, dispersion management seems to be necessary which makes the proposed system complex and expensive [78]. To overcome this problem, a straightforward solution is proposed [78, 79]. The accumulative dispersion in the SMF can be calculated as:

$$CD = D_{ps/nm/km} \cdot L_{km} \cdot \Delta\lambda_{nm}, \quad (4.19)$$

where D and L are dispersion factor and length of fiber, respectively, and $\Delta\lambda$ corresponds to the signal spectrum width. As D is fixed, to keep the CD the same for different lengths of L , $\Delta\lambda$ has to be modified accordingly. It is well known that, the signal spectrum width $\Delta\lambda$ is directly related to the laser chirp. By varying the laser operation point, e.g. modulation amplitude (V_{pp} peak-to-peak voltage) or laser bias current, the amount of the frequency chirp can be changed, which leads to the spectral width modification. The chirp variation versus the applied V_{pp} is measured based on a time-resolved chirp-measurement technique and presented in Fig. 4.12a. As can be seen, the signal chirp and the applied V_{pp} are linearly proportional.

4 UWB system design

For different driving voltages ($V_{pp} = 0.7$ and 1.2 V), the monocycle pulses are generated at the output of the CML and transmitted through different lengths of SMF. The obtained pulse shapes after the fiber transmission are compared to the theoretical doublet pulse via fidelity factor (F) using Matlab and shown in Fig. 4.12b. It can be seen from Fig. 4.12a that the chirp increases by increasing the V_{pp} . Consequently, in order to achieve a high fidelity, a shorter length of SMF is required. According to Fig. 4.12b and considering the $F = 0.95$ as the minimum acceptable fidelity, the transmitter can be adjusted for a transmission distance from 19 km to 57 km by varying the V_{pp} from 1.2 V to 0.5 V. Signal-to-noise-ratio (SNR) is the limiting factor for achieving a longer transmission length and a shorter one is limited by the maximum allowed driving voltage to the laser ($V_{pp} = 1.3$ V). Nevertheless, this region fulfills the standards of gigabit-capable passive optical networks (GPON) systems [ITU-T G.984.2]. The SMF can be replaced by a variable FBG as the dispersive media for the applications requiring a shorter coverage area.

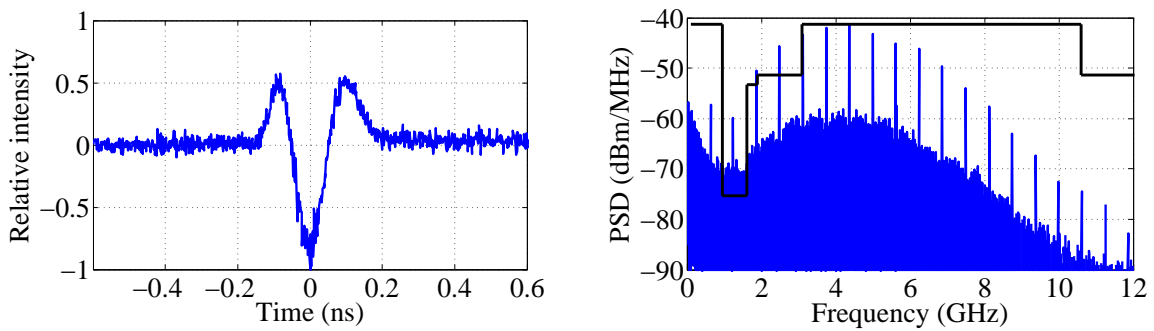


Figure 4.11: Obtained doublet pulse and corresponding spectrum after 25 km fiber transmission.

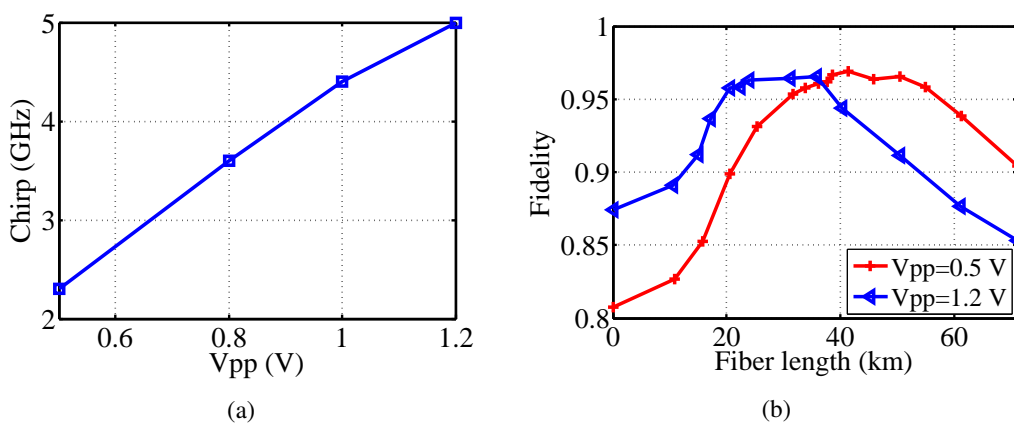


Figure 4.12: (a) Chirp measurement. (b) Fidelity vs. fiber length.

4.4.1 Bit-error-rate measurement

By setting the $V_{pp} = 0.85$ V, the doublet pulse is generated after 25 km of SMF, as shown in Fig. 4.11. Wireless transmission is then performed by employing the UWB antennas mentioned in Sec. 4.3. Fig. 4.13 shows the received waveform and the corresponding spectrum.

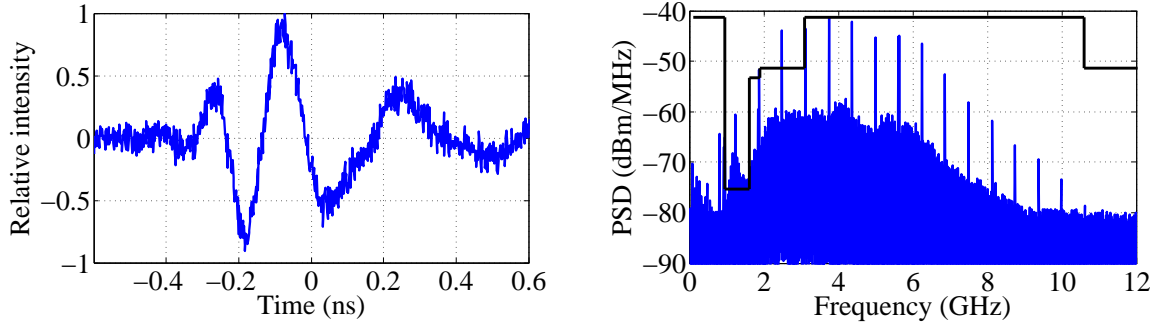


Figure 4.13: Received pulse after wireless transmission and corresponding spectrum.

After the wireless transmission, the received signal is down-converted to the baseband and amplified for BER measurement, in the same way as explained in Sec. 4.3.1. BER versus received optical power for each frequency component is illustrated in Fig. 4.14a. The received optical power for $BER = 10^{-4}$ for each spectral component is extracted and shown in Fig. 4.14b for fiber lengths of 15, 20, 25, 35 and 45 km, when V_{pp} is set to 1.3, 1.2, 0.85, 0.7 and 0.65 V, respectively. As can be seen, at higher fiber lengths, because of the low SNR of low-power frequency components (35 and 40 km), BER can be measured in a narrower range.

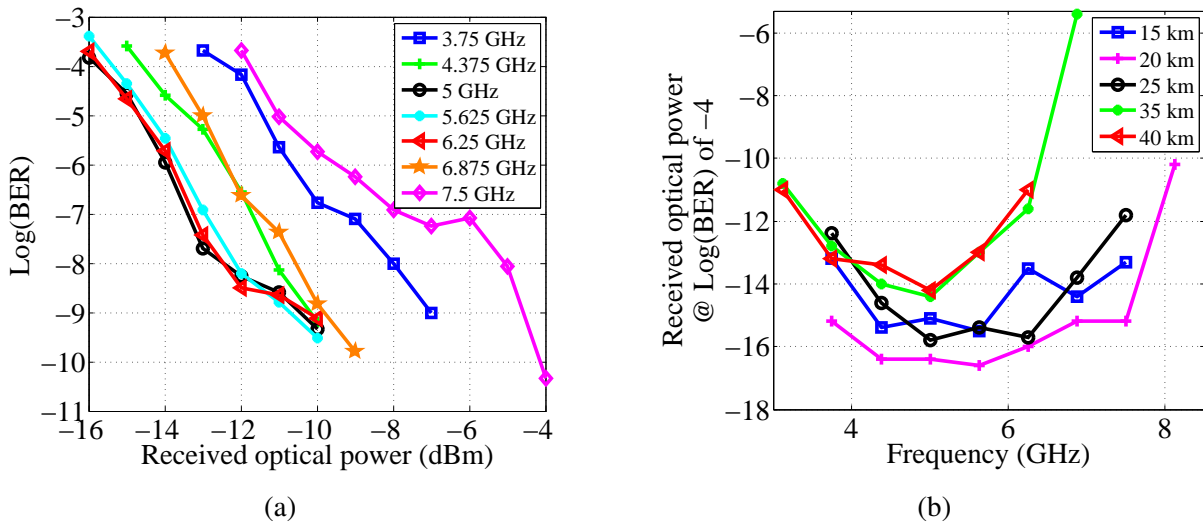


Figure 4.14: (a) Log(BER) vs. received optical power. (b) Receiver sensitivity for different lengths of fiber.

4.5 Summary

The theoretical background of the directly modulated semiconductor laser was provided. The principle of operation was explained through the basics of intensity modulation and frequency modulation of a directly modulated laser and performing a derivative operation after FM-to-IM conversion in an optical filter. Monocycle pulse generation was experimentally demonstrated, wireless transmission was performed and BER was measured. By taking advantage of the impact of the fiber chromatic dispersion on a chirped signal, the doublet pulses were experimentally generated after fiber transmission. The adaptability of the transmitter to the different lengths of the transmission fiber was numerically analyzed and experimentally proved. Fidelity factor results proved that when the transmission distance increases from 19 km to 57 km, doublet pulse can be achieved with a fidelity of at least 0.95, if the laser modulation amplitude is decreased from 1.2 V to 0.5 V. Finally, the wireless transmission of generated doublet pulses was performed, the BER measurement was executed and error free transmission was successfully shown. The presented work and results of this chapter are published in **IEEE** [74, 78–80] and **CLEO** [78].

Chapter 5

Integration to TDM-PON

In this chapter, the compatibility of the proposed technique in Chapter 4 with the time division multiplexing-passive optical network (TDM-PON) architecture is investigated. A novel and cost-efficient technique is introduced to generate UWB and non-return-to-zero (NRZ) signals in different time slots of TDM-PON by utilizing a single chirped controlled semiconductor laser associated with an optical bandpass filter. In this approach, the chirp of the laser is controlled by different bias burst amplitudes (BBA) for different time slots. Through the proper selection of the burst amplitudes, 10 Gbps NRZ and 1.25 Gbps UWB signals are generated in different time slots.

5.1 TDM-PON

By using a commercially available so-called chirped-managed-laser (CML) package, consisting of a distributed feedback (DFB) laser and an optical bandpass filter (OBPF), a very simple and cost efficient technique for generating the IR-UWB pulses was experimentally demonstrated in Chapter 4. From the other side, the main feature of CML is its large tolerance to fiber dispersion. CML can reach over 200 km in SMF at 10 Gbps without dispersion compensation, while the reach of external modulators are typically limited to 80 km. Employing the chirp of the directly modulated laser (DML) is the key point in CML for such an outstanding reach extension. The continuous phase shift of the optical carrier in association with the adiabatic chirp of the DML upon modulation together and the spectral reshaping performance of the OBPF establish a phase rule; in which, '1' bits separated by any odd number of '0' bits are π out of phase. This increases dispersion tolerance by the destructive interference of the energy in the bits that are leaving their time slots to spill into adjacent time slots. For instance, consider a "1 0 1" bit sequence from a DML. As this signal travels through the SMF, dispersion spreads the energy of the '1' bits into adjacent '0' bits. Consequently, the constructive interference between the '1' bits introduces errors in the '0' bits leading to a closed eye diagram. For the same "1 0 1" bit sequence in CML, the '1' bits have higher optical frequency than the '0' bits by $1/2$ of the bit rate ($\Delta\nu(0 \leftrightarrow 1) = \frac{1}{2T}$). This causes the phase of the output light to slip by π , making the second '1' bit π out of phase with the first '1' bit. This phase shift is the key for maintaining a clean '0' bit. The energy of the '1' bits still spreads into the middle '0' but due to

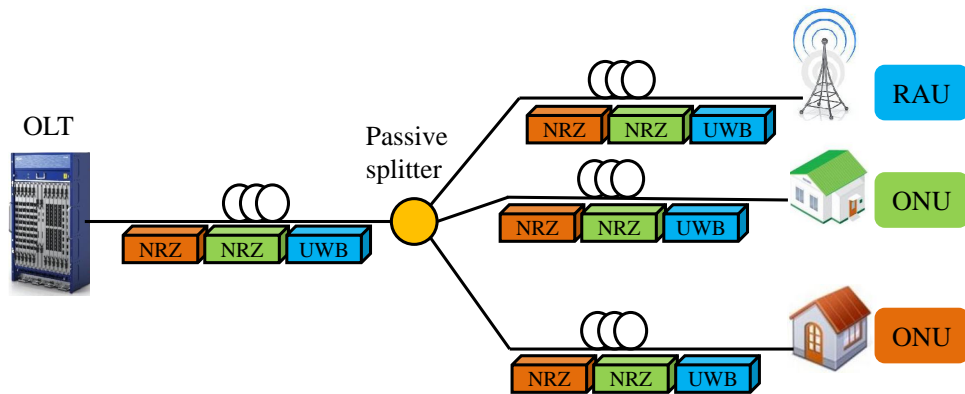


Figure 5.1: Downstream TDM-PON traffic.

the destructive interference, the eye remains open after more than 200 km of transmission [81].

Fixed fiber deployments for fiber to the home (FTTH) services are growing based on PON technology. Gigabit PON and Ethernet PON are both based on TDM architecture and provide services to N users, using passive 1: N power splitters with an aggregate bit rate [ITU-T G.984.2]. In the downstream TDM scenario, the optical line terminal (OLT) dedicates individual time slots to each subscriber. As depicted in Fig. 5.1, the optical network units (ONU) and radio antenna units (RAU) receive their own data through the address labels embedded in the signal and ignore the other time slots. To reduce the overall cost of the system, it is desirable to investigate the compatibility of the proposed system in Chapter 4 with the TDM-PON.

As explained, both NRZ and UWB signals can be generated by a single CML module. However, to generate the UWB signal, the signal spectrum should be placed on the filter's negative slope [79], whereas in the case of NRZ generation, the signal spectrum should be placed on the filter's positive slope [81]. A novel technique is proposed in this chapter to generate the NRZ and UWB signals from a single CML module in a TDM-PON system to reduce the cost and complexity of the transmitter. In this approach the laser operation point in each time slot of the TDM structure is controlled through the different bias burst amplitudes (BBA) at different time slots. In this way, the chirp of the laser is controlled and the spectrum of the optical signal is placed in the required position according to the central wavelength of the optical filter, to generate either a NRZ or UWB signal.

5.1.1 Chirp analysis of CML

The proposed technique takes advantage of the chirp of the DFB laser, therefore an analysis of laser chirp behavior has been performed below. The frequency deviation in a semiconductor laser is mainly due to three mechanisms [82]:

1. Transient chirp, associated with the relaxation oscillation.
2. Adiabatic chirp, introduced by the effect of the injection current on the refractive index of the cavity.

3. Thermal chirp, where the temperature affects both the refractive index and cavity length.

The thermal effect is the dominant mechanism in the low frequency region. In this region, the frequency deviation is almost independent of the bias current, but a large frequency deviation is caused by a temperature change induced by the modulation current [72]. The frequency deviation in the low frequency region is proportional to the temperature modulation in an active layer negatively ($-\Delta T(t)$) and subsequently to $-i(t)$ [72]. As a result, the FM and IM are expected to be out of phase in this region. The frequency chirp at frequencies higher than 10 MHz is governed by the carrier effect and can be expressed as:

$$\Delta\nu(t) = \frac{1}{2\pi} \frac{d\phi(t)}{dt} = \frac{\alpha}{4\pi} \left(\kappa P(t) + \frac{1}{P(t)} \frac{dP(t)}{dt} \right), \quad (5.1)$$

where $P(t)$ and $\phi(t)$ are the instantaneous optical power and phase, respectively. α is the linewidth enhance factor and κ is the adiabatic chirp coefficient. The first term in Eq. 5.1 stands for the adiabatic chirp. The second term denotes the transient chirp and can be neglected when the laser is biased far from the threshold. Therefore, Eq. 5.1 can be simplified as:

$$\Delta\nu(t) = \frac{\alpha}{4\pi} \kappa P(t). \quad (5.2)$$

Since $P(t)$ is proportional to the laser driving current $I(t)$, the frequency deviation is also directly proportional to $I(t)$. The chirp variation of the DFB laser versus modulation amplitude is reported in [72, 79]. In order to implement a TDM-PON compatible transmitter which can generate UWB and NRZ signals in different time slots of the TDM architecture, using the laser chirp in different modulation frequency regions is proposed here. In Chapter 4, the laser was directly modulated at 10 GHz in continuous-mode so the UWB pulses can be generated by using the adiabatic chirp in the high frequency region. In this chapter, the laser is modulated at a low frequency, in order to employ the thermal chirp in the low frequency region for establishing the TDM burst mode. Therefore, a chirp measurement of the CML has been performed to find a frequency with the sufficient chirp in the low frequency region. The central wavelength, input impedance and threshold current of the laser module are 1538 nm, 50 Ω and 15 mA, respectively. The laser bias current is set to 40 mA. The integrated OBPF is a multiple cavity filter with 3-dB bandwidth of 0.06 nm and 10-dB bandwidth of 0.12 nm. The laser is driven by a sinusoidal electrical signal at different frequencies. The filter of the CML is tuned by temperature regulation for each frequency so that the maximum eye diagram opening is obtained at the CML output. The chirp and the phase difference between FM and IM are measured by using the time-resolved chirp-measurement technique [76] and the results are presented in Fig. 5.2.

At frequencies around 1 kHz, a thermal chirp of 5 GHz/mA is recorded. As can be seen, in this region the phase difference between FM and IM is close to 180°. This confirms the negative sign in the theoretical discussion above on the relation between the thermal chirp and the modulation current. As expected for a 10 Gbps CML [81] and due to the adiabatic effect, the laser chirp in the high frequency region is about 5 GHz/mA. The phase difference in this region is close to 30°, which refers to the delay (τ) between IM and FM in Fig. 4.2. The thermal and adiabatic effects cancel each other out in the middle region which leads to a decrease in

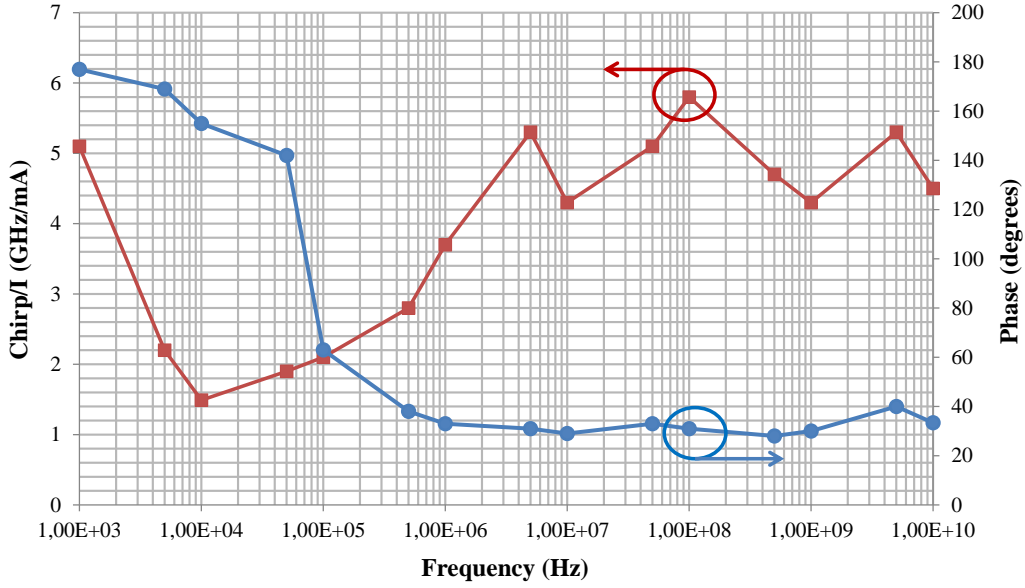


Figure 5.2: Chirp versus modulation frequency.

chirp. All in all, based on the theoretical discussion and the experimental measurement, it is expected that the chirp follows the intensity at high frequencies with a time delay τ and in the low frequency region, be 180° out of phase.

As mentioned in Sec. 5.1, the signal's spectrum should be placed on positive and negative filter slopes, in order to generate the NRZ and UWB signals, respectively. To do so, the burst frequency is chosen as 1 kHz, as the chirp at this frequency is sufficient to move the signal spectrum between the positive and negative slopes of the OBPF.

The key point of this technique is to generate different signal formats (NRZ and UWB) by changing the BBA without moving the central wavelength of the OBPF. A trial is organized to test this idea in the continuous-mode before moving to the main experiment. The laser bias current, laser temperature and filter temperature are set to 25 mA, 20°C and 41°C , respectively. First, an electrical NRZ signal with 0 mA dc-offset and modulation current of $i_{pp}=20$ mA ($v_{pp}=1$ V) is sent to the laser. The dc-offset is increased to change the laser operation point and consequently the frequency deviation, in order to place the optical spectrum of the laser on proper location with respect to the position of the filter. Best optical eye diagram is observed for $I_{dc-offset}=14.6$ mA ($V_{dc-offset}=0.73$ V). The experiment is repeated for UWB signal and $I_{dc-offset}=34$ mA ($V_{dc-offset}=1.7$ V) is recorded at the point of the best quality of the eye diagram. These levels are helpful for finding the appropriate intensity of the BBA in each time slot. This test was performed in continuous-mode and high frequency, where adiabatic chirp dominates. In this region, the frequency deviation is proportional to the laser operation point (Eq. 5.2). Therefore, a lower laser operation point was reported to place the signal spectrum on the positive slope of the filter (lower frequency) to generate the NRZ signal; a higher laser operation point was reported to place the spectrum on the negative one (higher frequency) to generate the UWB signal.

In the burst mode, the laser works at low frequencies (1 kHz), and regarding the theoretical analysis above and Fig. 5.2, the lower laser operation point in this region leads to a higher thermal chirp and vice versa. Figure. 5.3 explains this schematically. The NRZ and UWB signals are added to the time slots with the higher and lower intensity levels, respectively. From the other side, burst frequency is chosen around 1 kHz and therefore, the higher the driving current the lower the thermal chirp. As a result, the spectrum of the NRZ and UWB signals would be at lower frequency (positive filter slope) and higher frequency (negative filter slope), respectively.

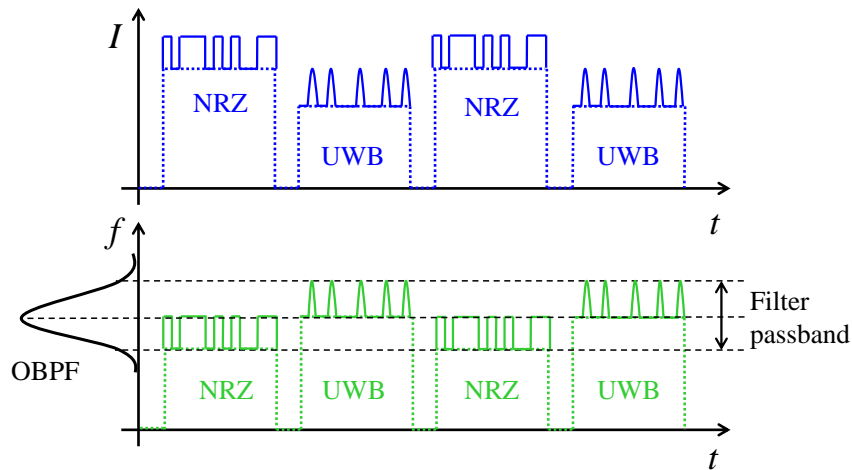


Figure 5.3: Semiconductor laser chirp behavior in burst mode.

5.2 Experimental setup and results

5.2.1 Burst mode

In order to investigate the effect of the thermal chirp on the signal quality, 1.25 Gbps UWB and 10 Gbps NRZ signals are separately generated in the burst mode. The same transmitter setup is used to perform both experiments (Fig. 5.4). For emulating the burst mode, a 10 Gbps PPG is programmed in the alternate (ALTN) mode. For the first experiment, ALTN-A contains a 1.25 Gbps coded electrical on-off-keying signal (PRBS $2^7 - 1$) generated by PPG at 10 Gbps and ALTN-B is all zeros. From the coding, a logical '1' is represented by "1000 0000" (one '1' bit every 8 bits), and a logical '0' is represented by "0000 0000". Simultaneously, a burst signal is generated by an arbitrary waveform generator (AWG) with an intensity of $i_{pp} = 20$ mA ($v_{pp} = 1$ V) at 1 kHz (Fig. 5.5). The duration of the high level time slot is 0.45 ms. The PPG and AWG are so synchronized that when PPG is in ALTN-A mode, the burst signal has a high level and when PPG is in ALTN-B mode, the amplitude of the burst signal is low. By employing an electrical coupler, the data and burst signals are then added together. An electrical low pass filter (LPF) with a bandwidth of 7.46 GHz is used to carve the electrical pulses into the Gaussian shape. The laser bias current and laser temperature are set to 20 mA, 20°C , respectively. The

filter temperature is tuned to 33.4°C , to generate the monocycle. The generated optical signal at the output of the transmitter is shown in Fig. 5.6(a). In the second experiment the ALTN-A is a 10 Gbps NRZ (PRBS $2^7 - 1$). To have the largest open eye diagram, filter temperature is set to 38.5°C . Figure. 5.6(b) shows the optical NRZ signal at the output of the transmitter.

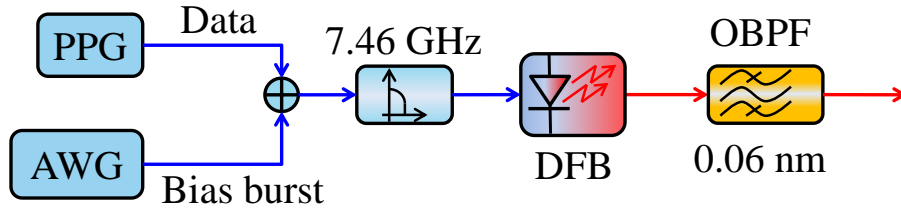


Figure 5.4: Common transmitter for NRZ and UWB generation.

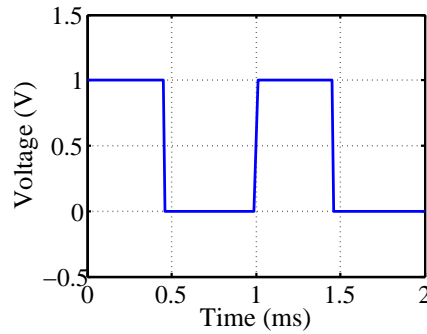


Figure 5.5: Bias burst signal.

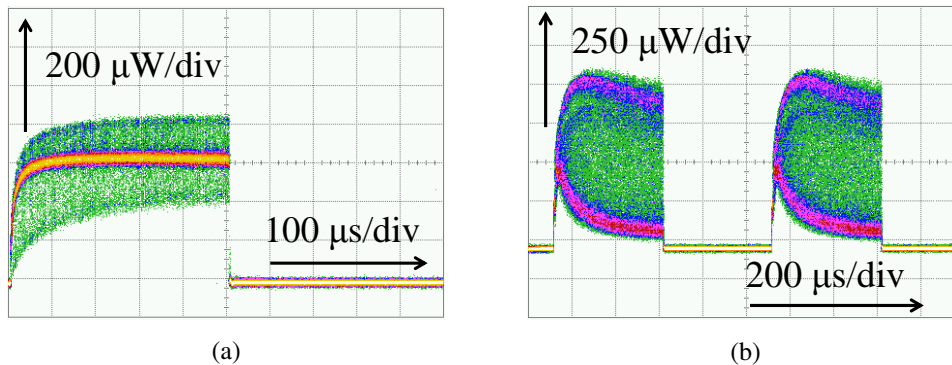


Figure 5.6: Transmitter output, (a) UWB and (b) NRZ.

For both experiments a common transmitter is used but in the receiver side two different receivers have to be implemented (Fig. 5.7). In both receivers, the BERT has to work in burst mode, in order to receive only the data and be off in the zero time slots. Therefore, an electrical

5 Integration to TDM-PON

signal is generated using a second AWG at 1 kHz to gate the BERT (Fig. 5.8); so the BER is measured, only when the gating signal is at the high level. As depicted in Fig. 5.9(a), the optical signal in the NRZ receiver is converted to the electrical one by employing an APD. As shown in Fig. 5.7(b), the UWB receiver is very similar to the one used earlier in Sec. 4.3. Figure. 5.9(b) shows the converted signal after APD. The electrical signal is then amplified and wireless transmission is performed utilizing the same UWB planar spiral antennas introduced in Sec. 4.3. A local oscillator is used to down-convert the signal. After the amplification, a low-pass filter with a 3-dB bandwidth of 1 GHz is used to remove residual high frequency components. It can be seen from Fig. 5.9(a) and 5.9(b) that the slow thermal chirp of the laser causes an undesired long rise time, which leads to the degradation of the eye diagram. Consequently, in order to obtain an open eye diagram, some portion of the data at the beginning of each time slot must be omitted. Therefore, the duration of the high level time slot of the gate control signal is chosen as 0.4 ms (Fig. 5.8), while the duration of the high level time slot of the burst signal in Fig. 5.5 is 0.45 ms. The black dashed lines in Fig. 5.9(a) and 5.9(b) show how the received data is gated. BER and the eye diagram of the received signals are depicted in Fig. 5.10.

It is important to note that it is also possible to speed up the burst response by operating the laser at higher burst frequencies. The key point is the chirp of the laser, which should be enough to shift the spectrum from one slope of the filter to the other one. As mentioned earlier, the amount of the required chirp is about 5 GHz. Referring to Fig. 5.2, the burst frequency is chosen as 1 kHz and therefore the thermal chirp is dominant which makes the burst response slow. By choosing a burst frequency higher than 10 MHz, which also causes a sufficient amount of chirp (e.g. 50 MHz in Fig. 5.2), the adiabatic chirp will be dominant, leading to a fast burst response. However, it has to be taken into account that these frequencies are higher than 10 MHz and as explained (Eq. 5.2), in this region the chirp is directly proportional to the applying current; therefore BBAs should be chosen carefully. For instance, since the burst frequency is 1 kHz in Fig. 5.3, the BBA of the NRZ is higher than the BBA of the UWB, in order to place the spectrum on the right position. But if we choose 50 MHz as the burst frequency, it should be vice versa.

As demonstrated, NRZ and UWB can be generated in the burst mode. NRZ and UWB sequences were added to the burst signal and applied to the laser. The filter position was adjusted in each case by thermal regulation to have the largest eye opening. In the receiver, some portion of the data was gated out to achieve an open eye diagram. These techniques can be considered for the PON upstream scenario. In the downstream scenario, both signals must be generated in the same burst signal. In this case, the filter position cannot be shifted for each time slot.

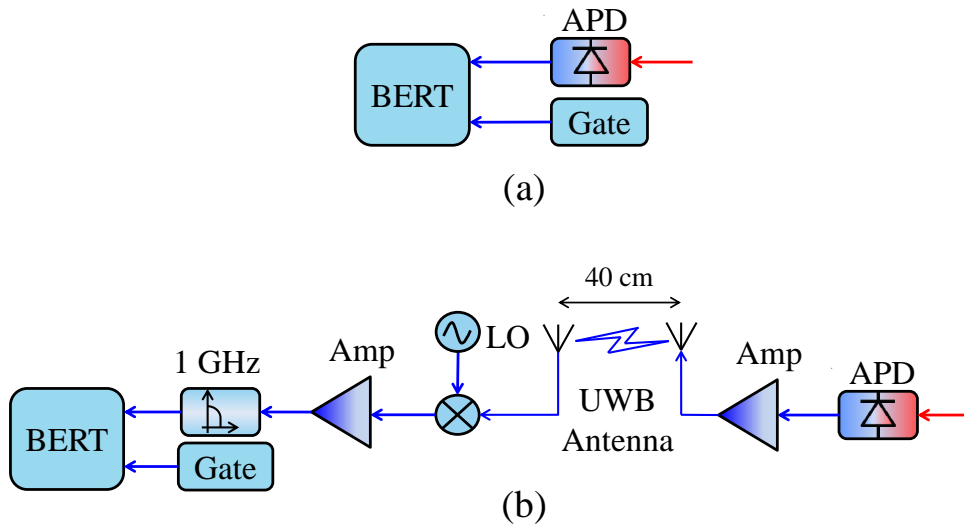


Figure 5.7: Receivers (a) NRZ and (b) UWB.

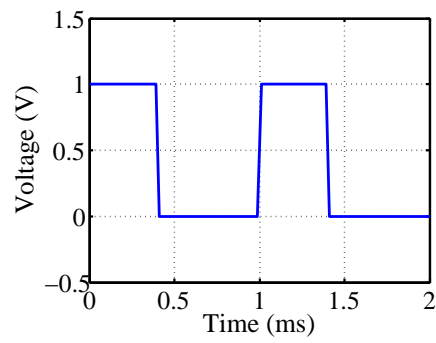


Figure 5.8: Gate control signal.

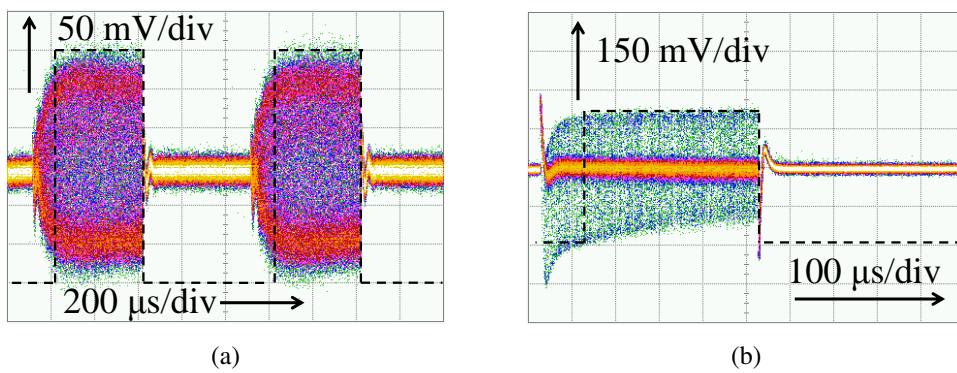


Figure 5.9: (a) Detected NRZ after APD. (b) Detected UWB after APD.

5 Integration to TDM-PON

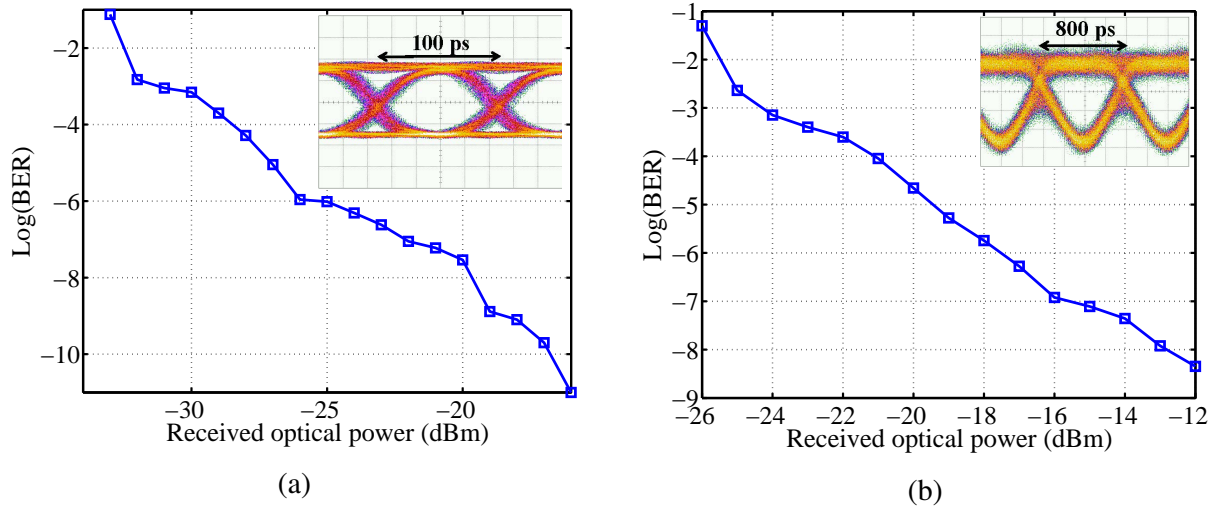


Figure 5.10: Log(BER) vs. received optical power in upstream scenario (a) 10 Gbps NRZ, (b) 1.25 Gbps UWB.

5.2.2 Downstream PON

As mentioned in Subsec. 5.2.1 it is not possible to move the filter position in different time slots of a burst signal in downstream. Instead, it is proposed here to keep the central wavelength of the OBPF fixed and adjust the position of the signal spectrum by controlling the BBA and subsequently, the chirp of the laser. The transmitter setup is the same as Fig. 5.4 but the difference is that this time both ALT-A and ALT-B contain data at the same time. ALT-N-A contains a 10 Gbps NRZ (PRBS $2^7 - 1$) and ALT-N-B is a 1.25 Gbps coded electrical on-off-keying signal (PRBS $2^7 - 1$) generated by PPG at 10 Gbps. This time, the burst signal is generated from AWG with two different intensity levels for NRZ and UWB signals at 1 kHz. When PPG generates NRZ, the burst signal has an amplitude of $i_{pp}=34$ mA ($v_{pp}=1.7$ V) and when PPG generates the coded on-off-keying, the amplitude of the burst signal is $i_{pp}=14.6$ mA ($v_{pp}=0.73$ V). By employing an electrical coupler, the data and burst signals are then added together (Fig. 5.11). The generated electrical pulses are carved by an electrical lowpass filter (LPF) with a bandwidth of 7.46 GHz to achieve the Gaussian shaped pulses, and sent to the laser. The laser bias current, laser temperature and filter temperature are set to 20 mA, 20°C and 41°C , respectively. Different intensity of the bursts leads to a different frequency deviation of the optical signal in each time slot. As a result, in each time slot, the optical spectrum is placed at different positions regarding the central wavelength of the OBPF. Figure 5.12(a) shows the generated optical signal at the output of the transmitter. It can be seen that optical NRZ and UWB signals are generated by using only a single light source.

The receivers are also the same as in Fig. 5.7. The detected electrical signal after APD in both receivers is the same as in Fig. 5.12(b). The gating signal to control the burst mode of BERT and receive only one signal format at a time is the same as in Fig. 5.8. In the case of NRZ, the gating signal is adjusted as shown by the dotted-line in Fig. 5.12(b), so received NRZ data is sent to BERT and UWB data is cut out. In the UWB receiver, the gating signal is set

5.2 Experimental setup and results

as shown by the dashed-line in Fig. 5.12(b). Consequently, the received UWB data is passed and NRZ data is gated out. BER and eye diagram of the received NRZ and UWB signals are depicted in Fig. 5.13(a) and 5.13(b), respectively. As can be seen, an open eye and BER of 10^{-9} is achieved at a power of -14 dBm and -12 dBm for NRZ and UWB transmission, respectively.

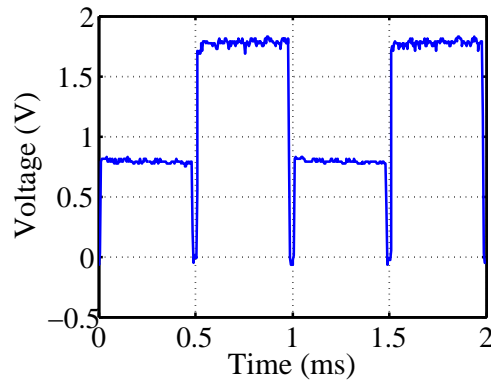


Figure 5.11: Burst signal.

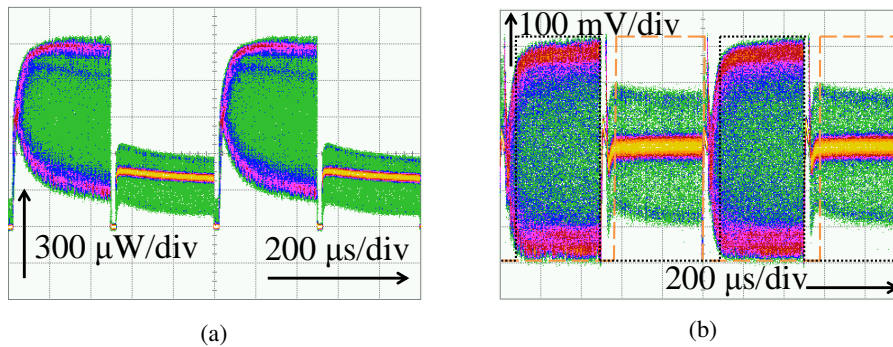


Figure 5.12: (a) transmitter output and (b) received signal after APD.

5 Integration to TDM-PON

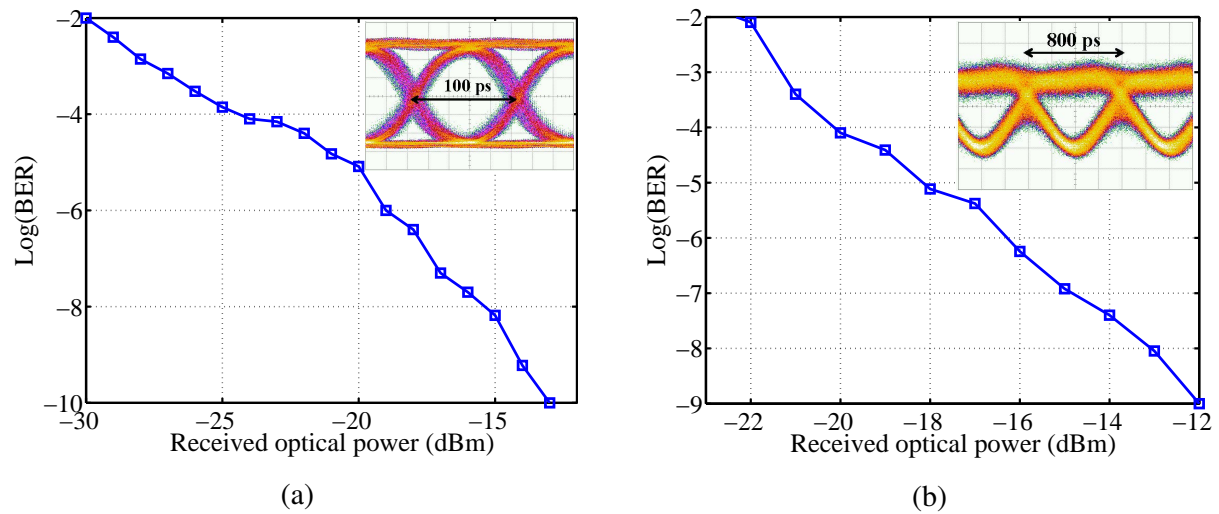


Figure 5.13: Log(BER) vs. received optical power in downstream scenario (a) 10 Gbps NRZ, (b) 1.25 Gbps UWB.

5.3 Summary

It was experimentally demonstrated that the proposed transmitter can be adapted to the TDM-PON and generate the NRZ and UWB signals with the use of only one single light source at different time slots of the TDM architecture. The chirp of the DFB laser was analyzed and principle of operation was explained. In upstream scenario, a 10 Gbps NRZ and a 1.25 Gbps UWB signal were generated separately in burst mode to study the influence of the thermal chirp effects on the signal quality at low frequencies. Through the proper selection of the burst amplitudes in the downstream scenario, a 10 Gbps NRZ and a 1.25 Gbps UWB signal were generated from a single light source at different time slots of the TDM architecture. The BER measurement was performed and an error free transmission was achieved. The presented work and results of this chapter are published in **Optics Express** [83].

Chapter 6

Integration to WDM-PON

In this chapter a novel bidirectional UWBoF system compatible with the WDM architecture is presented. In the proposed scheme, a 6th order Gaussian derivative is generated for UWB transmission in a downstream (DS) scenario, based on the directly modulated laser, accumulative chromatic dispersion in the transmission fiber and delay-line-interferometer (DLI). While the UWB signal is received from one of the DLI outputs, the other output is utilized to reuse the wavelength by injection locking a colorless Fabry-Perot laser diode (FP-LD). Due to the filtering effect of the FP-LD, a clear optical carrier without intensity modulation is then generated which can be used for upstream (US) baseband (BB) transmission by directly modulating the FP-LD.

6.1 WDM-PON

As mentioned earlier in Chapter. 3, for the sake of simplicity, the generation of monocycle and doublet pulses has mostly been reported in the microwave photonic research. However, the spectrum of monocycle and doublet does not comply with the FCC regulation. As shown in Chapter. 3, a fifth derivative of the Gaussian pulse is required at least, in order to meet the FCC regulation perfectly [37]. In chapter. 4 one of the simplest and most cost efficient techniques to generate monocycle and doublet UWB pulses was introduced. This approach is based on the direct modulation of a semiconductor laser (DML), optical filtering and accumulative chromatic dispersion in a transmission fiber. It was shown in Chapter. 4 that the proposed transmitter can adapt to different accumulative dispersion caused by different fiber lengths installed in the optical access network [79]. It was also demonstrated in Chapter. 5 that the transmitter is compatible with the TDM-PON and can generate NRZ and UWB signals at different time slots in the TDM architecture.

On the other hand, fiber to the home (FTTH) services are growing rapidly based on the PON technology. Future access networks will have advanced features such as aggregated bandwidth, attainable reach and allowable power budget [84], while the current PON technologies (Gigabit PON and Ethernet PON) are based on TDM and cannot fulfill the requirements. Therefore, the WDM-PON has been introduced as an ultimate broad-band access network due to its advantages, such as increased bandwidth per optical network unit (ONU), high security,

6.2 Proposed UWBoF-WDM-PON architecture

network flexibility and protocol transparencies. Nevertheless, WDM-PON is costlier and more complicated than TDM-PON, because of the need for wavelength selective optical components and frequency stable light sources.

In order to reduce the overall cost and complexity and enhance the compatibility between WDM-PON and UWBoF, it is preferable to simplify the operation and ease the maintenance. For instance, realizing a colorless ONU by reusing the downstream (DS) wavelength for the upstream (US) service is highly desirable [85]. Several different approaches have been proposed for reusing the wavelength, such as employing a separated optical carrier [86, 87], gain saturation of a reflective semiconductor optical amplifier (RSOA) [88, 89] and injection-locking of a Fabry-Perot laser diode (FP-LD) [90, 91]. The separated optical carrier technique is complicated, costly and inefficient, as the sharp optical filters or interleavers are required in this approach and also demodulation of the signal at the ONU is sophisticated. The major limitation of the schemes using a RSOA or a FP-LD is that the extinction ratio of the DS signal has to be low, which confines the network performance.

A very simple and cost efficient wavelength reuse technique for UWB over WDM-PON system is proposed in this chapter. Based on the proposed technique in Chapter 4 and taking advantage of the interference effect of a delay-line-interferometer (DLI) for the downlink, the 6th order derivative of the Gaussian function is generated in the ONU. The uplink is based on the injection locking, filtering effect and direct modulation of a FP-LD. The FCC compliance UWB signal is obtained from one of the DLI outputs and transmitted through the UWB antennas, while the second output of the DLI is utilized for injection locking the FP-LD to generate a clear optical carrier without intensity modulation for the US data transmitter. A bidirectional and symmetric transmission of 1.25 Gbps UWB signal over 60 km of SMF is experimentally demonstrated and the transmission performance in terms of BER and eye diagrams is evaluated. For both down and upstream scenarios, an error free transmission is achieved.

6.2 Proposed UWBoF-WDM-PON architecture

Figure. 6.1 shows the proposed UWBoF over WDM-PON architecture. At the OLT, the desired optical pulses for the downlink are generated in each transmitter by using a CML at a unique wavelength, so that each transmitter has its own and unique wavelength. A WDM multiplexer (MUX) is employed for multiplexing the optical DS signals from all transmitters and sending them to the remote node (RN). The DS signal in the RN is de-multiplexed utilizing a WDM de-multiplexer (DEMUX) and directed to the corresponding ONUs. In the ONU, the received signal is first passed through a DLI in order to take advantage of the interference effect and shape the desired 6th order Gaussian derivative. The optical UWB signal is then converted to an electrical signal by using an APD and sent to the user end through UWB antennas. Meanwhile, the second output of the DLI is redirected to a colorless FP-LD through a polarization controller (PC) and a circulator. The free running FP-LD is then injected and locked and an optical carrier at the same wavelength as the DS is generated for the US. From the other side, the US UWB data from the wireless user is received in the ONU, down converted to the baseband (BB) by a local oscillator and a low-pass filter (LPF) and directly modulated on the selected wavelength for the US. The US signals from different ONUs are then multiplexed

6 Integration to WDM-PON

at the RN using a MUX and sent to the OLT. The received US signals are de-multiplexed at the OLT by using a DEMUX and directed to the corresponding transceiver. The optical US BB signal is then converted to an electrical signal at each transceiver by utilizing an APD and detected by the receiver. A dual - fiber transmission architecture is used in the proposed setup, in order to eliminate the unwanted Rayleigh scattering induced noise in the bidirectional transmission [92].

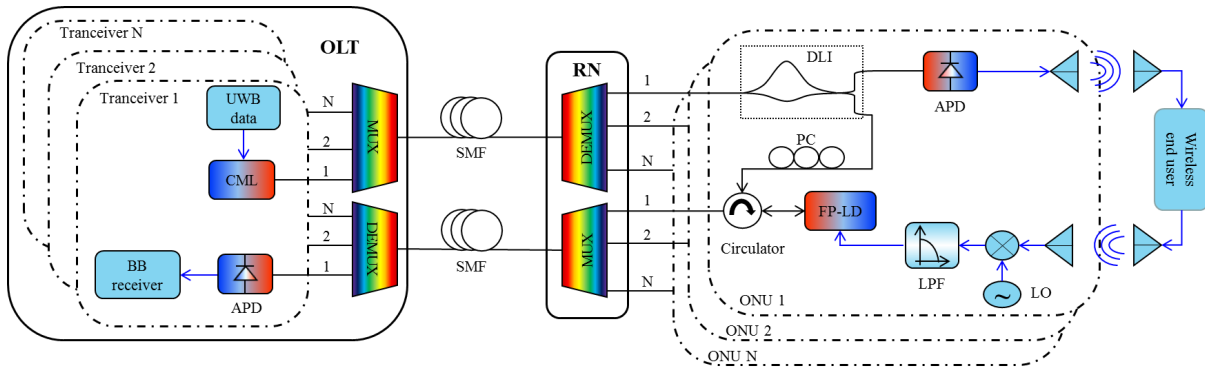


Figure 6.1: Proposed wavelength reused UWBoF over WDM-PON architecture.

6.3 Principle of operation

As explained in detail in Chapters 4 and 5, by applying the electrical signal to the DFB laser, not only the intensity, but also the optical frequency of the output light is modulated. It was discussed that the output intensity modulation (IM) is related to the photon density inside the cavity and the laser frequency modulation (FM) is a result of the carrier density change. It was demonstrated theoretically and experimentally in Chapter 5, that an UWB or NRZ signal can be generated from a single CML, by placing the spectrum of the DFB output on either the negative or positive slope of the OBPF, respectively. As in the previous chapters, in order to generate the required pulses for UWB generation in this chapter, a proper FM to IM conversion has to be carried out. The difference is that here both negative and positive slopes are simultaneously employed. In order to realize this idea, an optical signal is required, having positive and negative frequency deviation. An electrical pulse with a small distortion on the edge [Fig. 6.2(a)] is sufficient to generate the required optical signal. The CML is modeled in MATLAB in order to see the optical pulse shape and its corresponding chirp after DFB laser and analyze the effect of the OBPF. The laser rate equations [93, 94] are used for modeling the DFB and OBPF is considered as a Gaussian bandpass filter with the order of one and a 3-dB bandwidth of 0.06 nm. The intensity and chirp of the optical signal after the DFB are shown in Fig. 6.2(b). The desired pulse shape can be obtained at the output of the CML, by tuning the OBPF and placing the spectrum of the DFB output on the proper position with respect to the central wavelength of the OBPF. Figure 6.3(a) shows the achieved pulse shape after the optical filtering. Figure 6.4 describes how the FM of the signal from the DFB output [Fig. 6.3(b)]

is converted to IM and combined with the IM of the signal by the OBPF to obtain the pulse shape at the output of the CML [Fig. 6.3(a)]. Using the same model as in Sec. 4.4, the fiber transmission is also modeled in MATLAB. The obtained pulse shape after the fiber transmission and its corresponding chirp are shown in Fig. 6.3(b). In Sec. 4.4, the impact of the chromatic dispersion on a chirped signal was fully studied. It was demonstrated mathematically and experimentally, how the chromatic dispersion transfers the photon energy from the end to the beginning of a chirped pulse and modifies the waveform. It was also shown that the transmitter can be adapted to the different lengths of the fiber by controlling the laser operation point and the obtained pulse shape is independent from the length of the transmission fiber.

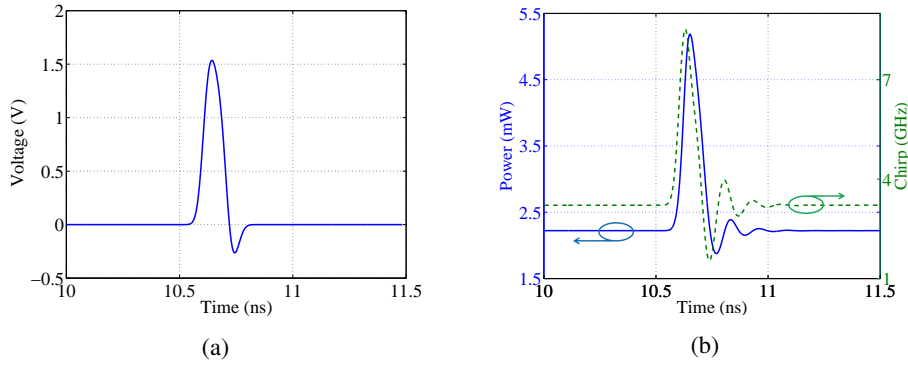


Figure 6.2: (a) Applied electrical signal to DML. (b) Output of modeled directly modulated DFB.

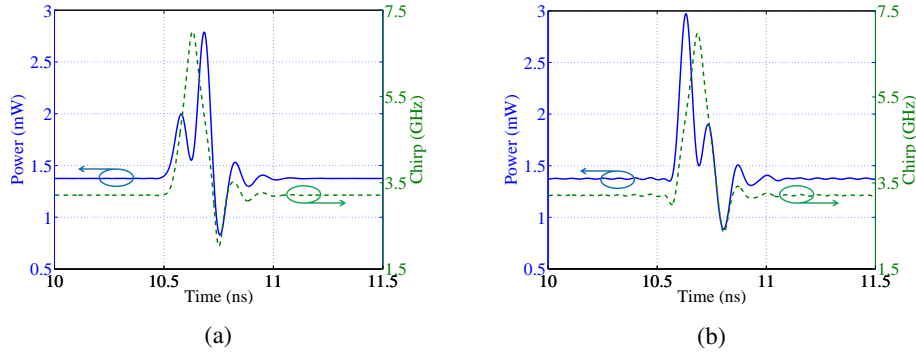


Figure 6.3: (a) Output of the modeled OBPF. (b) Output of the modeled fiber.

In order to take advantage of the interference effect of a DLI and shape the 6th order Gaussian derivative, the DLI is modeled at the end as:

$$E_{out1}(t) = \frac{1}{2}E_{in}(t - T) - E_{in}(t), \quad (6.1)$$

$$E_{out2}(t) = j\frac{1}{2}E_{in}(t - T) + jE_{in}(t). \quad (6.2)$$

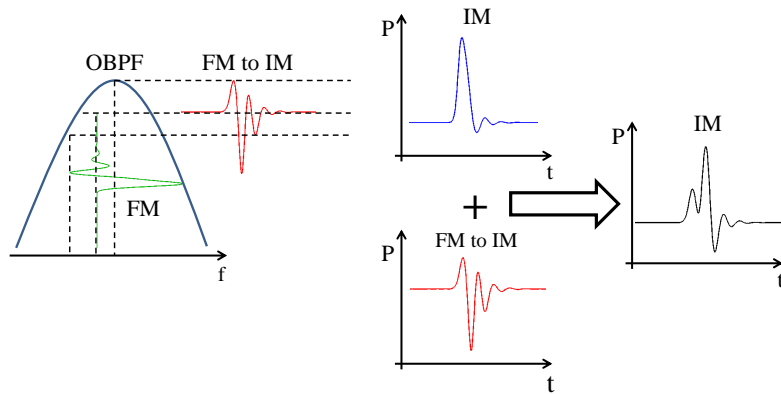


Figure 6.4: Optical FM-to-IM conversion by optical filtering.

E_{in} is the DLI input signal, which is the same as the fiber output signal [Fig. 6.3(b)]. T indicates the time delay between two branches of the DLI. The desired 6th order Gaussian derivative can be achieved by controlling the T and choosing a proper time shift between the branches of the DLI. From the simulation, T is reported as $T = 0.1$ ns. The outputs of the DLI and their corresponding electrical spectrum are shown in Fig. 6.5. The black mask in Fig. 6.5(a) determines the FCC regulation.

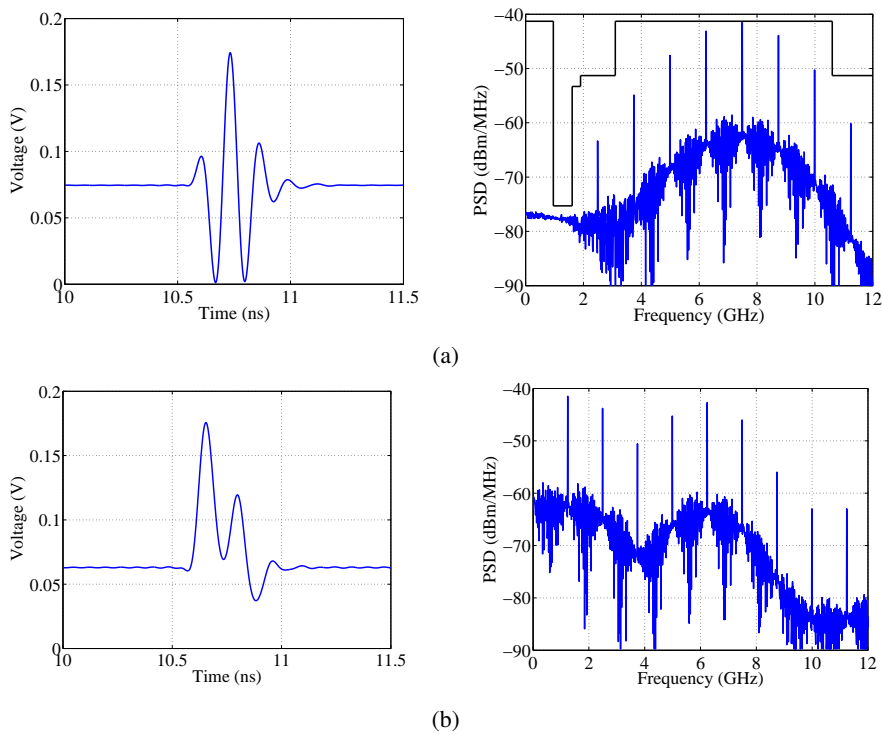


Figure 6.5: Outputs of the DLI and corresponding spectrum, (a) first output and (b) second output.

6.4 Experiment

6.4.1 Downstream

Figure 6.6 illustrates the experimental setup of the proposed wavelength reused UWBoF system. A 1.25 Gbps electrical on-off-keying signal (PRBS $2^{11} - 1$) is generated in the OLT by a programmed PPG at 10 Gbps. From the coding, a logical ‘1’ is represented by “1000 0000” (one ‘1’ bit every 8 bits), and a logical ‘0’ is represented by “0000 0000”. In order to generate the desired electrical pulse shape as in Fig. 6.2(a), the positive and negative outputs of the PPG are added together by using a 3-dB electrical coupler. By adjusting the duty cycle of the PPG outputs, the required pulse shape is obtained [Fig. 6.7(a)]. The peak-to-peak voltage is $V_{pp} = 1.8$ V. The DFB laser is then directly modulated. The electrical signal is then used to directly modulate the DFB laser. The central wavelength, input impedance and threshold current of the laser module are 1538.7 nm, 50Ω and 15 mA, respectively. By tuning the OBPF properly as described in Sec. 6.3, the desirable optical signal at the output of the CML is achieved [Fig. 6.7(b)]. The laser bias current, laser temperature and filter temperature are set to 50 mA, $20^\circ C$ and $42^\circ C$, respectively; and the 3-dB BW of the OBPF is 0.06 nm. The optical power at the output of the CML is reported as 2.9 dBm. The generated signal is then transmitted to the ONU through 25 km of SMF. The obtained waveform after the fiber transmission is shown in Fig. 6.8(a). The optical power after the fiber transmission is measured as -2.1 dBm. In the ONU, the optical signal is passed through a DLI in order to generate the 6th order Gaussian derivative. The Obtained waveform at the first output of the DLI is shown in Fig. 6.8(b) and the optical power is reported as -6 dBm. As mentioned earlier in Sec. 6.3, it was shown in Chapter 4 that this technique is independent from the length of the transmission fiber and the transmitter can be adapted to the different lengths of the fiber by controlling the laser operation point. To prove this, the experiment is repeated for 60 km of SMF and similar results are achieved by setting V_{pp} to 0.75 V. The optical power at the output of the CML, after 60 km SMF and at the output of the DLI are measured as 1.8 dBm, -10.4 dBm and -14.3 dBm, respectively. After the

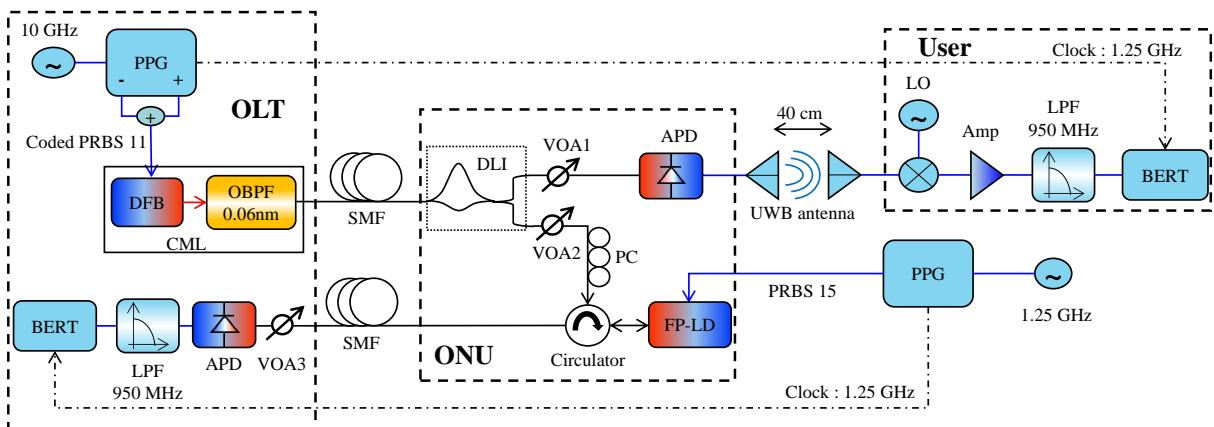


Figure 6.6: Experimental setup of the proposed wavelength reused UWBoF system.

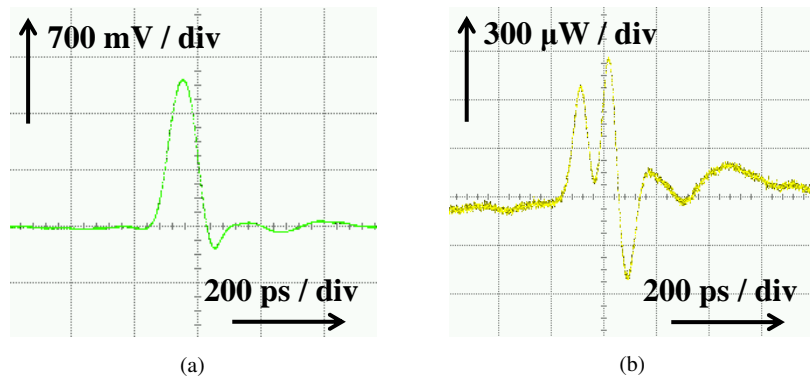


Figure 6.7: (a) Applied electrical signal to CML (b) CML output.

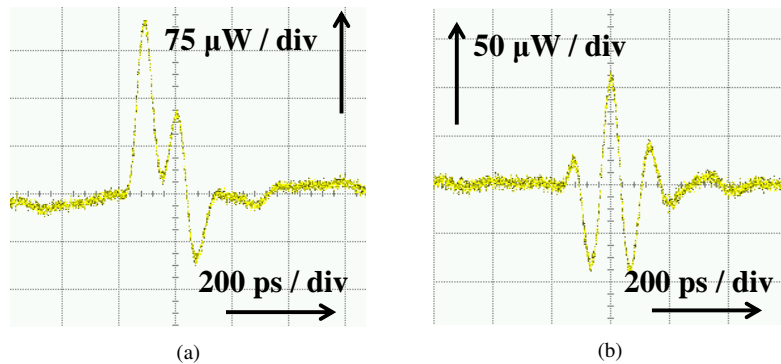


Figure 6.8: Obtained pulse shape, (a) after fiber transmission, (b) DLI output.

optical to electrical conversion, the DS signal is sent to the wireless user using the same UWB antenna introduced in Sec. 4.3. The UWB signal is then captured by another UWB antenna at the user side after 40 cm of wireless transmission. Figure. 6.9 shows the UWB pulses and their corresponding electrical spectra before and after wireless transmission. The black line in Fig. 6.9(a) and 6.9(b) indicates the FCC mask for indoor transmission and the red line in Fig. 6.9(b) shows the transfer function (S_{21}) of the used UWB antennas. As can be seen, the spectrum of the generated UWB signal fits perfectly into the FCC mask. In order to compare the pulse shapes before and after wireless transmission, the fidelity factor (F) is calculated and $F = 0.9168$ is found. This confirms that the signal is barely affected by the UWB antennas, as the spectrum of the UWB signal lies in the passband of the UWB antennas.

In the user-end, the received signal is down converted to the BB through an electrical mixer and a LO. Next, the BB signal is amplified and filtered to remove the high frequency components. The used electrical amplifier (Amp) and LPF have a 3-dB BW of 1.25 GHz and 950 MHz, respectively. Lastly, the frequency of the LO is tuned to each frequency component of the signal and the BER versus received optical power (by changing the attenuation at VOA1) is measured for different frequency components and the results are shown in Fig. 6.10(a). The inset in Fig. 6.10(a) shows the observed eye diagram of the down converted signal by LO at

7.5 GHz when the received optical power is -24 dBm. As mentioned above, this experiment was rerun for 60 km of transmission fiber. The BER performance of the proposed setup after transmission over 25 km and 60 km of SMF is compared in Fig. 6.10(b) for frequency components 6.25 GHz and 7.5 GHz. An error-free transmission (BER 10^{-9}) for both scenarios is achieved and the experimental results show good agreement with the numerical ones.

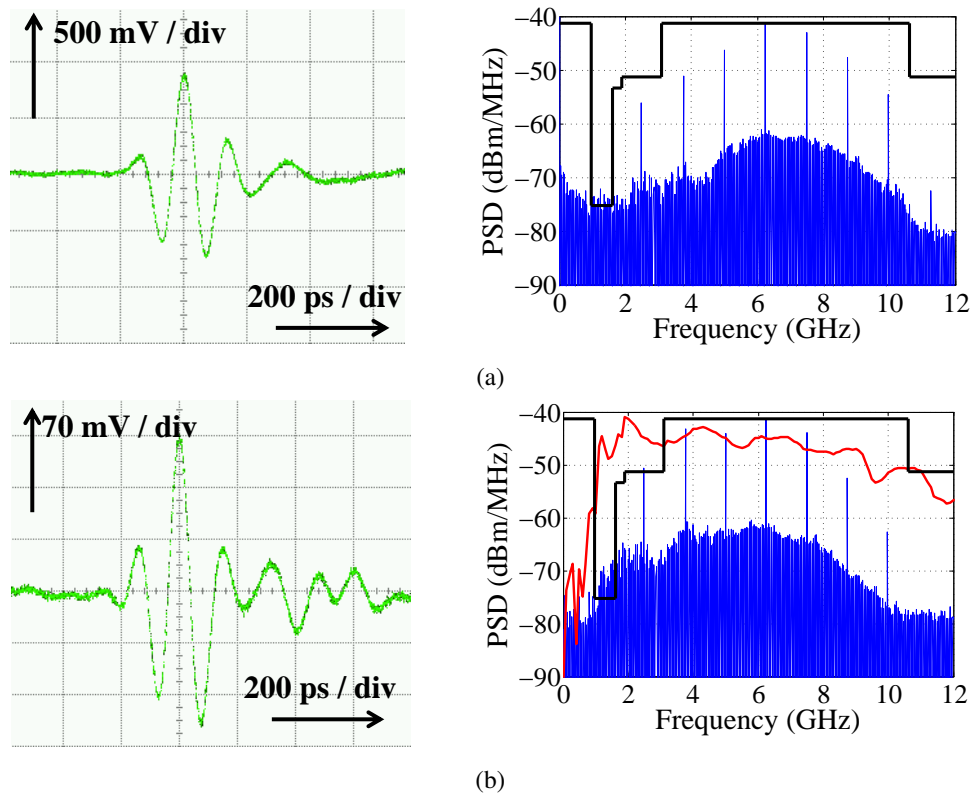
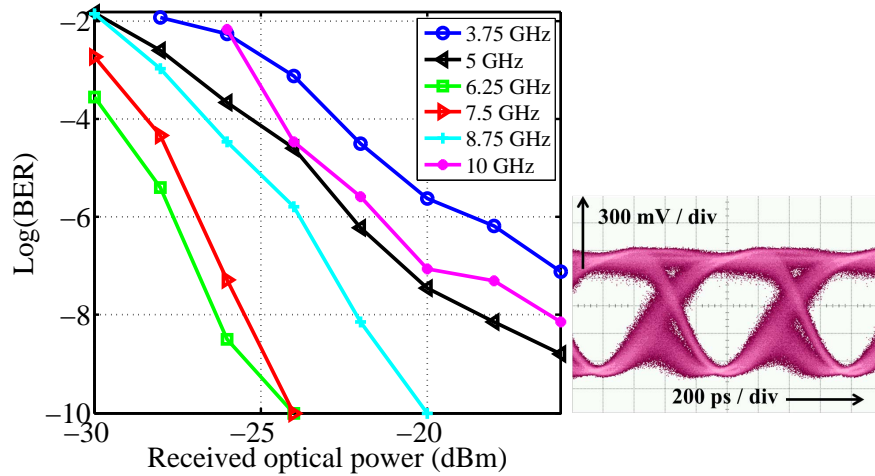


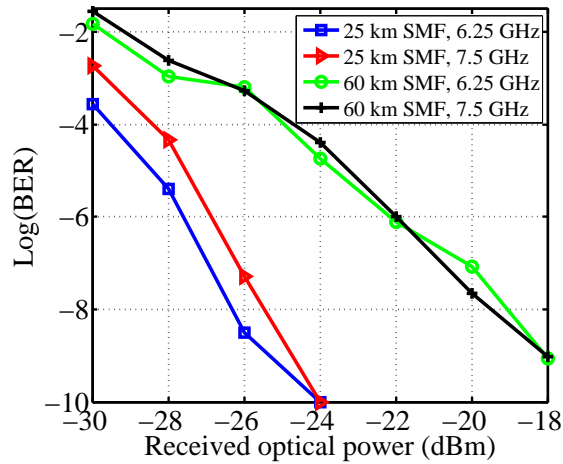
Figure 6.9: Electrical waveform and corresponding spectrum (a) before wireless transmission and (b) after wireless transmission.

6.4.2 Upstream

In order to establish the US carrier in the ONU, the second output of the DLI is injected to a colorless FP-LD through the second VOA, an optical circulator and a polarization controller (PC) (Fig. 6.6). As a result, the FP-LD is injection-locked and an optical carrier at the same wavelength as the DS is generated for the US. The spectrum of the free running FP-LD is illustrated in Fig. 6.11. The utilized FP-LD is intended for optical C-band with a channel range from 1531.12 nm to 1562.23 nm [Fig. 6.11(a)]. The enlarged spectrum is depicted in 6.11(c) to observe the modes and the channel spacing which is about 50 GHz. Figure 6.12 shows the spectrum of the injecting signal from the second output of the DLI. In order to demonstrate the successful injection locking, the power spectral density (PSD) of the generated optical carrier with respect to wavelengths in terms of different injection power is depicted in Fig. 6.13(a).



(a)



(b)

Figure 6.10: (a) Log(BER) vs. received optical power after 25 km SMF. (b) Comparison of BER performance after 25 km and 60 km SMF.

The maximum allowed injection power to the FP-LD is -5 dBm. Therefore, the injection power is changed from -6 dBm to -28 dBm with the use of the VOA2. The side mode suppression ratio (SMSR) versus the injection power is shown in Fig 6.13(b).

Comparing Fig. 6.11, Fig. 6.12 and Fig. 6.13, it is obvious that the FP-LD is locked to the same wavelength as the DS and all other modes are suppressed. The signal waveform and its corresponding electrical spectrum at the DLI output and before the injection are shown in Fig. 6.14(a). The injection signal to the FP-LD experiences the FP etalon effect in the FP cavity, which modifies the spectrum and the waveform consequently. The injection locked generated waveform and the corresponding electrical spectrum are captured at the third output of the circulator and depicted in Fig. 6.14(b). As can be seen, the frequency components below 1.25 GHz are cut off through the filtering effect of the FP-LD. As mentioned earlier, the US

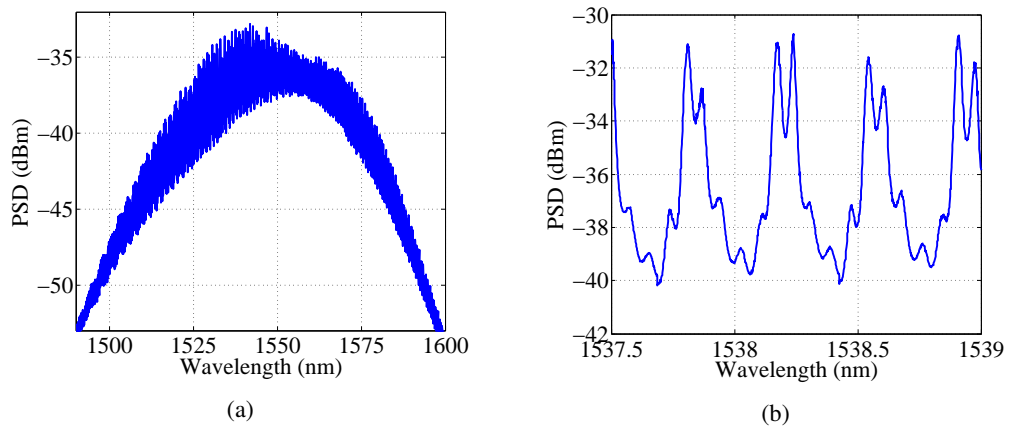


Figure 6.11: FP-LD spectrum.

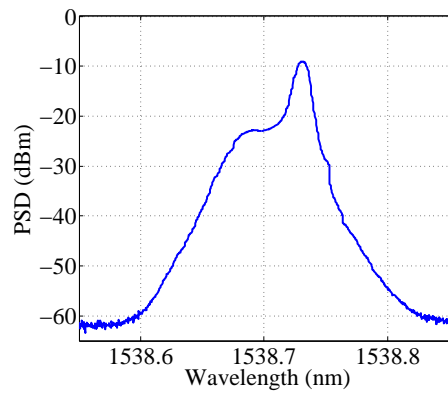


Figure 6.12: Spectrum of the injecting signal.

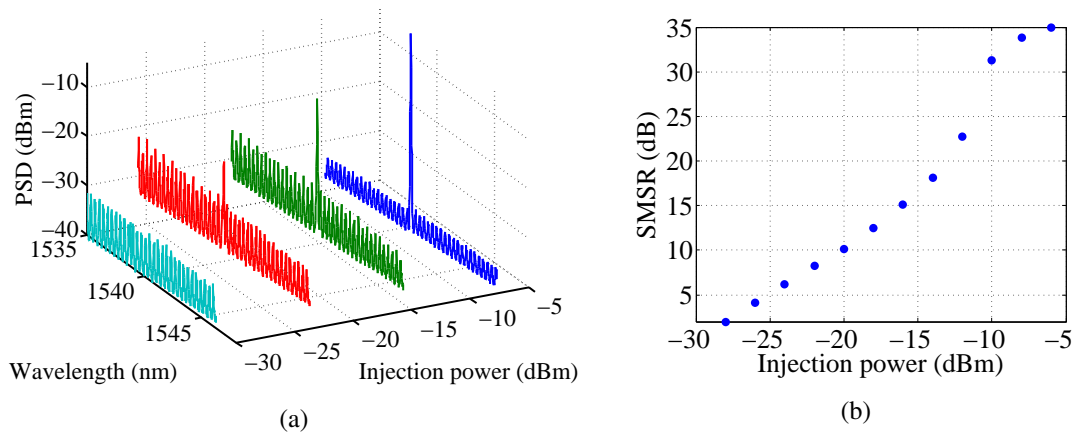


Figure 6.13: (a) Injection locked FP-LD. (b) SMSR vs. injection power.

6 Integration to WDM-PON

signal is a 1.25 Gbps BB and therefore, this suppression is very desirable as the noise level is minimized. Furthermore, the high frequency components will appear as an out-of-band noise and can be easily removed by a LPF in the receiver. Next, the generated optical carrier is sent to the OLT through 25 km of SMF. The optical signal is then converted to an electrical one in the receiver by employing an APD and the high frequency components are filtered out by using a LPF with a 3-dB BW of 950 MHz. Figure. 6.15 shows the temporal waveform of the optical carrier and the corresponding electrical spectrum after the LPF in the receiver, confirming that the DS data is completely erased from the US carrier. The clear optical carrier is then employed for establishing the US data transmission.

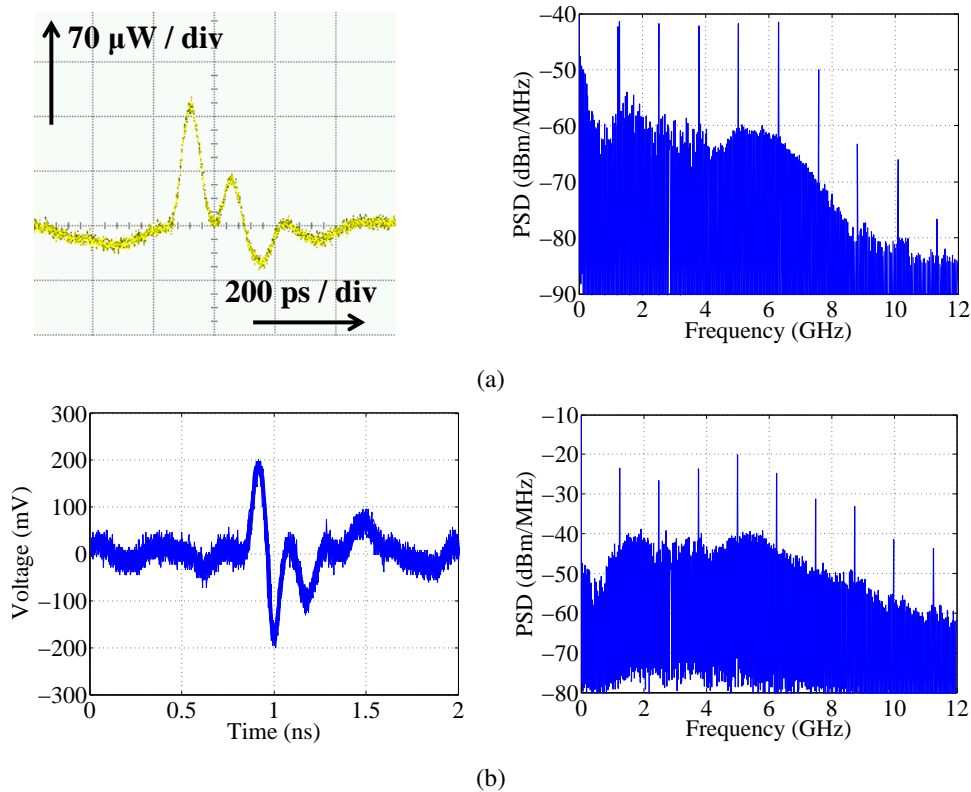


Figure 6.14: Waveform and electrical spectrum, (a) before injection locking and (b) after injection locking.

The received and down converted US UWB signal from the user-end in the ONU (Fig. 6.1), is emulated by generating a 1.25 Gbps BB on-off-keying signal ($\text{PRBS } 2^{15} - 1$) with the use of a PPG (Fig. 6.6). The injection-locked FP-LD is then directly modulated and the US signal is sent to the OLT through 25 km of SMF. The optical power after the injection-locking at the third output of the circulator and after the fiber transmission are measured as 1.4 dBm and -3.7 dBm, respectively. The received US signal in the OLT is then converted to an electrical signal by using an APD. Finally, the higher frequency components are removed by a LPF with a 3-dB BW of 950 MHz and the BER versus received optical power is measured (using VOA3). As mentioned before, the experiment is repeated for a symmetric 60 km of fiber transmission.

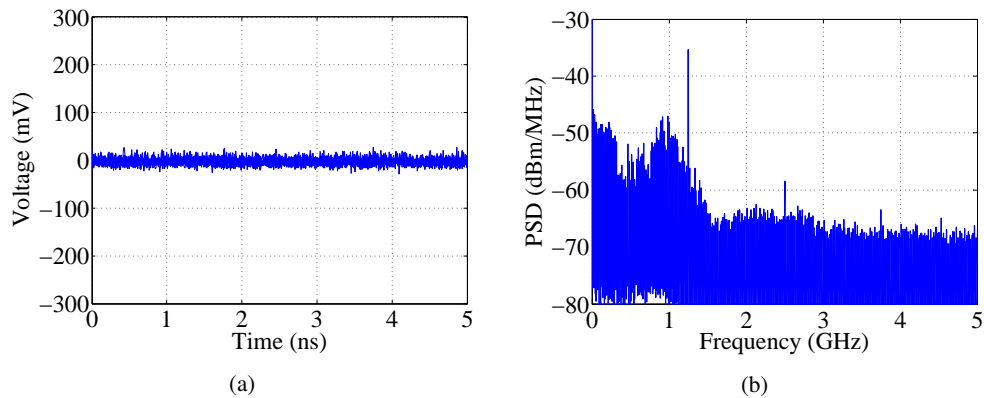


Figure 6.15: (a) The temporal waveform of the US carrier after photodetection and low-pass filtering. (b) Electrical spectrum of the US carrier.

In this case, the optical power before the FP-LD injection, after the injection and after 60 km of SMF are measured as, -14.3 dBm, 0.2 dBm and -13.1 dBm, respectively. Figure. 6.16 shows the BER measurement for US transmission over 25 km and 60 km of SMF. The inset in Fig. 6.16 shows the eye diagram after 25 km of fiber transmission, when the received optical power is -31 dBm. As can be seen, an error-free transmission (BER 10^{-9}) for both scenarios is achieved.

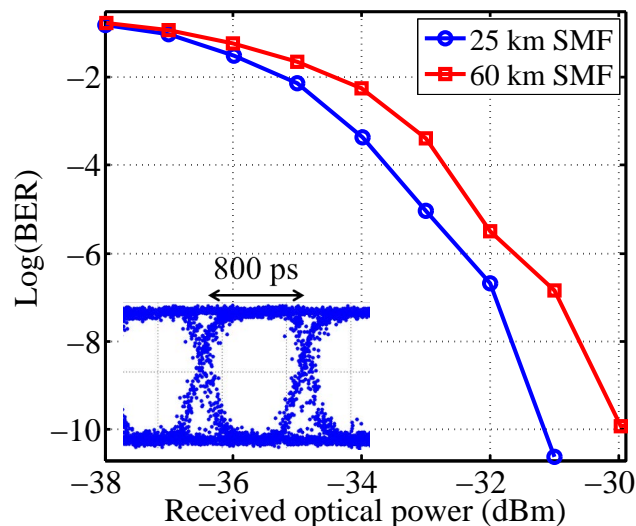


Figure 6.16: Upstream BER measurement.

6.5 Summary

A simple and cost efficient bidirectional UWBoF system over WDM-PON was presented. The principle of operation was explained through the numerical simulation. In the DS scenario, the 6th order Gaussian derivative was generated based on the direct modulation of a semiconductor laser, optical filtering, accumulative chromatic dispersion in transmission fiber and the interference effect of DLI. The second output of the DLI was employed for injection locking of a FP-LD in order to establish a clean optical carrier for the US. A bidirectional 1.25 Gbps data transmission was performed for symmetric transmission distance of 25 km of SMF and an error free transmission was obtained. The experiment was successfully repeated for the symmetric transmission distance over 60 km of SMF, proving that the transmitter can be adjusted with respect to the fiber length by controlling the laser operation point. The presented work and results of this chapter are published in **Optics Express** [95].

Chapter 7

Spectral efficiency and modulation format

The rapid growing demand for bandwidth is forcing network operators and equipment manufacturers to move toward high-capacity optical transmission systems. Advanced modulation formats with high spectral efficiency are known as a promising solution for fiber optic communication. In this chapter, first, the conventional modulation formats for UWBoF are briefly reviewed and their functionality with the proposed transmitter in Chapter 4 is discussed. In addition, a novel modulation format based on the pulse positioning modulation (PPM) is proposed, in order to increase the spectral efficiency and optimize the PSD of the signal for the FCC limit. As it will be shown, the higher modulation formats for UWBoF require a correlation receiver. Due to the lack of a correlation receiver in the laboratory at the time period of this thesis, the data detection is unfortunately not experimentally possible. Therefore, the signal is generated once experimentally, to observe and analyze the corresponding spectrum of each modulation format individually. Then, the whole signal generation, transmission and data detection is simulated in “OptiSystem” in association with “Matlab”, in order to demonstrate the reception performance.

7.1 UWB modulation formats

As shown in Table. 7.1 , the UWB modulation formats can be listed in two basic categories, namely, “shape-based” and “time-based” techniques. These modulation techniques are discussed below.

Table 7.1: Categorization of modulation techniques for UWBoF communication

Shaped-based techniques	Time-based techniques
Pulse amplitude modulation (PAM) Bi-phase modulation (BPM) Pulse shape modulation (PSM) On-off keying (OOK)	Pulse position modulation (PPM)

7.1.1 Pulse amplitude modulation

In Pulse amplitude modulation (PAM), different amplitudes of a pre-specified waveform correspond to different data being transmitted. A basic PAM signal can be represented as:

$$S_{PAM} = \sum_j a(j)w(t - jT_f), \quad (7.1)$$

where $a(j)$ is the amplitude of the j_{th} pulse, $w(t)$ can be any desired IR-UWB pulse shape and T_f is the pulse repetition interval, or frame duration. In order to encode more than one bit per symbol, more than two amplitude levels must be employed. Figure 7.1 shows the basic concept of the PAM schematically. The amplitude modulation is not the best choice for most of the short-range communication, as the modulated symbol with the smaller amplitude is more susceptible to noise interference than its larger amplitude counterpart. Additionally, more power is required to transmit the higher amplitude pulse, while power efficiency is of a high importance in most UWB applications.

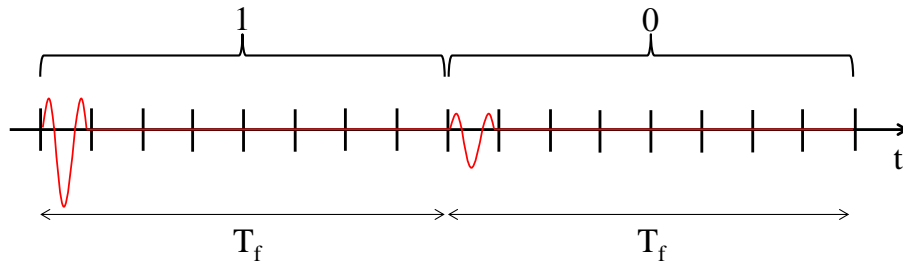


Figure 7.1: Schematic of a PAM signal.

PAM cannot be employed to modulate the signal in the proposed transmitter in this thesis. As explained earlier, the transmitter is based on the chirp of the signal and optical filtering. On the other hand, sending pulses with different amplitudes to the laser generates different amounts of chirp. Consequently, the filter needs to be placed at different positions corresponding to each amplitude's level, which is not possible.

7.1.2 Bi-phase modulation

Bi-phase modulation (BPM) employs the polarity of a particular IR-UWB pulse to encode the information. In other words, the polarity of the pulse is switched to represent "0" or "1". As there are only two polarities, only one bit per symbol can be encoded. The BPM signal can be expressed as:

$$S_{BPM} = \sum_j a(j)w(t - jT_f), \quad a(j) = +1, -1 \quad (7.2)$$

where $w(t)$ can be any desired IR-UWB pulse shape and T_f is the pulse repetition interval or frame duration. An optimal antipodal case can be achieved, by considering for instance, $a(j) = -1$ representing "0" and $a(j) = +1$ representing "1". The detection can be performed

7 Spectral efficiency and modulation format

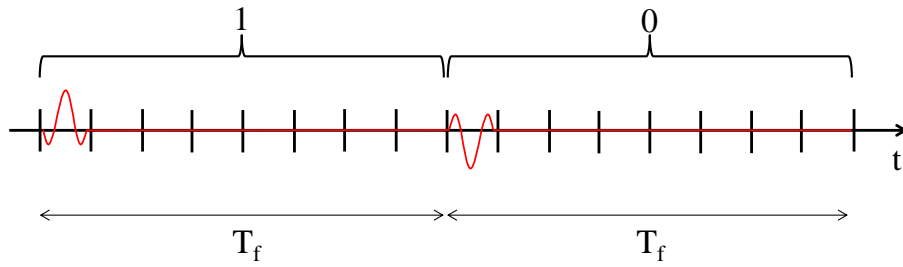


Figure 7.2: Schematic of a BPM signal.

by a correlation receiver using a normalized energy pulse $w(t)$ as the template signal. This will result in correlation values equal to -1 or $+1$. Figure 7.2 illustrates the concept of BPM.

The proposed transmitter in this thesis is able to generate different polarities, but it is not able to switch the polarities to modulate the signal. For instance in the entire thesis “1” was represented by “10000000” and “0” was represented by “00000000”, however, if “01111111” represents “1” and “11111111” represents “0”, IR-UWB pulses with inverted polarity can be achieved by placing the filter at the right position. However, switching the polarities is not possible as the optical filter has to be placed in a different position in each scenario. Therefore, BPM can not be employed by the proposed transmitter.

7.1.3 Pulse shape modulation

The main idea of Pulse shape modulation (PSM) is to utilize pulse shapes which are orthogonal to each other to represent the data bits. The conventional monocycle and doublet pulses have such a property. The PSM stream can be expressed as:

$$S_{PSM} = \sum_j w_j(t - jT_f), \quad (7.3)$$

where w_j is the appropriate waveform representing j_{th} data bit. M-ary PSM is possible by choosing more than two orthogonal pulse shapes. PSM can be detected by a correlation receiver, which benefits from orthogonality between the waveforms. Figure 7.3 describes the concept of PSM schematically.

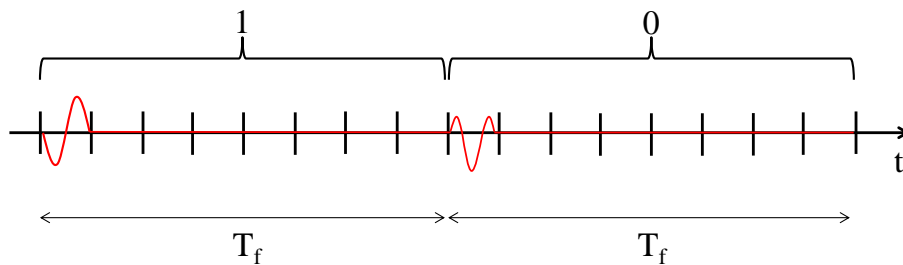


Figure 7.3: Schematic of a PSM signal.

As demonstrated in Chapter 4, by applying Gaussian electrical pulses to a DFB and optical filtering, monocycle pulses can be achieved and doublet pulses can be obtained after fiber transmission. Consequently, switching between monocycle and doublet is not possible and therefore, PSM cannot be used to modulate the signal in the proposed transmitter.

7.1.4 On-off keying

On-off keying (OOK), which has been employed in the entire thesis to transmit the data, is the simplest modulation format. In OOK, the transmission of a pulse represents “1” and its absence represents “0”. The OOK signal can be modeled as:

$$S_{BPM} = \sum_j a(j)w(t - jT_f), \quad a(j) = 1, 0 \quad (7.4)$$

where again, $w(t)$ is a prespecified waveform, T_f is the frame duration and $a(j)$ defines the presence or absence of the pulse. The concept of OOK is illustrated in Fig. 7.4 .

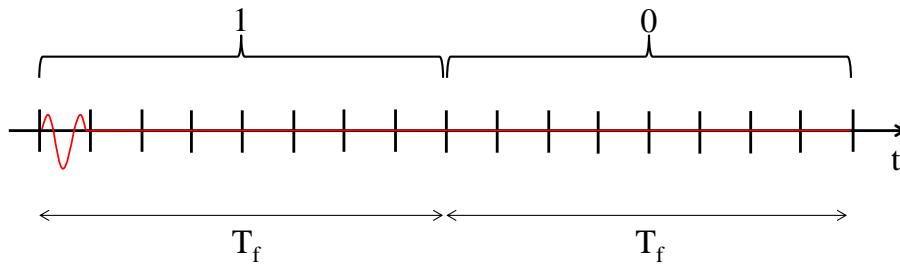


Figure 7.4: Schematic of a OOK signal.

The major limitation of using OOK in UWB communication is related to the echoes of the original pulses caused by multipath effects, which make it difficult to determine the absence of a pulse (i.e. “0”). Furthermore, OOK is a binary modulation scheme which cannot be extended to an M-ary modulation. Even though the OOK IR-UWB generation, transmission and detection has been fully explained throughout the thesis, the setup is one more time illustrated in Fig. 7.5 for the sake of the reader.

As mentioned earlier, in this technique, each data bit “1” is represented by “10000000” and each data bit “0” is represented by “00000000”. As depicted in Fig. 7.5, the detection can simply be performed by down-converting the signal after APD by using a local oscillator and lowpass filtering. The wireless transmission is left out in this section, as it is not the point of interest here. Figure 7.6 shows the electrical spectrum of the IR-UWB signal after the APD. As can be seen, the spectrum consists of continuous and discrete components. The data information is mainly contained in continuous spectral components and the power of the continuous spectral components has a direct relationship with the modulation efficiency, which also determines the receiver sensitivity [96]. As Fig. 7.6 shows, the discrete components contribute more to the PSD of an OOK modulated signal, therefore they would cause more interference to narrowband wireless systems. This is another disadvantage of OOK modulation for UWB communication [97].

7 Spectral efficiency and modulation format

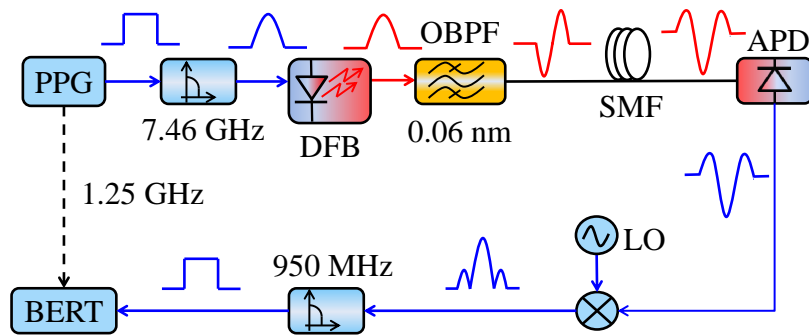


Figure 7.5: OOK IR-UWB transmission.

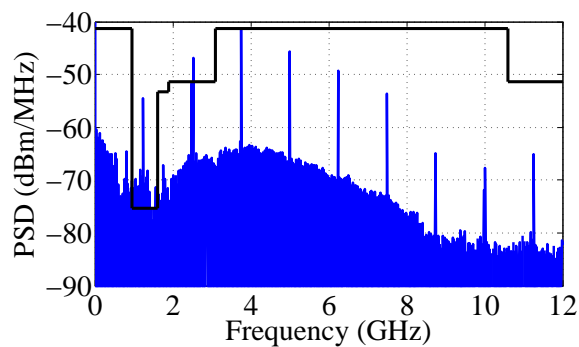


Figure 7.6: PSD of OOK signal.

The signal detection cannot be performed this simply for the rest of this chapter, as a signal correlation receiver is necessary. Unfortunately, at the time of this thesis, the signal correlation receiver was not available in the laboratory. Therefore, the signal generation, transmission and detection is simulated in “OptiSystem” in association with “Matlab” in order to evaluate the performance of the proposed techniques. To make sure that the simulation can be trusted and observe a good agreement between the simulation results and the measurements, in the first step, the OOK transmission is simulated. Figure. 7.7 shows the simulation setup.

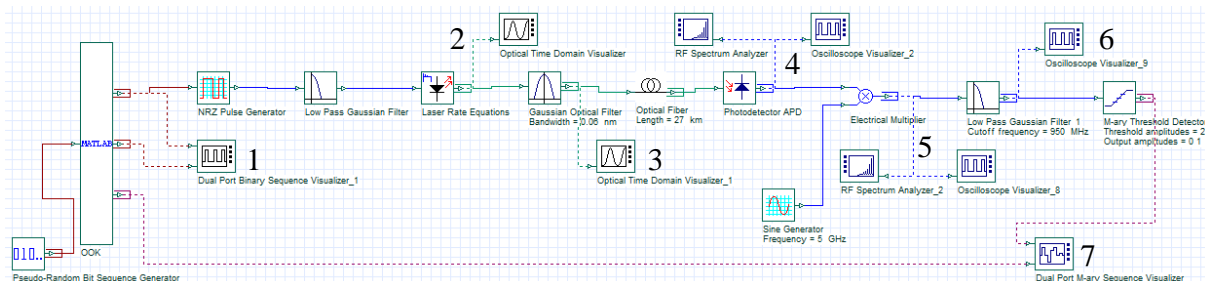


Figure 7.7: Simulation setup for OOK transmission.

First, a pseudo-random sequence is generated and sent to the “Matlab”, the Matlab codes the sequence (every data bit “1” is replaced by “10000000” and every data bit “0” is replaced by “00000000”) and sends it to an NRZ pulse generator. The coded sequence from the first output of the “Matlab” and the original sequence from the second output are compared at point 1 and shown in Fig. 7.8. The electrical pulses from the NRZ generator are then carved into the Gaussian shape by using a lowpass filter and sent to the laser. Figure 7.9a shows the laser output and the signal chirp at point 2. By utilizing an OBPF, the monocycles are generated at point 3 (Fig. 7.9b). Figure 7.10a and 7.10b show the obtained doublets and the corresponding PSD, respectively, after 27 km of fiber transmission and photodetection at point 4. Then, the UWB signal is downconverted, through a Sine generator at 5 GHz and an electrical mixer. Figure 7.11a and 7.11b illustrate the baseband signal and its corresponding PSD at point 5. A LPF is employed to integrate the symbol energy over the frame duration at point 6 (Fig. 7.12a). As the last step, a threshold detector is used in order to distinguish the “ones” from the “zeros” at point 7. Figure 7.12b compares the output of the threshold detector and the original data sequence from the third output of the “Matlab” coder. As can be seen, the original data is exactly recovered in the receiver. the reliability of the simulation is confirmed, as the simulation results show a very good agreement with the measurements.

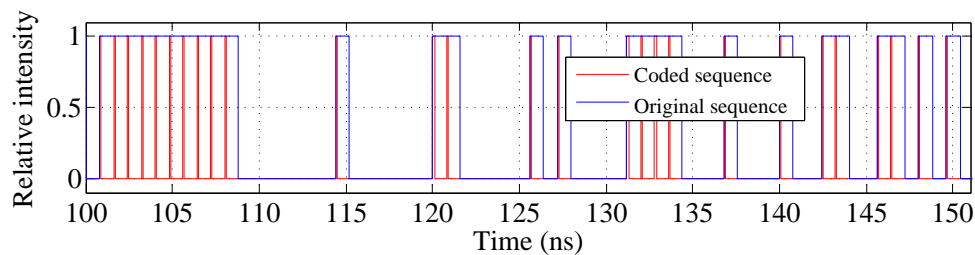


Figure 7.8: Original data and coded data.

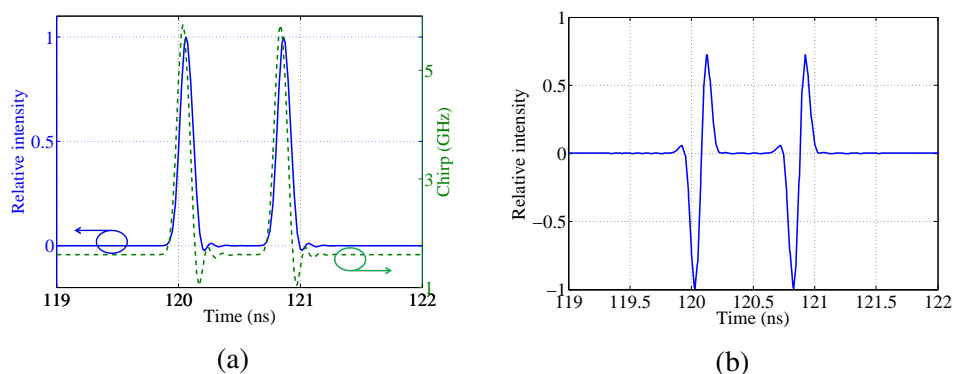


Figure 7.9: (a) Modulated laser output and corresponding chirp. (b) Monocycle pulses after OBPF.

7 Spectral efficiency and modulation format

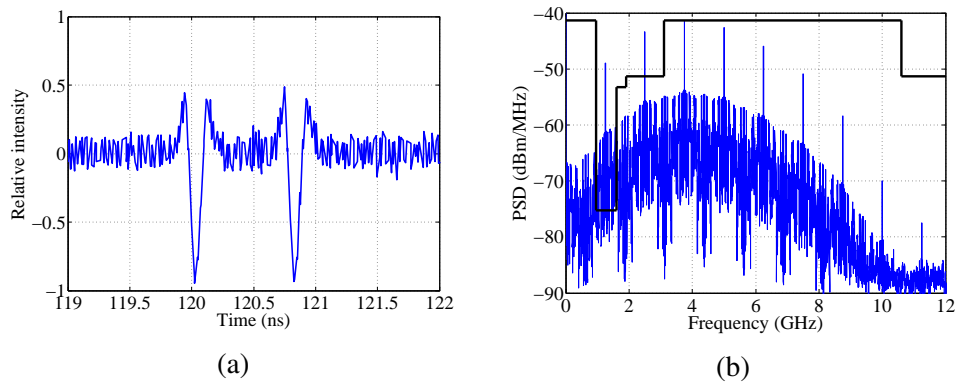


Figure 7.10: (a) Obtained doublet and (b) corresponding spectrum.

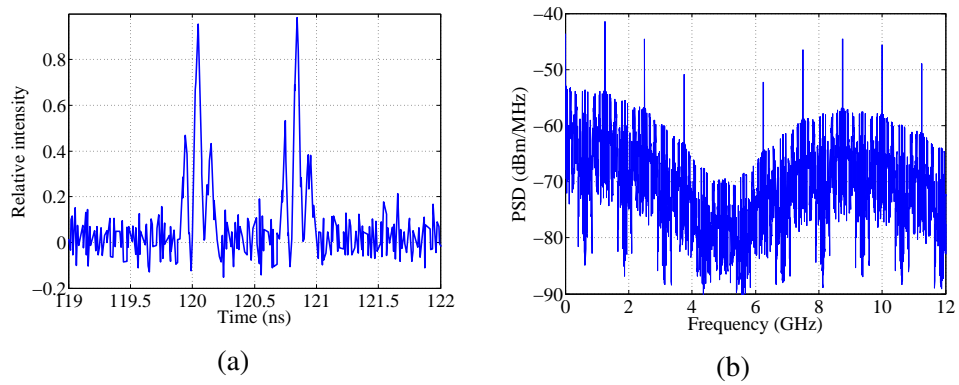


Figure 7.11: (a) Downconverted signal and (b) corresponding spectrum.

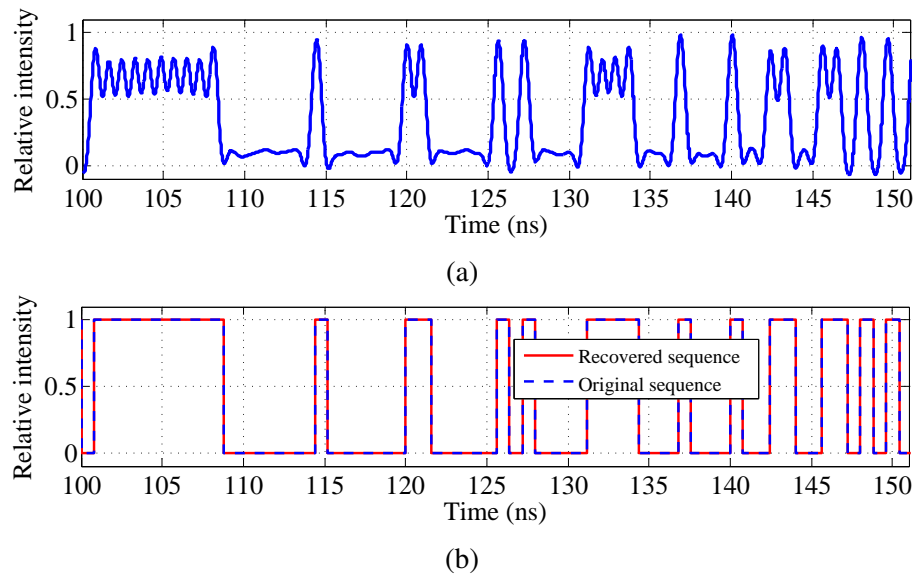


Figure 7.12: (a) Detected lowband signal after lowpass filtering. (b) Recovered data and the original data.

7.1.5 Pulse position modulation

As mentioned in Subsec. 7.1.4, the major problem of OOK is the echoes of the original pulses in the presence of multipath effects, which make it very difficult to determine the absence of a pulse (i.e. “0”). Therefore, pulse position modulation (PPM) is proposed to overcome this problem. Unlike all other modulation techniques, PPM is time-based. In PPM, the data is encoded by adding an extra time shift to the prespecified impulse. The PPM signal can be modeled as:

$$S_{PPM} = \sum_j w(t - jT_f - \tau_j), \quad (7.5)$$

where $w(t)$ can be any IR-UWB pulse shape, T_f is the frame duration and τ_j is an extra delay of j_{th} pulse corresponding to the symbol represented. Figure 7.13 shows the concept of the PPM schematically.

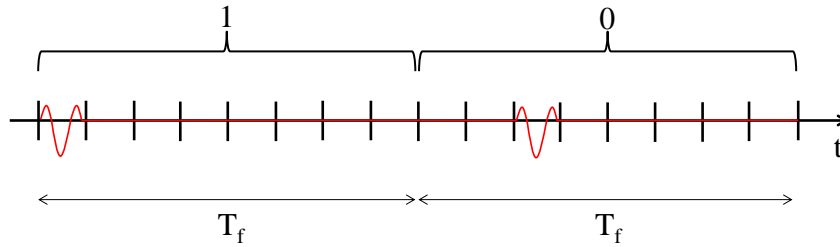


Figure 7.13: Schematic of a PPM signal.

As explained in [36, 98], both the discrete and continuous spectral components of a PPM signal, are the power spectrum of a UWB pulse multiplied by a cosine-based function, which is periodic in frequency. The frequency spacing between two adjacent notches is $1/\tau$, where τ is the time shift of the pulses for “0” and “1” bit. The signal generation is performed experimentally to study the spectrum of a PPM signal. Figure 7.14 shows the experiment setup.

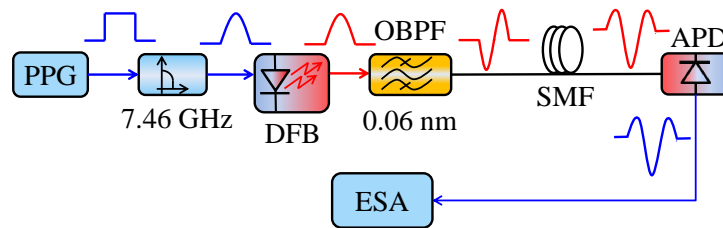


Figure 7.14: Experimental PPM signal generation.

A 1.25 Gbps coded PPM signal ($PRBS^7 - 1$) is generated by a PPG at 10 Gbps. From the coding, the logical “1” is represented by “10000000” and the logical “0” by “01000000”. As can be seen, the position of the “1” in the frame determines whether the symbol is representing the data bit “1” or “0”. The rest is the same as OOK transmission, with the difference being

7 Spectral efficiency and modulation format

that to detect the PPM signal, a correlation receiver is required. The electrical spectrum of the received PPM signal after the APD is recorded by an electrical spectrum analyzer (ESA). Figure 7.15 shows the captured spectrum for different τ . As expected, notches with the frequency spacing of $1/\tau$ appear in the PSD.

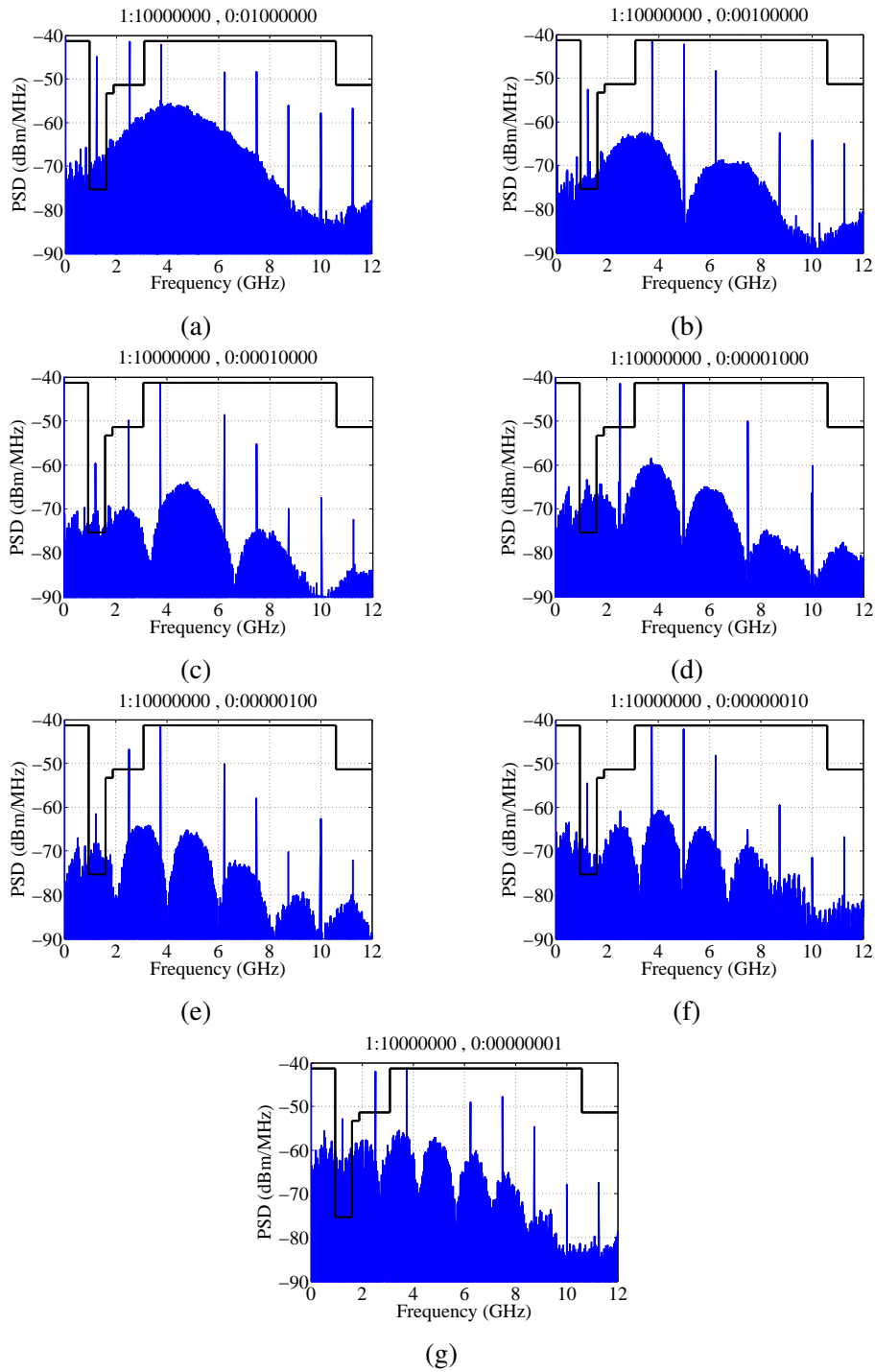


Figure 7.15: measured PPM spectrum for different τ .

As mentioned earlier, to detect a binary PPM signal a signal correlator with a special template waveform is required. The template waveform is the sum of two possible waveforms, when one of them is inverted and delayed by τ . This can be expressed as:

$$Temp(t) = w(t) - w(t - \tau), \quad (7.6)$$

this maximizes the distance between signals for binary PPM with IR-UWB pulses. A simulation is performed in order to study the detection of a PPM signal. The simulation setup is depicted in Fig 7.16.

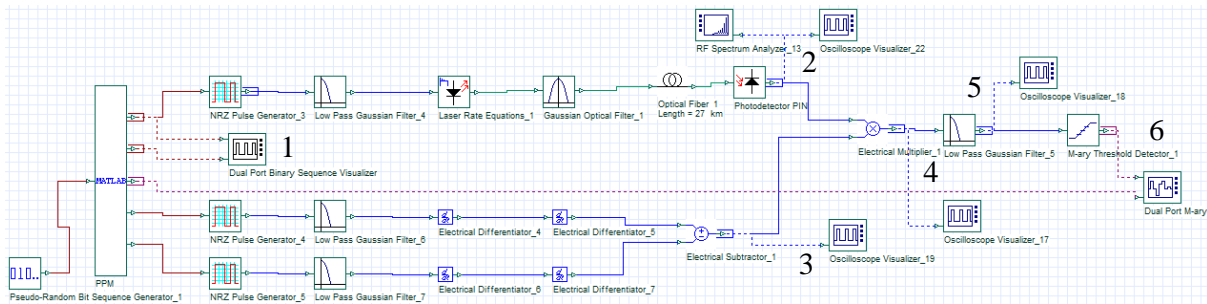


Figure 7.16: Simulation setup for PPM generation, transmission and detection.

First and before performing the PPM signal demodulation, it is interesting to repeat the experiment above, in the simulation and observe the electrical spectra for different τ and compare them to the measurement results from Fig 7.15. Therefore, a 1.25 Gbps PPM signal is generated at the first output of the “Matlab” coder and sent to the APD as before. Figure 7.17 shows the spectrum of the PPM signal at point 2 for different τ . As can be seen, the measurement and simulation results are in a very good agreement, which confirms the reliability of the simulation one more time. Next, in order to demonstrate the PPM signal detection, the case is chosen, in which the logical “1” is represented by “10000000” and the logical “0” is represented by “00001000”. The first and second outputs of the “Matlab” from Fig.7.16 are the coded and the original data sequences, respectively, which are compared together at point 1 (Fig. 7.18a). The coded signal is then modulated on the laser light, modified to UWB waveform and sent to the receiver. The PPM UWB signal is received by an APD at point 2 and illustrated in Fig.7.18b. The forth and fifth output of the “Matlab” are used to generate the template signal. The forth and fifth outputs are pulse trains of the fixed patterns “10000000” and “00001000”, respectively. By using a Gaussian LPF and two times differentiation, their waveform is shaped to doublet. After the subtraction at point 3, Eq.7.6 is realized (Fig. 7.18c). At point 4, the received signal from point 2 is downconverted through the multiplication with the template signal from point.3 (Fig.7.18d). A LPF with the 3-dB bandwidth of 950 MHz is employed to integrate the symbol energy over the frame duration at point 5 (Fig. 7.18e). At the end, the transmitted data is recovered by a threshold detector and compared to the original data at point 6 (Fig. 7.18f). As can be seen, the original data is exactly recovered in the receiver. Even though the PPM does not suffer from multipath effects as OOK, discrete frequency components still appear in its PSD and it is still a binary modulation format. It is noteworthy to mention,

7 Spectral efficiency and modulation format

that PPM can be expanded to M-ary format by using more than two positions to represent the data symbols, but then a costly and complicated receiver is required in order to perform the decorrelation.

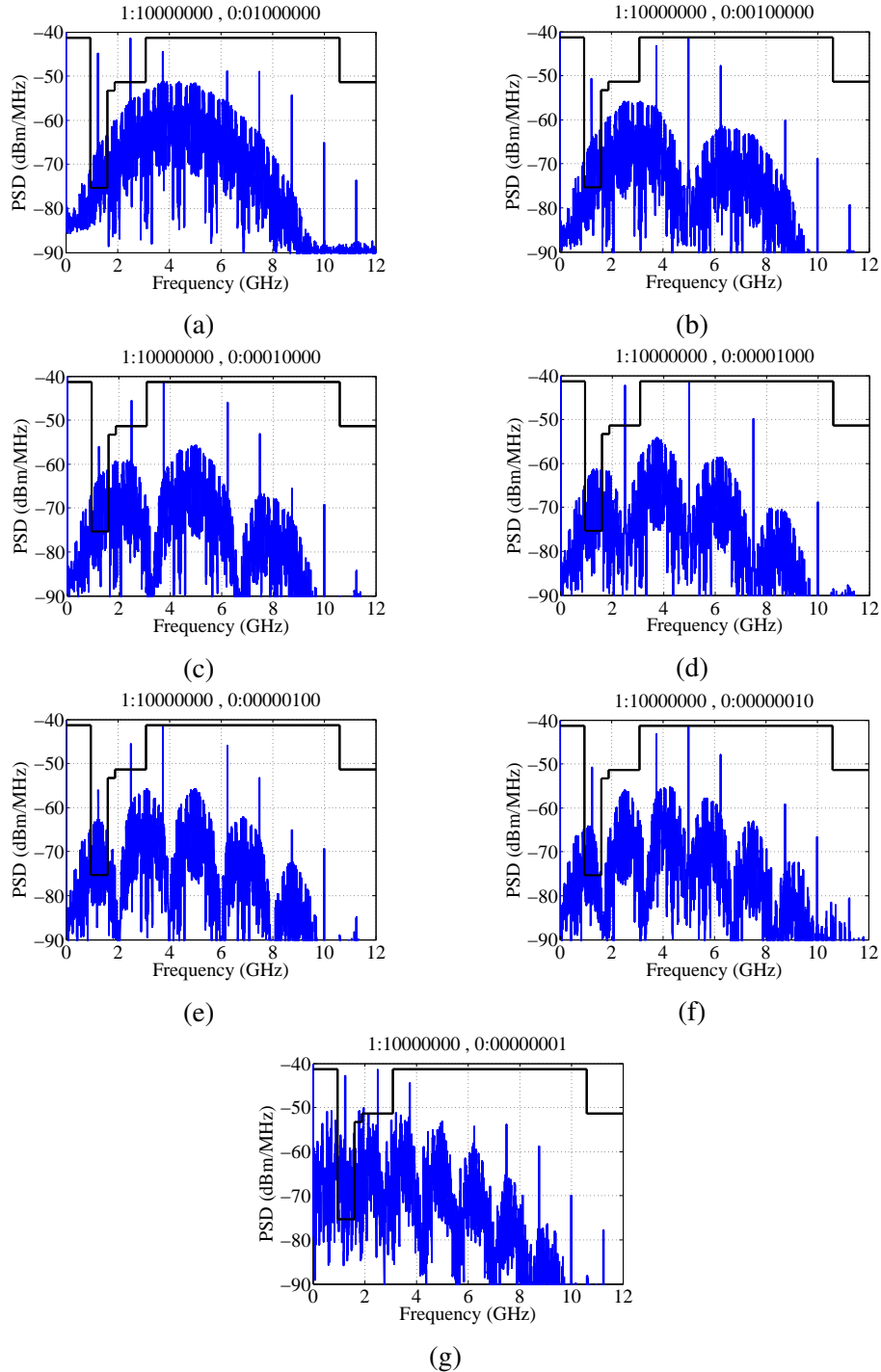


Figure 7.17: measured PPM spectrum for different τ .

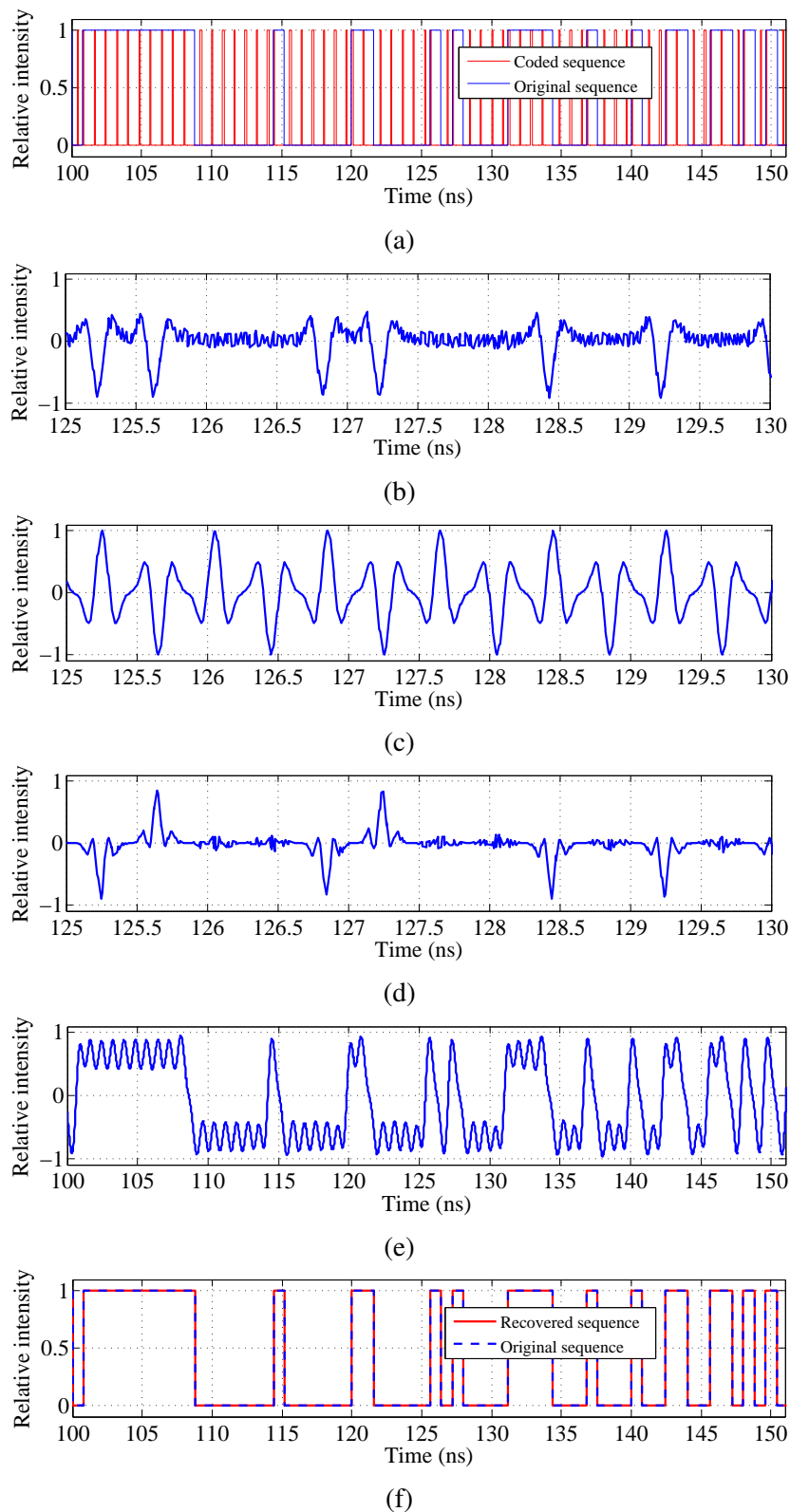


Figure 7.18: (a)Original and PPM coded sequences. (b)Received PPM signal. (c)Template signal. (d)Downconverted signal. (e)Obtained signal after lowpass filtering. (f)Recovered data and the original data.

7.2 Multipulse pulse position modulation

As discussed in Subsec. 7.1.4, the OOK is not the desired modulation method for IR-UWB communication due to its three major limitations: first, the detection of the absence of a pulse (i.e. “0”) due to multipath effects is very difficult. Second, the discrete frequency components appear in its PSD, which lead to a reduction of total power in order to avoid the violation of the FCC limit. Third, it is a binary modulation format and cannot be expanded to M-ary. In Subsec. 7.1.5, the PPM was studied as a solution for the first drawback. But the other two problems are still not answered. In this section a new modulation technique is proposed in order to address the mentioned drawbacks all at once. The new modulation format is called “multipulse pulse position modulation” (MPPPM). Even though the title “MPPPM” has been used in [99–101] and many other publications, to the best of the author’s knowledge, the proposed concept and aspect of the modulation and demodulation in this thesis are new.

7.2.1 Concept of MPPPM

In the conventional MPPPM, every symbol carries more than one bit, by sending more than one pulse within every frame duration and with different configurations [102]. This is demonstrated in Table 7.2. As can be seen, the binary modulation has been expanded to M-ary and transmitting more than one bit per symbol is possible through the classical MPPPM. However, this technique has two major drawbacks. First of all, the PSD of a classical MPPPM signal contains a huge portion of lowband frequency components, which is not suitable for UWB communication. This is due to the appearance of the pulses next to each other (i.e. “1100”), which leads to a larger total pulse width and makes the forming of IR-UWB impulses very difficult in fiber optic communication. Perhaps, this is the reason that the PSD of a MPPPM signal has never been mentioned in any publication considering the conventional MPPPM for UWBoF communication. The second problem of the conventional MPPPM is the higher cost and complexity of the receiver in comparison with the PPM which makes it unattractive for the communication industry [100, 102, 103].

Table 7.2: Coding scheme for classical MPPPM

Information bits	Classical MPPPM
11	0110
10	1001
01	1010
00	1100

A novel MPPPM coding based on Table 7.3, is proposed in this section. The same detection technique as PPM is required in order to receive and demodulate a coded signal based on the proposed MPPPM method. Therefore, regarding Eq.7.6, the constellation consists of positive and negative values. Furthermore, since an integration over the frame duration is performed before the threshold detection, the symbols containing three pulses will end up with a larger

intensity. Consequently, the constellation map shown in Fig. 7.19 is expected in the receiver for the proposed MPPPM coding technique.

Table 7.3: Coding scheme for proposed MPPPM

Information bits	proposed MPPPM
11	10101000
10	00100000
01	00010000
00	01010100

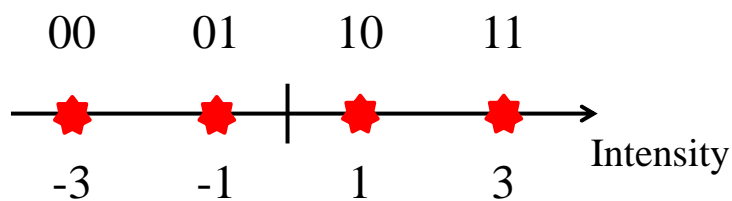


Figure 7.19: Constellation map of the proposed MPPPM coding in the receiver.

As it will be shown, the corresponding PSD of the new coding method complies with the FCC mask, the discrete spectral components are vanished, a higher order modulation format is enabled and yet the entire transmission and reception setup is the same as the PPM (Fig.7.16).

7.2.2 MPPPM signal generation and detection

In the first step, and the same as in Subsec. 7.1.4 and 7.1.5, the IR-UWB signal is generated experimentally in order to study its PSD. Figure 7.20 shows the experimental setup for proposed MPPPM coded IR-UWB signal generation. The setup is the same as Fig. 7.14. The only difference is the coding of the PPG. A 1.25 Giga symbol per second (Gsps) MPPPM coded electrical signal based on Table7.3 is generated by the PPG at 10 Gbps. Since every symbol represents two data bits, the total bit rate is 2.5 Gbps. With the same scenario as before, the optical signal is generated and sent to the receiver. The optical signal is detected by an APD and the electrical spectrum is captured by utilizing an ESA (Fig. 7.21). As can be seen, the discrete spectral components from 2 GHz to 8 GHz are completely vanished and this allows the continuous part to contain more power without violating the FCC regulation. As discussed earlier, this leads to a better receiver sensitivity. The only part of the spectrum violating the FCC limit, is the one from 0.96 GHz to 1.61 GHz, which can be simply filtered out by a well designed UWB antenna, without harming the data.

A simulation is performed in order to demonstrate the reception and demodulation of the proposed MPPPM coded signal. Figure 7.22 shows the simulation setup and as can be seen the setup is the same as the one from Fig. 7.16. In order to have a better vision, the original data sequence is mapped to the constellation points at the second output of the “Matlab” and is compared to the MPPPM coded signal from the first output of the “Matlab” at point 1

7 Spectral efficiency and modulation format

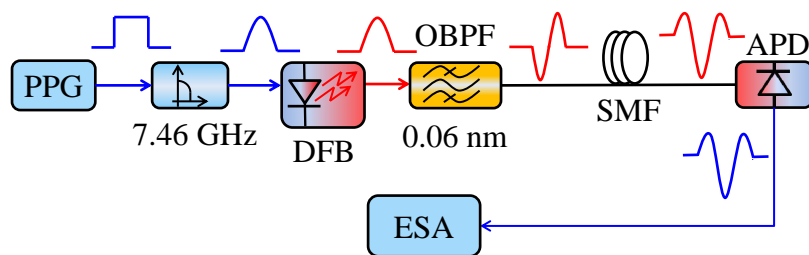


Figure 7.20: Experimental MPPPM signal generation.

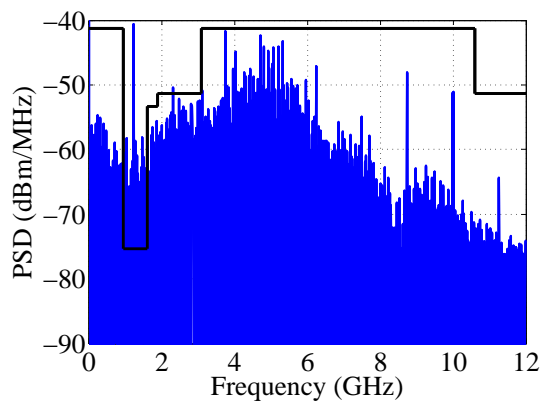


Figure 7.21: PSD of proposed MPPPM coded signal.

(Fig. 7.23). The IR-UWB pulses are formed and sent to the receiver with the same scenario as before. Figure 7.24 illustrates the electrical spectrum of the received signal at point 2, which is in good agreement with the experimental result shown in Fig. 7.21. The received electrical signal at point 2 is also depicted in Fig. 7.25. The fourth and fifth outputs of “Matlab” are pulse trains with the fixed patterns “1010100” and ‘0101010’, respectively. By using a LPF and two times differentiation, the waveform is modified into the doublet. The template signal is obtained at point 3, where the embedded one-pulse template signal is described by Eq. 7.6 (Fig. 7.26). The received signal at point 2 is multiplied by the template signal from point 3, by using an electrical mixer at point 4. (Fig. 7.27). By employing a LPF at point 5, the signal energy is integrated over the frame duration. As can be seen in Fig. 7.28, the frames containing more than one pulse per frame, end up with a larger intensity after the lowpass filtering. Finally, the recovered data after the threshold detector at point 6 are compared to the original data from the third output of the “Matlab” (Fig. 7.29). As can be seen, the original data is exactly recovered in the receiver. Even though the constellation of the MPPPM signal after the demodulation looks like a PAM signal, the proposed MPPPM technique does not suffer from the same problem explained in Subsec. 7.1.1 for PAM. This is because the information is not modulated on the amplitude of the pulses, but on the position and number of pulses in a frame duration.

7.2 Multipulse pulse position modulation

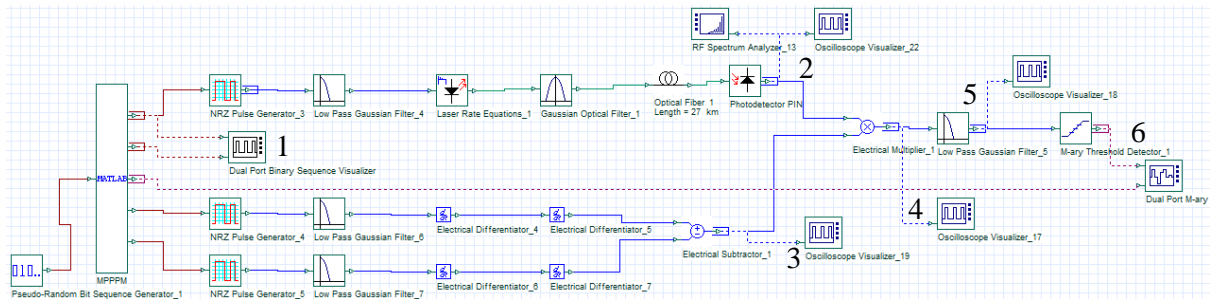


Figure 7.22: Simulation setup for MPPPM coded signal.

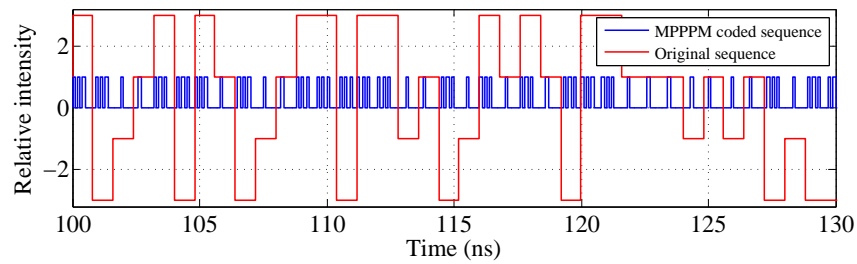


Figure 7.23: MPPPM coded signal and constellation mapped original signal.

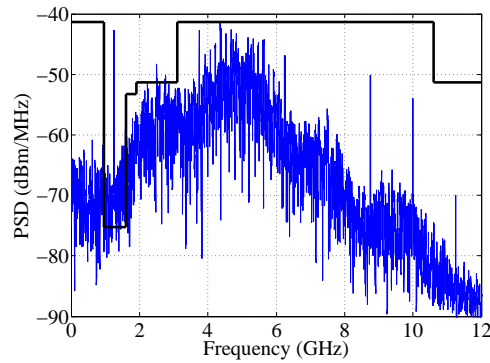


Figure 7.24: PSD of simulated MPPPM coded signal.

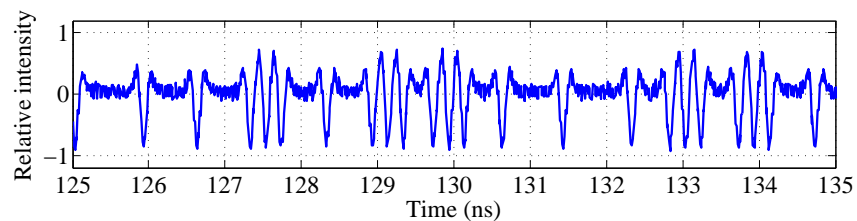


Figure 7.25: Received MPPPM IR-UWB signal after APD.

7 Spectral efficiency and modulation format

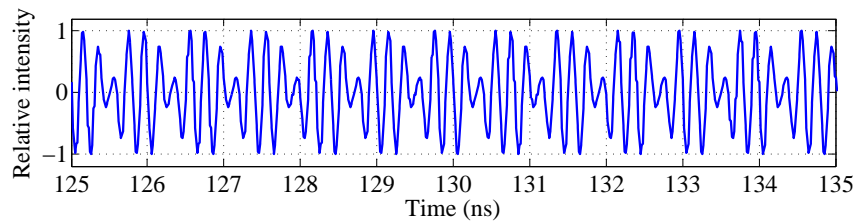


Figure 7.26: Template signal.

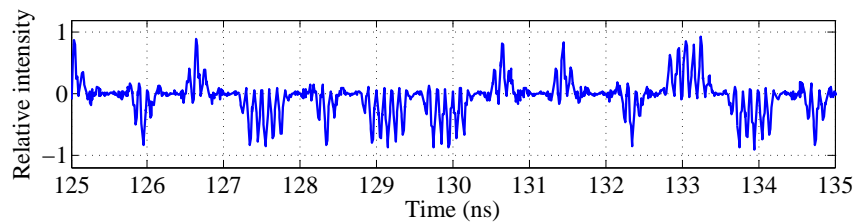


Figure 7.27: Downconverted signal.

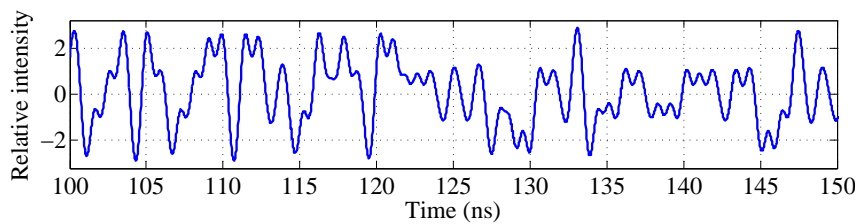


Figure 7.28: Obtained signal after lowpass filtering.

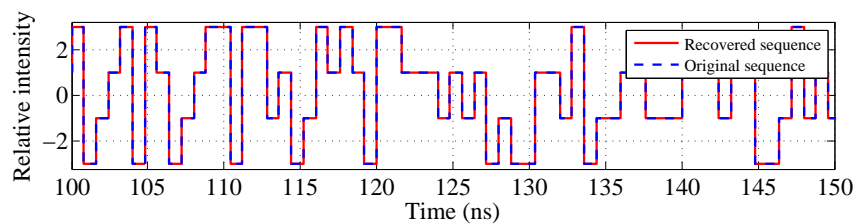


Figure 7.29: Recovered and original data.

7.3 Summary

An overview about the conventional modulation techniques for UWBoF communication was performed. It was explained that PAM, BPM and PSM cannot be employed for data modulation in the proposed transmitter. The performance of the OOK method was analyzed experimentally as well as through the simulation. The three main drawbacks of OOK were concluded in:

1. Challenging determination of the absence of a pulse (i.e. “0”), due to the echoes of the

original pulses in the presence of multipath effects. 2. Being binary and not capable to carry more than one bit per symbol. 3. Large discrete frequency components in the corresponding PSD. Next, the PPM was studied as an alternative for OOK. It was demonstrated that even though the PPM does not suffer from the first problem, the other two are not addressed by PPM. A new modulation technique based on the position and number of the impulses in every frame duration was proposed. The new method was called multipulse pulse position modulation (MPPPM). The generation and transmission of a 2.5 Gbps MPPPM coded IR-UWB signal was experimentally performed. The signal reception and demodulation was explained with the help of a simulation. It was demonstrated that the proposed scheme does not suffer from any of the aforementioned drawbacks.

Chapter 8

Conclusion and Outlook

8.1 Conclusion

As stated in the beginning of this dissertation, growing impact of the mobile data trafficking on modern life is undeniable. By the increasing penetration of handheld devices such as smart phones, tablets, laptops and notebooks in the modern world, the demand for high bandwidth in wireless communication has been growing rapidly. This has put a tremendous pressure on the communication industry and has allowed for new research opportunities, in order to cope with this data traffic avalanche and eventually satisfy the demand for high data rate.

One of the strongest solutions for meeting this growing demand is the deployment of optical fibers and photonic technologies in access and in-building networks as the transmission medium for both wired and wireless services. Accordingly, RoF has been introduced and is playing a crucial role in fiber distributed antenna systems. On the other hand, the next generation WLAN and WPAN are expected to have less complexity, be less expensive, consume less power and offer wireless connectivity at a bit rate exceeding 1 Gbps. UWB technology is proposed as a promising approach to fulfilling these requirements due to its low power consumption, immunity to multipath fading, interference mitigation, being carrier free, offering high data rates and capability to penetrate through obstacles.

This dissertation has focused on UWBoF technology for broadband indoor communication application. Accordingly, in this thesis, a novel concept for photonic generation of the gigabit UWB signal, fiber transmission and wireless communication has been proposed. The proposed technique has targeted the requirements and demands of the future fiber optic based indoor wireless communication.

Direct modulation of a semiconductor laser in combination with optical filtering was proven to be able to generate different UWB pulse shapes. Starting from the basics of intensity modulation and frequency modulation of the directly modulated laser, a derivative operation was performed after FM-to-IM conversion in an optical filter. Monocycle pulse generation was experimentally demonstrated, wireless transmission was performed and BER was measured.

It was experimentally demonstrated that in association with the accumulative fiber dispersion, doublet pulses can be obtained. It was proven that the transmitter can be adapted for different fiber transmission distances, by controlling the signal chirp. For different fiber lengths,

8 Conclusion and Outlook

the laser chirp had to be controlled (by changing the laser modulation amplitude) in order to keep the accumulative chromatic dispersion constant. Fidelity factor results showed that when the transmission distance increases from 19 km to 57 km, doublet pulse can be achieved with a fidelity of at least 0.95, if the laser modulation amplitude is decreased from 1.2 V to 0.5 V. The BER performance after the wireless transmission of generated doublets showed an error-free transmission.

The transmitter was developed further in order to be integrated into the TDM-PON. The chirp behavior of the CML was measured and studied. Based on the chirp analysis, the bias point of the laser was controlled through a burst signal with different amplitudes for the different time slots of the TDM architecture. By a proper selection of the burst amplitudes, 10 Gbps NRZ and 1.25 Gbps UWB signals were generated from a single light source at different time slots in the TDM architecture. The BER measurement was performed and an error free transmission was successfully demonstrated.

A bidirectional UWBoF system compatible with WDM-PON was presented. The 6th order Gaussian derivative was generated experimentally for UWB transmission in the downstream scenario by taking advantage of the interference effect of a DLI in the ONU. A 1.25 Gbps UWB transmission over 25 km of SMF was performed for the downstream scenario and an error free transmission was obtained. For the upstream scenario a colorless FP-LD was injection locked, by the second output of the DLI and a clear optical carrier was established. Data erasing of the upstream carrier was demonstrated. A 1.25 Gbps NRZ transmission over 25 km of SMF was performed by the direct modulation of the injection locked FP-LD and an error free transmission was demonstrated. The experiment was successfully repeated for the symmetric transmission distance over 60 km of SMF, proving that the transmitter can be adjusted with respect to the fiber length by controlling the laser operation point.

The classical UWBoF modulation formats were briefly reviewed. It was explained that the modulation techniques such as PAM, BPM and PSM cannot be used to modulate the data in the proposed transmitter. As the main used modulation technique in the entire thesis was OOK, its drawbacks were investigated and highlighted. A new modulation technique was proposed based on the position and number of the impulses in each frame duration. The new method was called multipulse pulse position modulation (MPPPM). The generation and transmission of a 2.5 Gbps MPPPM coded IR-UWB signal was experimentally performed. The signal reception and demodulation was explained with the help of a simulation. It was demonstrated that the proposed scheme improves the spectral efficiency by enabling M-ary modulation and optimizing the PSD of the signal for the FCC regulation.

8.2 Outlook

All WDM-PON approaches try to solve one of the main challenges which is to provide cost effective light sources at the OLT. Tunable vertical-cavity surface-emitting lasers (VCSEL) are highly desirable components for WDM-PON networks for several reasons. For instance, in order to supply a 100-channel WDM system, one would need 100 different DFB lasers with fixed wavelengths. This matter leads to several disadvantages. First, the laser manufacturers would need to introduce expensive selection processes for supplying the ONUs with lasers

of the appropriate wavelength. Moreover, the network operators would need to stock many different lasers and keep inventories of spare parts for each laser wavelength in the event that transmitters fail in the field and need to be replaced. A tunable VCSEL would be able to compensate all of these disadvantages [104]. The significant advantages of VCSELs compared with the conventional DFB lasers include considerably lower production costs, smaller threshold- and driving current and consequently lower power consumption, higher direct digital modulation rate, smaller footprint, wafer-level testing, efficient fiber coupling (due to circular-symmetric Gaussian beam profile), much shorter cavity length enabling larger free spectral range (FSR), and easier micro electro mechanical system (MEMS) integration [64]. The aspect of having wide, continuous and mode-hop free tuning around a telecommunication band enhances the reliability of the system and reduces its costs. The proposed UWBoF scheme in this dissertation can be developed further by changing the semiconductor type from edge-emitting DFB working at a fixed predetermined wavelength, to a wavelength tunable MEMS-VCSEL. The photonics group of TU-Darmstadt is the pioneer in fabricating the tunable MEMS-VCSELs with over 60 nm tunability [64]. This will open a new research opportunity in FM-IM conversion based UWBoF.

All in all, the results from this dissertation make hybrid PON more realizable for the fiber optic based communication industry. This was demonstrated by the fact that NRZ and UWB can be generated from only a single light source, the transmitter can be adjusted for different fiber lengths installed in optical access network infrastructures, simple and inexpensive RAUs can be easily implemented, the system is compatible with hybrid PON, and it can also be upgraded for the future PON.

List of Figures

1.1	PON standardization roadmap [8]. EPON: ethernet passive optical network, GPON: gigabit passive optical network, 10GE-PON: 10 Gbps ethernet passive optical network, XG-PON: 10-gigabit-capable passive optical network, NG-PON1: The first next-generation passive optical network, NG-PON2: The second next-generation passive optical network.	2
1.2	Throughput and allocated frequency of some wireless services. UWB: ultra-wide band, GSM: Global System for Mobile Communications, LTE: Long Term Evolution, UMTS: Universal Mobile Telecommunications System, WiMAX: Worldwide Interoperability for Microwave Access.	4
1.3	Wireless technology trends Ref. [12], Fig. 1.	5
1.4	Cisco Forecasts 49 Exabytes per month of mobile data by 2021 [13].	6
1.5	Devices responsible for mobile data traffic growth (Laptops and smartphones lead traffic growth) [13].	6
2.1	FCC emission limit for indoor UWB systems.	12
2.2	UWB intended bands for communications for different regions (Ref. [21], Fig. 1).	13
2.3	RoF architecture.	16
3.1	Examples of derivatives of Gaussian pulse.	21
3.2	PSD of higher order derivatives of Gaussian pulses.	22
3.3	Peak frequency versus pulse shaping factor.	22
3.4	Bandwidth versus pulse shaping factor.	23
3.5	UWB pulse generator based on PM-IM conversion (Ref. [35], Fig. 6).	24
3.6	Concept of two- or three-tap delay line generation of an IR-UWB pulse (Ref. [35], Fig. 8 and Fig. 11).	25
3.7	Concept of two MZMs biased at complementary slopes (Ref. [47], Fig. 2).	26
3.8	UWB monocycle generation based on a two-tap photonic microwave delay-line filter using an SOA (Ref. [34], Fig. 19).	27
3.9	UWB monocycle generation using a two-tap microwave delay-line filter based on a PolM. (Ref. [34], Fig. 21).	27
3.10	(a) Block diagram of the all-fiber UWB signal generation system. (b) All-fiber spectrum shaper configuration. EDFA: erbium-doped fiber amplifier. OC: optical coupler (Ref. [59], Fig. 1).	28
3.11	Block diagram of the UWB waveform generator (Ref. [61], Fig. 3).	29

LIST OF FIGURES

4.1	Optical UWB signal generation based on direct modulation of semiconductor laser.	34
4.2	(a) Optical FM and IM generated by a directly modulated semiconductor laser, (b) Optical FM-to-IM conversion by the optical band-pass filter, (c) Optical waveform at the filter output. Δf : frequency deviation, $15 \text{ ps} < \tau < 25 \text{ ps}$ (Ref. [74], Fig. 1).	35
4.3	(a) Output of the modeled DFB. (b) Output of the modeled OBPF.	36
4.4	Monocycle generation based on FM-IM conversion.	36
4.5	Obtained monocycle pulse and corresponding spectrum.	37
4.6	UWB spiral antenna and corresponding S_{21}	38
4.7	Received pulse after wireless transmission and corresponding spectrum.	38
4.8	(a) Log(BER) vs. received optical power. (b) Receiver sensitivity for different frequency components.	39
4.9	Doublet generation using chromatic dispersion in SMF associated with the laser chirp.	40
4.10	Obtained pulse shapes at different fiber lengths. (a) Calculation. (b) Experiment.	41
4.11	Obtained doublet pulse and corresponding spectrum after 25 km fiber transmission.	42
4.12	(a) Chirp measurement. (b) Fidelity vs. fiber length.	42
4.13	Received pulse after wireless transmission and corresponding spectrum.	43
4.14	(a) Log(BER) vs. received optical power. (b) Receiver sensitivity for different lengths of fiber.	43
5.1	Downstream TDM-PON traffic.	47
5.2	Chirp versus modulation frequency.	49
5.3	Semiconductor laser chirp behavior in burst mode.	50
5.4	Common transmitter for NRZ and UWB generation.	51
5.5	Bias burst signal.	51
5.6	Transmitter output, (a) UWB and (b) NRZ.	51
5.7	Receivers (a) NRZ and (b) UWB.	53
5.8	Gate control signal.	53
5.9	(a) Detected NRZ after APD. (b) Detected UWB after APD.	53
5.10	Log(BER) vs. received optical power in upstream scenario (a) 10 Gbps NRZ, (b) 1.25 Gbps UWB.	54
5.11	Burst signal.	55
5.12	(a) transmitter output and (b) received signal after APD.	55
5.13	Log(BER) vs. received optical power in downstream scenario (a) 10 Gbps NRZ, (b) 1.25 Gbps UWB.	56
6.1	Proposed wavelength reused UWBoF over WDM-PON architecture.	60
6.2	(a) Applied electrical signal to DML. (b) Output of modeled directly modulated DFB.	61
6.3	(a) Output of the modeled OBPF. (b) Output of the modeled fiber.	61

LIST OF FIGURES

6.4	Optical FM-to-IM conversion by optical filtering.	62
6.5	Outputs of the DLI and corresponding spectrum, (a) first output and (b) second output.	62
6.6	Experimental setup of the proposed wavelength resued UWBoF system.	63
6.7	(a) Applied electrical signal to CML (b) CML output.	64
6.8	Obtained pulse shape, (a) after fiber transmission, (b) DLI output.	64
6.9	Electrical waveform and corresponding spectrum (a) before wireless transmission and (b) after wireless transmission.	65
6.10	(a) Log(BER) vs. received optical power after 25 km SMF. (b) Comparision of BER performance after 25 km and 60 km SMF.	66
6.11	FP-LD spectrum.	67
6.12	Spectrum of the injecting signal.	67
6.13	(a) Injection locked FP-LD. (b) SMSR vs. injection power.	67
6.14	Waveform and electrical spectrum, (a) before injection locking and (b) after injection locking.	68
6.15	(a) The temporal waveform of the US carrier after photodetection and low-pass filtering. (b) Electrical spectrum of the US carrier.	69
6.16	Upstream BER measurement.	69
7.1	Schematic of a PAM signal.	73
7.2	Schematic of a BPM signal.	74
7.3	Schematic of a PSM signal.	74
7.4	Schematic of a OOK signal.	75
7.5	OOK IR-UWB transmission.	76
7.6	PSD of OOK signal.	76
7.7	Simulation setup for OOK transmission.	76
7.8	Original data and coded data.	77
7.9	(a)Modulated laser output and corresponding chirp. (b)Monocycle pulses after OBPF.	77
7.10	(a)Obtained doublet and (b)corresponding spectrum.	78
7.11	(a)Downconverted signal and (b)corresponding spectrum.	78
7.12	(a)Detected lowband signal after lowpass filtering. (b) Recovered data and the original data.	78
7.13	Schematic of a PPM signal.	79
7.14	Experimental PPM signal generation.	79
7.15	measured PPM spectrum for different τ	80
7.16	Simulation setup for PPM generation, transmission and detection.	81
7.17	measured PPM spectrum for different τ	82
7.18	(a)Original and PPM coded sequences. (b)Received PPM signal. (c)Template signal. (d)Downconverted signal. (e)Obtained signal after lowpass filtering. (f)Recovered data and the original data.	83
7.19	Constellation map of the proposed MPPPM coding in the receiver.	85
7.20	Experimental MPPPM signal generation.	86
7.21	PSD of proposed MPPPM coded signal.	86

LIST OF FIGURES

7.22	Simulation setup for MPPPM coded signal.	87
7.23	MPPPM coded signal and constellation mapped original signal.	87
7.24	PSD of simulated MPPPM coded signal.	87
7.25	Received MPPPM IR-UWB signal after APD.	87
7.26	Template signal.	88
7.27	Downconverted signal.	88
7.28	Obtained signal after lowpass filtering.	88
7.29	Recovered and original data.	88

List of Tables

2.1	UWB APPLICATION IN MILITARY AND COMMERCIAL SECTORS [24]	15
4.1	PARAMETERS FOR 1550 nm DFB LASERS [71]	34
4.2	FIDELITY FOR MEASURED AND THEORETICAL WAVEFORMS	39
7.1	Categorization of modulation techniques for UWBoF communication	72
7.2	Coding scheme for classical MPPPM	84
7.3	Coding scheme for proposed MPPPM	85

Bibliography

- [1] “White paper: Cisco VNI Forecast and Methodology, 2015-2021,” CISCO, Tech. Rep., 2016.
- [2] D. Nessel, “PON Roadmap [Invited],” *J. Opt. Commun. Netw.*, vol. 9, no. 1, pp. A71–A76, Jan 2017.
- [3] K. i. Sato and H. Hasegawa, “Optical Networking Technologies That Will Create Future Bandwidth-Abundant Networks [Invited],” *IEEE/OSA Journal of Optical Communications and Networking*, vol. 1, no. 2, pp. A81–A93, July 2009.
- [4] H. Rohde, S. Smolorz, E. Gottwald, and K. Kloppe, “Next generation optical access: 1 Gbit/s for everyone,” in *2009 35th European Conference on Optical Communication*, Sept 2009, pp. 1–3.
- [5] C. Lin, *Broadband Optical Access Networks and Fiber-to-the-Home: Systems Technologies and Deployment Strategies*. John Wiley & Sons Ltd, 2006.
- [6] J. Prat, *Next-Generation FTTH Passive Optical Networks*, J. Prat, Ed. Springer, 2008.
- [7] A. Banerjee, Y. Park, F. Clarke, H. Song, S. Yang, G. Kramer, K. Kim, and B. Mukherjee, “Wavelength-division-multiplexed passive optical network (WDM-PON) technologies for broadband access: a review [Invited],” *J. Opt. Netw.*, vol. 4, no. 11, pp. 737–758, Nov 2005.
- [8] FSAN Standard Roadmap 2.0. [Online]. Available: <https://www.fsan.org/roadmap/>
- [9] P. K. Bondyopadhyay, “Guglielmo Marconi - The father of long distance radio communication - An engineer’s tribute,” in *1995 25th European Microwave Conference*, vol. 2, Sept 1995, pp. 879–885.
- [10] C. Park and T. S. Rappaport, “Short-Range Wireless Communications for Next-Generation Networks: UWB, 60 GHz Millimeter-Wave WPAN, And ZigBee,” *IEEE Wireless Communications*, vol. 14, no. 4, pp. 70–78, August 2007.
- [11] M. Jacobsson, I. Niemegeers, and S. H. d. Groot, *Personal Networks: Wireless Networking for Personal Devices*. John Wiley & Sons, Ltd, 2010.

-
- [12] A. Ng'oma, H. Yang, and J. George, "Integrated fiber-wireless networks: What, why and how," in *AFRICON, 2011*, Sept 2011, pp. 1–6.
- [13] "White paper : Cisco Visual Networking Index: Global Mobile Data Traffic Forecast Update, 2016 - 2021," CISCO, Tech. Rep., 2016.
- [14] K. David, D. Dixit, and N. Jefferies, "2020 Vision," *IEEE Vehicular Technology Magazine*, vol. 5, no. 3, pp. 22–29, Sept 2010.
- [15] R. Bendlin, T. Ekpenyoung, and D. Greenstret, "White paper: Paving the path for wireless capacity expansion," Texas Instruments Incorporated, Tech. Rep., February 2012.
- [16] J. Foerster, E. Green, S. Somayazulu, and D. Leeper, "Ultra-Wideband Technology for Short-or Medium-Range Wireless Communications," *Intel Technology Journal*, vol. 2, pp. 1–11, 2001.
- [17] Z. Sahinoglu, S. Gezici, and I. Gvenc, *Ultra-wideband Positioning Systems: Theoretical Limits, Ranging Algorithms, and Protocols*. New York, NY, USA: Cambridge University Press, 2011.
- [18] C. c. Chong, F. Watanabe, and H. Inamura, "Potential of UWB Technology for the Next Generation Wireless Communications," in *2006 IEEE Ninth International Symposium on Spread Spectrum Techniques and Applications*, Aug 2006, pp. 422–429.
- [19] S. Gezici and H. V. Poor, "Position Estimation via Ultra-Wide-Band Signals," *Proceedings of the IEEE*, vol. 97, no. 2, pp. 386–403, Feb 2009.
- [20] A. Yarovoy, "Ultra-Wideband Systems," in *2003 33rd European Microwave Conference*, Oct 2003, pp. 597–600.
- [21] J. R. Fernandes and D. Wentzloff, "Recent advances in IR-UWB transceivers: An overview," in *Proceedings of 2010 IEEE International Symposium on Circuits and Systems*, May 2010, pp. 3284–3287.
- [22] U.S. Federal Communications Commission, "Revision of Part 15 of the Commissions Rules Regarding Ultra-Wideband Transmission Systems," *First Report and Order, ET Docket 98-153*, April 2002.
- [23] M.-G. D. Benedetto and G. Giancola, *Understanding Ultra Wide Band Radio Fundamentals*. Upper Saddle River, NJ, USA: Prentice Hall Press, 2004.
- [24] F. Nekoogar, *Ultra-wideband Communications: Fundamentals and Applications*, 1st ed. Upper Saddle River, NJ, USA: Prentice Hall Press, 2005.
- [25] M. Ghavami, L. Michael, and R. Kohno, *Ultra Wideband Signals and Systems in Communication Engineering*. Jhon Wiley & Sons, Ltd, 2007.
- [26] H. Nikookar, *Introduction to Ultra Wideband for Wireless Communications*. Springer Netherlands, 2010.

BIBLIOGRAPHY

- [27] X. Chen, S. Xu, H. Yin, and W. Wang, "Potential of IR-UWB Technology for Ubiquitous Computing," in *2009 5th International Conference on Wireless Communications, Networking and Mobile Computing*, Sept 2009, pp. 1–6.
- [28] R. S. Kshetrimayum, "An introduction to UWB communication systems," *IEEE Potentials*, vol. 28, no. 2, pp. 9–13, March 2009.
- [29] S. Gezici, "A survey on wireless position estimation," *Wireless personal communications*, vol. 44, no. 3, pp. 263–282, 2008.
- [30] A. A. M. Saleh, A. Rustako, and R. Roman, "Distributed Antennas for Indoor Radio Communications," *IEEE Transactions on Communications*, vol. 35, no. 12, pp. 1245–1251, December 1987.
- [31] H. B. Kim and A. Wolisz, "A Radio over Fiber Based Wireless Access Network Architecture for Rural Areas," in *14th IST Mobile and Wireless Communications Summit*, 2005.
- [32] D. Mynbaev and L. Scheiner, *Fiber-optic Communications Technology*. Prentice Hall, 2001. [Online]. Available: <https://books.google.de/books?id=o3CFQgAACAAJ>
- [33] H. Al-Raweshidy and S. Komaki, *Radio over Fiber Technologies for Mobile Communications Networks*. Artech House, 2002.
- [34] J. Yao, F. Zeng, and Q. Wang, "Photonic Generation of Ultrawideband Signals," *J. Lightwave Technol.*, vol. 25, no. 11, pp. 3219–3235, Nov 2007.
- [35] J. Yao, "Photonics for ultrawideband communications," *IEEE Microwave Magazine*, vol. 10, no. 4, pp. 82–95, June 2009.
- [36] S. Pan and J. Yao, "UWB-Over-Fiber Communications: Modulation and Transmission," *Journal of Lightwave Technology*, vol. 28, no. 16, pp. 2445–2455, Aug 2010.
- [37] H. Sheng, P. Orlik, A. M. Haimovich, L. J. Cimini, and J. Zhang, "On the spectral and power requirements for ultra-wideband transmission," in *Communications, 2003. ICC '03. IEEE International Conference on*, vol. 1, May 2003, pp. 738–742 vol.1.
- [38] A. Popa, "An Optimization of Gaussian UWB Pulses," *Development and Application Systems*, p. 50, 2010.
- [39] S. Wang, H. Chen, M. Xin, M. Chen, and S. Xie, "Optical ultra-wide-band pulse bipolar and shape modulation based on a symmetric PM-IM conversion architecture," *Opt. Lett.*, vol. 34, no. 20, pp. 3092–3094, Oct 2009. [Online]. Available: <http://ol.osa.org/abstract.cfm?URI=ol-34-20-3092>
- [40] F. Zeng and J. Yao, "An approach to ultrawideband pulse generation and distribution over optical fiber," *IEEE Photonics Technology Letters*, vol. 18, no. 7, pp. 823–825, April 2006.

- [41] ———, “Optical Generation and Distribution of UWB Signals (Invited Paper),” in *2006 International Conference on Communications, Circuits and Systems*, vol. 3, June 2006, pp. 2024–2029.
- [42] F. Zeng, Q. Wang, and J. Yao, “All-optical UWB impulse generation based on cross-phase modulation and frequency discrimination,” *Electronics Letters*, vol. 43, no. 2, pp. 121–122, January 2007.
- [43] J. Dong, X. Zhang, J. Xu, D. Huang, S. Fu, and P. Shum, “Ultrawideband monocycle generation using cross-phase modulation in a semiconductor optical amplifier,” *Opt. Lett.*, vol. 32, no. 10, pp. 1223–1225, May 2007. [Online]. Available: <http://ol.osa.org/abstract.cfm?URI=ol-32-10-1223>
- [44] F. Liu, T. Wang, Z. Zhang, M. Qiu, and Y. Su, “On-chip photonic generation of ultrawideband monocycle pulses,” *Electronics Letters*, vol. 45, no. 24, pp. 1247–1249, November 2009.
- [45] J. Yao, “A Tutorial on Microwave Photonics,” *IEEE Photon. Soc. Newsletter*, vol. 26, no. 2, pp. 4–12, Apr 2012.
- [46] S. Sales, J. Capmany, J. Marti, and D. Pastor, “Experimental demonstration of fibre-optic delay line filters with negative coefficients,” *Electronics Letters*, vol. 31, no. 13, pp. 1095–1096, Jun 1995.
- [47] Y. Yu, J. Dong, X. Li, and X. Zhang, “Ultra-Wideband Generation Based on Cascaded Mach-Zehnder Modulators,” *IEEE Photonics Technology Letters*, vol. 23, no. 23, pp. 1754–1756, Dec 2011.
- [48] M. Bolea, J. Mora, B. Ortega, and J. Capmany, “Optical UWB pulse generator using an N tap microwave photonic filter and phase inversion adaptable to different pulse modulation formats,” *Opt. Express*, vol. 17, no. 7, pp. 5023–5032, Mar 2009. [Online]. Available: <http://www.opticsexpress.org/abstract.cfm?URI=oe-17-7-5023>
- [49] ———, “High-order UWB pulse generation based on a microwave photonic filter using incoherent optical sources,” in *2011 International Topical Meeting on Microwave Photonics jointly held with the 2011 Asia-Pacific Microwave Photonics Conference*, Oct 2011, pp. 462–465.
- [50] J. Li, S. Fu, K. Xu, J. Wu, J. Lin, M. Tang, and P. Shum, “Photonic ultrawideband monocycle pulse generation using a single electro-optic modulator,” *Opt. Lett.*, vol. 33, no. 3, pp. 288–290, Feb 2008. [Online]. Available: <http://ol.osa.org/abstract.cfm?URI=ol-33-3-288>
- [51] J. Li, K. Xu, S. Fu, M. Tang, P. Shum, J. Wu, and J. Lin, “Photonic Polarity-Switchable Ultra-Wideband Pulse Generation Using a Tunable Sagnac Interferometer Comb Filter,” *IEEE Photonics Technology Letters*, vol. 20, no. 15, pp. 1320–1322, Aug 2008.

BIBLIOGRAPHY

- [52] Q. Wang, F. Zeng, S. Blais, and J. Yao, "Optical ultrawideband monocycle pulse generation based on cross-gain modulation in a semiconductor optical amplifier," *Opt. Lett.*, vol. 31, no. 21, pp. 3083–3085, Nov 2006. [Online]. Available: <http://ol.osa.org/abstract.cfm?URI=ol-31-21-3083>
- [53] H. Chen, M. Chen, C. Qiu, J. Zhang, and S. Xie, "UWB monocycle pulse generation by optical polarisation time delay method," *Electronics Letters*, vol. 43, no. 9, pp. 542–543, April 2007.
- [54] H. Chen, M. Chen, C. Qiu, and S. Xie, "A Novel Composite Method for Ultra-Wideband Doublet Pulses Generation," *IEEE Photonics Technology Letters*, vol. 19, no. 24, pp. 2021–2023, Dec 2007.
- [55] H. Chen, M. Chen, J. Zhang, and S. Xie, "UWB monocycle and doublet pulses generation in optical domain," in *Microwave Photonics, 2007 International Topical Meeting on*, Oct 2007, pp. 145–148.
- [56] H. Chen, M. Chen, T. Wang, M. Li, and S. Xie, "Methods for Ultra-Wideband Pulse Generation Based on Optical Cross-Polarization Modulation," *Journal of Lightwave Technology*, vol. 26, no. 15, pp. 2492–2499, Aug 2008.
- [57] Q. Wang and J. Yao, "Switchable optical UWB monocycle and doublet generation using a reconfigurable photonic microwave delay-line filter," *Opt. Express*, vol. 15, no. 22, pp. 14 667–14 672, Oct 2007. [Online]. Available: <http://www.opticsexpress.org/abstract.cfm?URI=oe-15-22-14667>
- [58] J. Chou, Y. Han, and B. Jalali, "Adaptive RF-photonic arbitrary waveform generator," *IEEE Photonics Technology Letters*, vol. 15, no. 4, pp. 581–583, April 2003.
- [59] C. Wang, F. Zeng, and J. Yao, "All-Fiber Ultrawideband Pulse Generation Based on Spectral Shaping and Dispersion-Induced Frequency-to-Time Conversion," *IEEE Photonics Technology Letters*, vol. 19, no. 3, pp. 137–139, Feb 2007.
- [60] M. Abtahi, M. Mirshafiei, J. Magne, L. A. Rusch, and S. LaRochelle, "Ultra-Wideband Waveform Generator Based on Optical Pulse-Shaping and FBG Tuning," *IEEE Photonics Technology Letters*, vol. 20, no. 2, pp. 135–137, Jan 2008.
- [61] M. Abtahi, J. Magne, M. Mirshafiei, L. A. Rusch, and S. LaRochelle, "Generation of Power-Efficient FCC-Compliant UWB Waveforms Using FBGs: Analysis and Experiment," *Journal of Lightwave Technology*, vol. 26, no. 5, pp. 628–635, March 2008.
- [62] V. Torres-Company, K. Prince, and I. T. Monroy, "Fiber transmission and generation of ultrawideband pulses by direct current modulation of semiconductor lasers and chirp-to-intensity conversion," *Opt. Lett.*, vol. 33, no. 3, pp. 222–224, Feb 2008. [Online]. Available: <http://ol.osa.org/abstract.cfm?URI=ol-33-3-222>

- [63] ———, “Ultrawideband Pulse Generation Based on Overshooting Effect in Gain-Switched Semiconductor Laser,” *IEEE Photonics Technology Letters*, vol. 20, no. 15, pp. 1299–1301, Aug 2008.
- [64] S. Paul, C. Gierl, J. Cesar, Q. T. Le, M. Malekizandi, B. Kögel, C. Neumeyr, M. Ortsiefer, and F. Küppers, “10-Gb/s Direct Modulation of Widely Tunable 1550-nm MEMS VCSEL,” *IEEE Journal of Selected Topics in Quantum Electronics*, vol. 21, no. 6, pp. 436–443, Nov 2015.
- [65] T. L. Paoli and J. E. Ripper, “Direct modulation of semiconductor lasers,” *Proceedings of the IEEE*, vol. 58, no. 10, pp. 1457–1465, Oct 1970.
- [66] R. Tucker, “High-speed modulation of semiconductor lasers,” *Journal of Lightwave Technology*, vol. 3, no. 6, pp. 1180–1192, Dec 1985.
- [67] J. Bowers, “High speed semiconductor laser design and performance,” *Solid-State Electronics*, vol. 30, no. 1, pp. 1 – 11, 1987, special Issue-Optoelectronics. [Online]. Available: <http://www.sciencedirect.com/science/article/pii/0038110187900232>
- [68] R. Olshansky, P. Hill, V. Lanzisera, and W. Powazinik, “Frequency response of 1.3 micro meter InGaAsP high speed semiconductor lasers,” *IEEE Journal of Quantum Electronics*, vol. 23, no. 9, pp. 1410–1418, September 1987.
- [69] T. L. Koch and J. E. Bowers, “Nature of wavelength chirping in directly modulated semiconductor lasers,” *Electronics Letters*, vol. 20, no. 25, pp. 1038–1040, December 1984.
- [70] C. Henry, “Theory of the linewidth of semiconductor lasers,” *IEEE Journal of Quantum Electronics*, vol. 18, no. 2, pp. 259–264, February 1982.
- [71] J. C. Cartledge and R. C. Srinivasan, “Extraction of DFB laser rate equation parameters for system simulation purposes,” *Journal of Lightwave Technology*, vol. 15, no. 5, pp. 852–860, May 1997.
- [72] S. Kobayashi, Y. Yamamoto, M. Ito, and T. Kimura, “Direct frequency modulation in AlGaAs semiconductor lasers,” *IEEE Journal of Quantum Electronics*, vol. 18, no. 4, pp. 582–595, Apr 1982.
- [73] R. S. Vodhanel, A. F. Elrefaie, R. E. Wagner, M. Z. Iqbal, J. L. Gimlett, and S. Tsuji, “Ten-to-twenty gigabit-per-second modulation performance of 1.5- μ m distributed feedback lasers for frequency-shift-keying systems,” *Journal of Lightwave Technology*, vol. 7, no. 10, pp. 1454–1460, Oct 1989.
- [74] Q. T. Le, D. Briggmann, and F. Kueppers, “Ultrawideband signal generation based on directly modulated semiconductor laser and optical filtering,” in *2013 IEEE International Topical Meeting on Microwave Photonics (MWP)*, Oct 2013, pp. 340–343.

BIBLIOGRAPHY

- [75] J. Liang, "Antenna Study and Design for Ultra Wideband Communication Applications," Ph.D. dissertation, Department of Electronic Engineering Queen Mary, University of London, 2006. [Online]. Available: <http://qmro.qmul.ac.uk/jspui/handle/123456789/1768>
- [76] R. A. Saunders, J. P. King, and I. Hardcastle, "Wideband chirp measurement technique for high bit rate sources," *Electronics Letters*, vol. 30, no. 16, pp. 1336–1338, Aug 1994.
- [77] A. F. Elrefaie, R. E. Wagner, D. A. Atlas, and D. G. Daut, "Chromatic dispersion limitations in coherent lightwave transmission systems," *Journal of Lightwave Technology*, vol. 6, no. 5, pp. 704–709, May 1988.
- [78] M. Malekizandi, Q. Le, H. Nessling, A. Emsia, D. Briggmann, and F. Küppers, "Adaptive Doublet Pulse Generation for UWB Transmission in Hybrid Wireless-Optical Access Networks," in *2015 European Conference on Lasers and Electro-Optics - European Quantum Electronics Conference*. Optical Society of America, 2015. [Online]. Available: http://www.osapublishing.org/abstract.cfm?URI=CLEO_Europe-2015-CI_P_6
- [79] M. Malekizandi, Q. T. Le, A. Emsia, D. Briggmann, and F. Küppers, "Generation of UWB Doublet Pulse Based on Directly Modulated Laser and Chromatic Dispersion," *IEEE Photonics Technology Letters*, vol. 28, no. 3, pp. 343–346, Feb 2016.
- [80] M. Malekizandi, Q. T. Le, D. Briggmann, A. Emsia, and F. Küppers, "Radio transmission and BER performance of UWB pulse generation based on directly modulated semiconductor laser," in *2015 IEEE Optical Interconnects Conference (OI)*, April 2015, pp. 74–75.
- [81] D. Mahgerefteh, Y. Matsui, X. Zheng, and K. McCallion, "Chirp Managed Laser and Applications," *IEEE Journal of Selected Topics in Quantum Electronics*, vol. 16, no. 5, pp. 1126–1139, Sept 2010.
- [82] A. Zadok, H. Shalom, M. Tur, W. D. Cornwell, and I. Andonovic, "Spectral shift and broadening of DFB lasers under direct modulation," *IEEE Photonics Technology Letters*, vol. 10, no. 12, pp. 1709–1711, Dec 1998.
- [83] M. Malekizandi, Q. T. Le, A. Emsia, D. Briggmann, A. Chipouline, and F. Küppers, "TDM-PON compatible generation of 10 Gbps NRZ and 1.25 Gbps UWB signals by a single light source," *Opt. Express*, vol. 24, no. 15, pp. 17 018–17 026, Jul 2016. [Online]. Available: <http://www.opticsexpress.org/abstract.cfm?URI=oe-24-15-17018>
- [84] K. Grobe and J. P. Elbers, "PON in adolescence: from TDMA to WDM-PON," *IEEE Communications Magazine*, vol. 46, no. 1, pp. 26–34, January 2008.
- [85] G. K. Chang, A. Chowdhury, Z. Jia, H. C. Chien, M. F. Huang, J. Yu, and G. Ellinas, "Key Technologies of WDM-PON for Future Converged Optical Broadband Access Networks [Invited]," *IEEE/OSA Journal of Optical Communications and Networking*, vol. 1, no. 4, pp. C35–C50, September 2009.

- [86] L. Chen, H. Wen, and S. Wen, "A Radio-Over-Fiber System With a Novel Scheme for Millimeter-Wave Generation and Wavelength Reuse for Up-Link Connection," *IEEE Photonics Technology Letters*, vol. 18, no. 19, pp. 2056–2058, Oct 2006.
- [87] Z. Jia, J. Yu, and G. K. Chang, "A full-duplex radio-over-fiber system based on optical carrier suppression and reuse," *IEEE Photonics Technology Letters*, vol. 18, no. 16, pp. 1726–1728, Aug 2006.
- [88] I. Papagiannakis, M. Omella, D. Klionidis, J. A. L. Villa, A. N. Birbas, J. Kikidis, I. Tomkos, and J. Prat, "Design Characteristics for a Full-Duplex IM/IM Bidirectional Transmission at 10 Gb/s Using Low Bandwidth RSOA," *Journal of Lightwave Technology*, vol. 28, no. 7, pp. 1094–1101, April 2010.
- [89] M. Presi, R. Proietti, K. Prince, G. Contestabile, and E. Ciaramella, "A 80 km reach fully passive WDM-PON based on reflective ONUs," *Opt. Express*, vol. 16, no. 23, pp. 19 043–19 048, Nov 2008. [Online]. Available: <http://www.opticsexpress.org/abstract.cfm?URI=oe-16-23-19043>
- [90] F. Xiong, W. D. Zhong, and H. Kim, "A Broadcast-Capable WDM-PON Based on Polarization-Sensitive Weak-Resonant-Cavity Fabry-Perot Laser Diodes," *Journal of Lightwave Technology*, vol. 30, no. 3, pp. 355–361, Feb 2012.
- [91] S. M. Lee, K. M. Choi, S. Mun, J. H. Moon, and C. H. Lee, "Dense WDM-PON based on wavelength-locked Fabry-Pe acute;rot laser diodes," *IEEE Photonics Technology Letters*, vol. 17, no. 7, pp. 1579–1581, July 2005.
- [92] G. Talli and P. D. Townsend, "Hybrid DWDM-TDM long-reach PON for next-generation optical access," *Journal of Lightwave Technology*, vol. 24, no. 7, pp. 2827–2834, July 2006.
- [93] J. C. Cartledge and G. S. Burley, "The effect of laser chirping on lightwave system performance," *Journal of Lightwave Technology*, vol. 7, no. 3, pp. 568–573, March 1989.
- [94] N. D. GP. Agrawal, *Semiconductor lasers*. Springer Science & Business Media, 2013.
- [95] M. Malekizandi, A. Chipouline, and F. Küppers, "Bidirectional UWB over fiber for WDM-PON system," *Opt. Express*, vol. 25, no. 6, pp. 6840–6850, Mar 2017. [Online]. Available: <http://www.opticsexpress.org/abstract.cfm?URI=oe-25-6-6840>
- [96] S. Pan and J. Yao, "IR-UWB-Over-Fiber Systems Compatible With WDM-PON Networks," *Journal of Lightwave Technology*, vol. 29, no. 20, pp. 3025–3034, Oct 2011.
- [97] —, "Performance evaluation of UWB signal transmission over optical fiber," *IEEE Journal on Selected Areas in Communications*, vol. 28, no. 6, pp. 889–900, Aug 2010.
- [98] —, "IR-UWB-Over-Fiber Systems Compatible With WDM-PON Networks," *Journal of Lightwave Technology*, vol. 29, no. 20, pp. 3025–3034, Oct 2011.

BIBLIOGRAPHY

- [99] T. T. Nguyen and L. Lampe, "Coded multipulse pulse-position modulation for free-space optical communications," *IEEE Transactions on Communications*, vol. 58, no. 4, pp. 1036–1041, April 2010.
- [100] H. Selmy, H. M. H. Shalaby, and Z. Kawasaki, "Enhancing optical multi-pulse pulse position modulation using hybrid QPSK-modified MPPM," in *2014 IEEE Photonics Conference*, Oct 2014, pp. 617–618.
- [101] K. Katsu, D. Anzai, and J. Wang, "Performance evaluation on correlation detection and energy detection for ultra wideband-impulse radio communication with multi-pulse position modulation scheme in implant body area networks," *IET Communications*, vol. 7, no. 13, pp. 1430–1436, September 2013.
- [102] M. Herceg, D. Zagar, and D. Galic, "Multi Pulse Position Amplitude Modulation for ultra-high speed time-hopping UWB communication systems over AWGN channel," in *2010 4th International Symposium on Communications, Control and Signal Processing (ISCCSP)*, March 2010, pp. 1–4.
- [103] Y. Q. Wang, Y. h. Lu, Y. Xu, P. F. He, and N. Zhang, "UWB High Data-Rate Wireless Communication System Base on Multi-Pulse Position Modulation," in *2006 International Conference on Wireless Communications, Networking and Mobile Computing*, Sept 2006, pp. 1–4.
- [104] S. J. H. A. D. F. K. P. M. T. G. C. G. M. C. A. A. D. B. C. B. K. A. H. J. G. P. W. A. L. P. D. M. O. C. Gierl, K. Zogal, "Tuneable VCSEL aiming for the application in interconnects and short haul systems," *Proc.SPIE*, vol. 7959, no. 16, pp. 7959 – 7959, January 2011. [Online]. Available: <https://doi.org/10.1117/12.881247>

Acronyms

ALTN	Alternate
Amp	Amplifier
APD	Avalanche photodiode
ATT	Attenuator
AWG	Arrayed waveguide grating
BB	Baseband
BBA	Bias burst amplitude
BER	Bit-error-rate
BERT	Bit-error-rate tester
BPM	Bi-phase modulation
BS	Base station
BW	Bandwidth
CD	Chromatic dispersion
CS	Central station
CML	Chirped-managed laser
DAS	Distributed antennas system
DAA	Detect and avoid
DEMUX	Demultiplexer
DFB	distributed feedback
DL	Delay line
DLI	Delay-line-interferometer
DML	Directly modulated laser
DS	Downstream
EPON	Ethernet passive optical network

FBG	Fiber Bragg Grating
FCC	Federal communications commission
FP-LD	Fabry-Perot laser diode
FTTH	Fiber-to-the-home
FM	Frequency modulation
FWHM	Full-width half maximum
GPON	Gigabit passive optical network
GPS	Global positioning systems
GSM)	Global system for mobile communications
HD	High definition
HDTV	High definition television
ICT	Information and communication technology
IM	Intensity modulation
IR-UWB	Impulse radio UWB
ITS	Intelligent transport systems
LoS	Line of sight
MPC	Multipath components
LD	Laser diode
LO)	Local oscillator
LPF	Low pass filter
LTE	Long term evolution
MAN	Metropolitan area networks
MB-OFDM	Multi-band-OFDM
MIMO	Multiple input multiple output
MLFL	Mode-locked fiber laser
MPPPM	Multipulse pulse position modulation
MU	Mobile user
MUX	Multiplexer
MZM	Mach-Zehnder modulator
M2M	Machine to machine
NF	Noise figure

NLoS	Non-LoS
NRZ	Non-return-to-zero
OAM	Operations administration maintenance
OBPF	Optical bandpass filter
OFDM	Orthogonal frequency-division multiplexing
OLT	Optical line termination
ONU	Optical network unit
OOK	On-off keying
PAM	Pulse amplitude modulation
PC	Polarization controller
PDA	Personal digital assistance
PM	Phase modulation
PMF	Polarization maintaining fiber
PolM	Polarization modulation
PPG	Pulse pattern generator
PPM	Pulse position modulation
PSD	Power spectral density
PSK	Phase shift keying
PSM	Pulse shape modulation
QAM	Quadrature amplitude modulation
RAU	Remote antenna unit
RIN	Relative intensity noise
RN	Remote node
RoF	Radio-over-fiber
RSOA	Reflective semiconductor optical amplifier
SCM	Sub-carrier modulation
SE	Spectral efficiency
SMF	Single mode fiber
SMSR	Side mode suppression ratio
SNR	Signal to noise ratio
SOA	Semiconductor optical amplifier

TDM	Time-division multiplexing
UMTS	Universal mobile telecommunication systems
US	Upstream
UWB	Ultra-wideband
UWBoF	UWB-over-fiber
VOA	Variable optical attenuator
VoD	Video-on-demand
VoIP)	Voice-over-IP
WDM	Wavelength division multiplexing
WiMAX	Worldwide interoperability for microwave access
WLAN	Wireless local area network
WPAN	Wireless personal area network
WWAN	Wireless wide area network
XPM	Cross-phase modulation
XPoIM	Cross-Polarization modulation

Symbols

f	Frequency
σ	Shaping factor of the Gaussian pulse
τ	Time delay
κ	Adiabatic chirp coefficient
λ	Wavelength
CD	Chromatic dispersion
D	Dispersion factor
L	Length
V_{pp}	Peak-to-peak voltage
ϕ	Phase
c	Speed of light
$\Delta\nu$	Frequency deviation
F	Fidelity factor

Publications

Journal

1. A. Emsia, Q. T. Le, **M. Malekizandi**, D. Briggmann, I. B. Djordjevic and F. Küppers, "WDM-TDM NG-PON Power Budget Extension by Utilizing SOA in the Remote Node," in *IEEE Photonics Journal*, vol. 6, no. 2, pp. 1-10, April 2014. doi: 10.1109/JPHOT.2014.2314108.
2. S. Paul, C. Gierl, J. Cesar, Q. T. Le, **M. Malekizandi**, B. Kogel, C. Neumeyr, M. Ortsiefer and F. Küppers, "10-Gb/s Direct Modulation of Widely Tunable 1550-nm MEMS VCSEL," in *IEEE Journal of Selected Topics in Quantum Electronics*, vol. 21, no. 6, pp. 436-443, Nov.-Dec. 2015. doi: 10.1109/JSTQE.2015.2418218.
3. **M. Malekizandi**, Q. T. Le, A. Emsia, D. Briggmann and F. Küppers, "Generation of UWB Doublet Pulse Based on Directly Modulated Laser and Chromatic Dispersion," in *IEEE Photonics Technology Letters*, vol. 28, no. 3, pp. 343-346, Feb.1, 1 2016. doi: 10.1109/LPT.2015.2496215.
4. S. Paul, M. Haidar, J. Cesar, **M. Malekizandi**, B. Kögel, C. Neumeyr, M. Ortsiefer, and F. Küppers, "Far-field, linewidth and thermal characteristics of a high-speed 1550-nm MEMS tunable VCSEL," *Opt. Express* 24, 13142-13156 (2016).
5. **M. Malekizandi**, Q. Le, A. Emsia, D. Briggmann, A. Chipouline, and F. Küppers, "TDM-PON compatible generation of 10 Gbps NRZ and 1.25 Gbps UWB signals by a single light source," *Opt. Express* 24, 17018-17026 (2016).
6. **M. Malekizandi**, A. Chipouline, and F. Küppers, "Bidirectional UWB over fiber for WDM-PON system," *Opt. Express* 25, 6840-6850 (2017).
7. V. Lyubopytov, A. Porfirev, S. Gurbatov, S. Paul, M. Schumann, J. Cesar, **M. Malekizandi**, M. Haidar, M. Wegener, A. Chipouline, and F. Küppers, "Simultaneous wavelength and orbital angular momentum demultiplexing using tunable MEMS-based Fabry-Perot filter," *Opt. Express* 25, 9634-9646 (2017).

Conference

1. A. Emsia, **M. Malekizandi**, T. Q. Le, I. B. Djordjevic and F. Küppers, "1 Tb/s WDM-OFDM-PON power budget extension techniques," 2013 IEEE Photonics Conference, Bellevue, WA, 2013, pp. 529-530. doi: 10.1109/IPCon.2013.6656670.
2. **M. Malekizandi**, A. Emsia, D. Briggmann, Q. T. Le, I.B. Djordjevic, F. Küppers, "Power budget extension for OFDM-TDM-WDM PON," in DokDok, October 2013, Jena, Germany.
3. A. Emsia, **M. Malekizandi**, D. Briggmann, Q. T. Le, F. Küppers, "DPSK-based reach extension for NGbit/s NG-PON," in DokDok, October 2013, Jena, Germany.
4. A. Emsia, **M. Malekizandi**, D. Briggmann, Q. T. Le, I. B. Djordjevic, F. Küppers, "Experimental Demonstration of NG-PONs Power Budget Enhancement Techniques," in Photonics West, SPIE, December 2013, San Francisco, California, USA. doi:10.1117/12.2040133.
5. **M. Malekizandi**, A. Emsia, D. Briggmann, Q. T. Le, I. B. Djordjevic, F. Küppers, "Power budget extension for higher order modulation formats in PONs," in Photonics West, SPIE, December 2013, San Francisco, California, USA. doi:10.1117/12.2038524.
6. A. Emsia, Q. T. Le, **M. Malekizandi**, D. Briggmann, and F. Küppers, "10 Gbit/s PON Upstream Burst-mode Equalization Based on SOAs," in Asia Communications and Photonics Conference 2014, OSA Technical Digest (online) (Optical Society of America, 2014), paper ATH1H.2.
7. **M. Malekizandi**, Q. T. Le, D. Briggmann, A. Emsia and F. Küppers, "Radio transmission and BER performance of UWB pulse generation based on directly modulated semiconductor laser," 2015 IEEE Optical Interconnects Conference (OI), San Diego, CA, 2015, pp. 74-75. doi: 10.1109/OIC.2015.7115707.
8. **M. Malekizandi**, Q. Le, H. Nessler, A. Emsia, D. Briggmann, and F. Küppers, "Adaptive Doublet Pulse Generation for UWB Transmission in Hybrid Wireless-Optical Access Networks," in 2015 European Conference on Lasers and Electro-Optics - European Quantum Electronics Conference, (Optical Society of America, 2015), paper CI-P-6.
9. S. Paul, C. Gierl, J. Cesar, Q. T. Le, **M. Malekizandi**, F. Küppers, B. Koegel, J. Roskopf, C. Grus, M. Görblich, Y. Xu, C. Neumeyr, and M. Ortsiefer, "High Speed Surface Micromachined MEMS Tunable VCSEL for Telecom Wavelengths," in CLEO: 2015, OSA Technical Digest (online) (Optical Society of America, 2015), paper AM3K.1.
10. **M. Malekizandi**, Q. T. Le, A. Emsia and F. Küppers, "Generating 6th order Gaussian derivative for UWBoF using directly modulated laser and accumulative chromatic dispersion of fiber," 2015 IEEE Photonics Conference (IPC), Reston, VA, 2015, pp. 112-113.

11. A. Emsia, Q. T. Le, R. E. Gündogdu, **M. Malekizandi**, E. I. Betou, M. Olson, J. Keck, R. Herber, K. Rienecker, M. Fricke, F. Küppers, "Cost-efficient Upstream Transmitter Using Injection Locked Fabry-Perot Laser Diodes for Multi-Gbit/s WDM-PON," Photonic Networks; 17. ITG-Symposium; Proceedings of, Leipzig, Germany, 2016, pp. 1-8.
12. S. Paul, V. S. Lyubopytov, M. F. Schumann, J. Cesar, **M. Malekizandi**, M. T. Haidar, A. P. Porfirev, S. O. Gurbatov, M. Wegener, A. Chipouline, F. Küppers, "Vortex-MEMS filters for wavelength-selective orbital-angular-momentum beam generation," Proc. SPIE 10120, Complex Light and Optical Forces XI, 101200G (February 27, 2017); doi:10.1117/12.2252494.
13. S. Paul, J. Cesar, **M. Malekizandi**, M. T. Haidar, N. Heermeier, M. Ortsiefer, C. Neumeyer, C. Gréus, M. H. Eiselt, I. Ibrahim, H. Schmidt, J. Schmidt, F. Küppers, "Towards a SFP+ module for WDM applications using an ultra-widely-tunable high-speed MEMS-VCSEL," Proc. SPIE 10122, Vertical-Cavity Surface-Emitting Lasers XXI, 1012209 (February 25, 2017); doi:10.1117/12.2252059.
14. V. Lyubopytov, T. von Lerber, M. Lassas, **M. Malekizandi**, A. Chipouline, F. Küppers, "Amplitude Noise Suppression and Orthogonal Multiplexing Using Injection-Locked Single-Mode VCSEL," in Optical Fiber Communication Conference, OSA Technical Digest (online) (Optical Society of America, 2017), paper Tu3C.3; doi:10.1364/OFC.2017.Tu3C.3.
15. S. Paul, N. Heermeier, **M. Malekizandi**, J. Cesar, M. T. Haidar, C. Greus, C. Neumayer, F. Küppers, "10-Gbps direct on-off-keying modulation across 85 nm continuous tuning range using telecom MEMS-VCSEL," 2017 Conference on Lasers and Electro-Optics Europe and European Quantum Electronics Conference (CLEO/Europe-EQEC), Munich, Germany, 2017, pp. 1-1. doi: 10.1109/CLEOE-EQEC.2017.8086351
16. A. Chipouline, V. S. Lyubopytov, **M. Malekizandi**, T. von Lerbet, M. Lassas and F. Küppers, "Injection-locked single-mode VCSEL for orthogonal multiplexing and amplitude noise suppression," 2017 Conference on Lasers and Electro-Optics Europe and European Quantum Electronics Conference (CLEO/Europe-EQEC), Munich, Germany, 2017, pp. 1-1. doi: 10.1109/CLEOE-EQEC.2017.8086943
17. V. S. Lyubopytov, A. P. Porfirev, S. O. Gurbatov, S. Paul, M. F. Schuman, J. Cesar, **M. Malekizandi**, M. T. Haidar, M. Wegner, A. Chipouline and F. Küppers, "MEMS-based wavelength and orbital angular momentum demultiplexer for on-chip applications," 2017 Conference on Lasers and Electro-Optics Europe and European Quantum Electronics Conference (CLEO/Europe-EQEC), Munich, Germany, 2017, pp. 1-1. doi: 10.1109/CLEOE-EQEC.2017.8087118

Curriculum Vitae

Personal Profile

Name: Mohammadreza Malekizandi
Date of Birth: 09.09.1985
Place of Birth: Tehran, Iran

Education

Dec. 2013 - current	Ph.D. candidate at the Department for Photonics and Optical Communications, Institute for Microwave Engineering and Photonics, Technische Universität Darmstadt. Dissertation: All optical ultra-wideband-over-fiber.
Oct. 2010 - Aug. 2013	M.Sc. in Electrical Technology and Information Technology, Technische Universität Darmstadt, Germany. Dissertation: Power budget management in PON for higher order modulation formats.
May. 2013 - Aug. 2013	Visiting researcher at College of Optical Sciences, University of Arizona, USA. Topic: Power budget extension for PON.
May. 2012 - Aug. 2012	Internship at College of Optical Sciences, University of Arizona, USA. Topic: OFDM for optical communication.
Sep. 2003 - Sep. 2008	B.Sc. in Electrical Engineering and communication, Islamic Azad University, Shahr-e-Rey Branch, Tehran, Iran. Dissertation: Design and fabrication of ultra-wideband antenna.